# ROLE OF THROMBOSPONDIN-1 (TSP1)-CD47 SIGNALING IN TRACHEAL REPAIR AND REGENERATION

by

**Johannes Craig Kutten**

B. S. Biomedical Engineering, Rensselaer Polytechnic Institute, 2011

M. S., Biomedical Engineering, Rensselaer Polytechnic Institute, 2011

Submitted to the Graduate Faculty of

the School of Medicine in partial fulfillment

of the requirements for the degree of

Doctor of Philosophy

University of Pittsburgh

2016

UNIVERSITY OF PITTSBURGH

SCHOOL OF MEDICINE

This dissertation was presented

by

Johannes Craig Kutten

It was defended on

August 11, 2016

and approved by

Wendy M. Mars, Ph. D., Associate Professor, Department of Pathology

Stephen F. Badylak, D. V. M., Ph. D., M. D., Professor, Department of Surgery

Peter Di, Ph. D., Assistant Professor, Department of Environmental and Occupational Health

Justin S. Weinbaum, Ph. D., Research Assistant Professor, Department of Bioengineering

Donna Beer Stolz, Ph. D., Associate Professor, Department of Cell Biology

Dissertation Advisor: Jeffrey S. Isenberg, M. D., M. P. H, Associate Professor, Department

of Medicine

# ROLE OF THROMBOSPONDIN-1 (TSP1)-CD47 SIGNALING IN TRACHEAL REPAIR AND REGENERATION

Johannes Craig Kutten, Ph. D.

University of Pittsburgh, 2016

**Background:** Loss of the trachea and proximal airway from congenital disorders, acute injury or chronic disease is a life-threatening complication. The lack of suitable native replacements has led to attempts to bioengineer tracheas. Recent clinical cases of bioengineered tracheal transplants have been hampered by an inability to maintain growing cell populations. The majority of cases have ended in significant acute and chronic complications, morbidity and death. A growing body of literature has found that a ligand-receptor interaction between the secreted protein thrombospodin-1 (TSP1) and its high affinity receptor CD47, which is upregulated in tissue injury, constitutively restricts multiple key transcription factors that modulate self-renewal and pluripotency.

**Hypothesis:** TSP1-CD47 signaling is maladaptively induced in injured airways and bioengineered tracheas to inhibit cellular dedifferentiation, proliferation and restoration of engineered tracheal transplants.

**Methods:** This dissertation first describes a murine orthotopic tracheal transplant model and second describes methods to characterize the effects of TSP1-CD47 signaling on airway epithelial cells. *In vitro*, airway epithelial cell wound healing and tissue angiogenic capacity was assessed using a variety of techniques. *In vivo*, naphthalene injury and orthotopic transplantation of decellularized tracheal grafts was performed in wild-type mice or in mice that lacked TSP1-CD47 signaling, and epithelial restoration and transplant healing were assessed.

**Results:** Decellularized tracheal grafts support re-epithelization within seven days and epithelial differentiation within eight weeks after transplantation. Disruption of TSP1-CD47 signaling restores self-renewal gene expression in tracheal epithelial cells exposed to hypoxic stress and stimulates more rapid wound healing in an *in vitro* model of airway injury. TSP1 inhibits proliferation of airway epithelial cells while antibody blockade of CD47 restores cell proliferation. Further, TSP1 is upregulated following airway epithelial cell seeding onto decellularized and synthetic tracheal scaffolds. TSP1-CD47 signaling is induced in the airways of WT mice after injury. CD47 null mice displayed enhanced tracheal healing of both chemically injured airways and following orthotopic transplantation of decellularized tracheal grafts.

**Conclusion:** TSP1-CD47 signaling is maladaptively upregulated in stressed tracheal epithelial cells, in injured airways, in cells seeded on decellularized and synthetic tracheal grafts, and in engineered tracheal transplants to limit self-renewal gene expression and inhibit cell proliferation, airway healing and cellular incorporation of bioengineered tracheal transplants.

# TABLE OF CONTENTS

**DAPI-labeled objects were sorted into four groups based on the degree of fluorescence intensity relative to a user-defined threshold: (1) K5-low/K14-low**

**DAPI-labeled objects were sorted into four groups based on the degree of fluorescence intensity relative to a user-defined threshold: (1) K5-low/K14-low**

# LIST OF TABLES

# LIST OF FIGURES

# PREFACE

This document would not exist without the help of many friends and colleagues along the way. First, I'd like to thank my parents, Johnnilyn and James Kutten, my brother Kwame, and my sister Rachel. I am inspired by your example, and I couldn't have made it to this point without you. Thanks for teaching me what it means to persevere.

Next, I would like to thank my mentors: Dr. Jeffrey S. Isenberg, my primary research mentor, who hosted me in his lab for three years as his graduate student. I learned quite a bit about mentorship (and how to be an attentive mentee), and for that I will be forever grateful. Thanks for encouraging me to do things I might not have tried otherwise. Thanks also to Dr. Thomas Gilbert, who initiated the trachea project and hosted me during my first research rotation in Pittsburgh in Summer 2011.

I'd like to thank members of my committee for their unending patience: Dr. Stephen F. Badylak, Dr. Donna Stolz, Dr. Wendy Mars.; Dr. Peter Di; Dr. Justin Weinbaum. Thanks as well to Drs. Richard Steinman and Dr. Tim Oury, who were indispensable in helping me navigate the difficult challenges of graduate school.

Next, I would also like to thank my friends here in Pittsburgh and elsewhere, who offered a listening ear and were always willing to carry extra weight when I needed to focus on school: Hugo Cheng, Micki Sundheim, Kristen and Josh Lippert, Bobby Seto, Cindy Seto, Jessica Hsu, Daniel Bucknell.

Thanks to my lab mates past and present: Natasha Rogers MD, PhD; Caitlin Czajka, PhD; Maryam Sharifi-Sanjani, PhD; Raquel Bienes-Martinez, PhD; Heather Knupp, MS; Kedar Ghimire PhD, Takuto Chiba, PhD, and Lynda Ihrig, whose technical assistance (and occasional commiseration) were invaluable.

Finally, I dedicate this dissertation to the patients, past and future, who inspire all I do.

# 1.0    INTRODUCTION


Tracheal injuries and defects are rare, but are in many instances fatal.  Despite the development of reparative protocols such as slide tracheoplasty, there remains a population of patients for whom there are no therapies available. These include pediatric patients with congenital defects and adults with tracheal tumors.  In these patients, tracheal transplantation or replacement with a bioengineered graft would be a life-saving therapy.  In spite of this, attempts to prepare bioengineered tracheal transplants have been unsuccessful, and new approaches are needed to generate grafts which support functional cell populations.

Thrombpsondin-1 (TSP1)-CD47 signaling represents a particular cell matrix interaction which may limit the survival of cells in tissues after transplantation.  TSP1 is deposited in the extracellular matrix by cells under stress.  It ligates with its high affinity cell receptor, CD47. TSP1 activation of CD47 redundantly inhibits tissue survival through effects on angiogenesis and self-renewal. Thus, TSP1 which is (1) retained in the extracellular matrix, or (2) is secreted by cells migrating into and repopulating decellularized or synthetic tracheal scaffold, can limit the survival of grafts and whole transplants.

**I hypothesize that TSP1, via cell-surface receptor CD47, inhibits cellular survival and engraftment within decellularized tracheal grafts.**  The aims of this dissertation project were as follows: (1) to establish a murine model of tracheal transplantation for studies examining the role of specific cell-matrix interactions in airway repair and regeneration.  (2) to examine the

1

effects of TSP1-CD47 signaling on airway epithelial cells *in vitro*, and (3) to demonstrate that interference with the TSP1-CD47 signaling axis (via the use of mutant mouse models) can improve outcomes in orthotopic decellularized tracheal transplantation.

This project describes a novel mechanism by which cell-matrix interactions limit cell survival and reconstitution of bioengineered decellularized and putatively synthetic tracheal grafts. The knowledge generated by this project will support the use of CD47-blocking therapeutics to improve outcomes in tissue engineered transplants.

## 1.1    DESCRIPTION OF CONTENTS

Chapter 2 describes the anatomy, development, physiology, and pathology on the trachea and provides some background on airway transplantation.  It also describes the publically available data on the first human trials of bioengineered tracheal transplants, as these preliminary cases and the results therein have already had an impact on the field of tracheal tissue bioengineering specifically and tissue engineering in general.  Chapter 3 describes the murine orthotopic tracheal transplant model. It borrows heavily from my publication in *Tissue Engineering Part A* (2015) [1].  Chapter 4 provides background on thrombospondin-1 (TSP1) and CD47 signaling, and describes our efforts to generate a floxed CD47 mouse for future work examining cell-specific CD47 knockouts. Chapter 5 explores a technique which was developed here in the Isenberg lab to determine whether or not the CD47 null genotype leads to increased numbers of basal cells within the airway epithelium. Finally, Chapter 6 describes our experience transplanting decellularized tracheal grafts into wild type (CD47 positive) and CD47 null mice.

## 2.0    BACKGROUND

The trachea is a vital organ which functions as the conduit between the external environment and the respiratory epithelium. There is a subset of patients with long-segment tracheal defects for whom current surgical protocols are insufficient. For these patients, tracheal transplantation represents a potentially lifesaving intervention.

Tracheal anatomy, development, physiology, and pathology are reviewed in this introduction. Present techniques of tracheal repair and associated pitfalls are examined.    Finally, a discussion of matricellular signaling within decellularized grafts forms the rationale for my research plan.

## 2.1    THE TRACHEA

### 2.1.1   Anatomy

The trachea is a vascularized tube extending from the larynx to the level of the fourth thoracic vertebra. In adult humans it is about 10-13 centimeters in length and 1.5-2 centimeters in diameter. It is surrounded by the *adventitia*, a layer of loose connective tissue which anchors it to surrounding structures [2].

The lumen is lined by a pseudostratified columnar epithelium comprised of three major cell types: (1) *ciliated cells* which provide mucociliary clearance; (2) *club secretory cells*, which fulfill a variety of roles related to the maintenance of the immune barrier; and (3) *basal cells*, which act as the progenitor cells of the proximal airway epithelium. The epithelium and the highly vascularized *lamina propria* together comprise the tracheal mucosa.

Patency of the trachea is maintained by up to 20 equally-spaced hyaline *cartilaginous rings*. These rings are "incomplete" (C-shaped) with their opening on the dorsal side. This opening is covered by a layer of smooth muscle (*m. trachealis*) which narrows the trachea under autonomic stimuli and separates the tracheal lumen from the esophagus.

The cervical trachea is perfused by tracheoesophageal branches of the inferior thyroidal artery, whereas the inferior trachea and carina are supplied by the bronchial arteries [3, 4]. Venous drainage is provided by the inferior thyroid venous plexus [4]. The adult tracheal microvasculature within the lamina propria provides segmental perfusion to the epithelium. Circumferentially-oriented arterioles and venules are found in the intercartilaginous zones, whereas longitudinal capillaries cross cartilaginous rings [5, 6].

### 2.1.2 Development

The trachea is comprised of tissue of both endodermal and mesodermal origin. Interactions between these two germ layers are responsible for the formation of the primitive gut tube and the development of the airways [7, 8].

The tracheal epithelium is derived from the foregut endoderm which initially expresses *Foxa1*, *Foxa2*, *Gata4* and *Gata6* [8]. Around developmental day E9.0 (day 22 in humans), epithelial cells of the ventral foregut endoderm are driven toward a respiratory lineage by the

expression of *Nkx2.1* (also known as *Ttf1* or *T/EBP*) [9]. *Nkx2.1* (expressed ventrally) and *Sox2* (expressed dorsally) are thought to counter-regulate each other [10]. Cells of the dorsal foregut endoderm take on characteristics of the esophageal epithelium through expression of high levels of *Sox2* [8, 9, 11], whereas moderate-to-low *Sox2* expression defines the conducting airway phenotype.

Proper *Sox2* signaling is critical for maintenance of the conducting airway epithelium in adults. The presence of *Sox2* is thought to specify the airway epithelium toward a proximal (versus distal) phenotype [12], and precise levels of *Sox2* are necessary for maintenance of the respiratory epithelium's club, ciliated, and basal cells [13]. *Sox2* deletion (after birth) leads to an excess number of mucus-producing cells, and a lower proportion of p63-positive basal cells [10]. Total loss of *Sox2* expression leads to a cuboidal and squamous cell phenotype [14]. Further, *Sox2* is necessary to maintain the self-renewal capacity of airway basal cells *in vitro*, and is required for regeneration of the tracheal epithelium in models of airway injury [15].

Tracheal cartilage is of splanchnic mesodermal origin. Transcription factors *Tbx4, Tbx5* and *Sox9* are critical for the patterning and development of the cartilaginous rings. Specification of the splanchnic mesoderm immediately adjacent to the foregut endoderm begins with expression of transcription factors *Tbx4* and *Tbx5*. By E11.5 *Tbx4/5* are expressed throughout the mesenchyme surrounding the primitive tracheal tube [16]. By E13.5, *Sox9* expression appears in a ring-like pattern corresponding to sites of future cartilaginous rings. Cells in these regions express collagen 2a, and exert negative feedback to suppress expression of *Tbx4/5* [16, 17]. Thus, by E15.5, *Tbx4/5* are only expressed in the spaces between the *Sox9*-expressing cartilaginous rings [17]. Loss of *Sox9* expression in mesenchymal cells is associated with a failure to develop tracheal rings and death due to tracheal collapse [17].

Studies of mouse tracheal development have indicated that the embryonic trachea is supplied by a primitive, highly anastomotic vascular plexus, structurally similar to that of the yolk sac [5]. This plexus is pruned to its segmental, hierarchal adult form between days E16.5 and P7. During this period, blood vessels crossing the cartilaginous rings regress and are replaced by longitudinally-oriented capillaries. Vessels in intercartilaginous sites are replaced with circumferential arterioles and venules. Variances in VEGF signaling, oxygen tension, and bio-mechanical load are thought to be responsible for this effect [5, 6].

### 2.1.3   Physiology

In the context of regenerative medicine, the physiology of the native tissue defines the design requirements of a tissue engineered graft.

### 2.1.3.1 Epithelial physiology

The tracheal epithelium of the mouse is histologically similar to the human trachea and main stem bronchi [2]. This pseudostratified epithelium consists of ciliated, club, and basal cells. It is characterized by (1) the presence of intracellular junctions, (2) secretion of antimicrobial products, (3) a mucociliary elevator. It is therefore a component of the innate immune barrier. This barrier function is particularly important because the trachea and thus engineered tracheal transplants sits at the interface between the non-sterile external environment and underlying sterile tissues. This localization distinguishes the trachea from prostheses which have been implanted in sterile mesenchymal tissues (such as vascular grafts and heart valves) [18, 19]. Rapid reconstitution of the tracheal epithelium is thought to limit scar tissue formation following injury and/or transplantation [20]. Published reports have made note of the presence of

6

granulation tissue along the luminal surface of tracheal grafts, which creates iatrogenic stenosis [18]. Re-epithelializaiton, when it does occur, halts the fibrotic process. Thus, a functioning epithelium is critical for any engineered tracheal transplant.

*Basal cells* are widely considered to be the progenitor cells of the proximal airway epithelium, and the trachea [7, 21-25]. These cells are relatively undifferentiated at baseline and are characterized by expression of the transcription factor p63 and the structural protein keratin-5. A second intermediate filament protein, keratin-14, is upregulated after injury as basal cells proliferate and differentiate. In naphthalene [22, 26-28], sulfur dioxide [27, 29], polidocanol [27], and chlorine [30] injury models, basal cells reconstitute the various cell types of the airway epithelium. The exact intracellular processes governing basal cell differentiation are unknown, though it has been proposed that a Notch signaling event converts these basal cells into a p63-negative, keratin-8-positive early progenitor, from which other cells differentiate [29].

*Ciliated cells* express the transcription factor *FoxJ1* and are identified histologically by expression of acetylated tubulin. They propel mucus toward the larynx where it can be expelled. The total volume of mucus produced in a given day averages 10 ml, but this amount can increase significantly in patients who are ill as the body attempts to remove cellular debris and microbial components [3]. Failure to clear airway secretions can lead to fatal airway obstruction. Thus, ciliated cells are another key component of any engineered tracheal graft, and an analysis of ciliary beat has been included in several models of tracheal repair [1].

*Club cells* (formerly known as Clara cells) are a tall, dome-shaped secretory cell population present in both the trachea and the bronchioles [31]. They produce a variety of molecules involved in creating the innate immune barrier of the airway epithelium, including proteases, antimicrobial peptides, and cytokines [31]. They have also been implicated in the

production of surfactant [32]. The presence of cytochrome P450 enzymes in these cells gives them the capacity to detoxify inhaled substances. A particular subpopulation of club cells within the bronchioles is thought to have a limited capacity to differentiate into other cell types, and thus can act as a progenitor cell population [30, 31, 33]. Despite their heterogeneity, club cells are uniformly identified through their production of the immunoregulatory peptide club cell secretory protein (CCSP, also known as CC10, secretogobulin 1a1 [SCGB1A1], and uterogobulin) [30].

### 2.1.3.2 Cartilaginous rings

The C-shaped cartilaginous rings consist of hyaline cartilage and primarily act to maintain the patency of the trachea. Signals from the cartilaginous rings may regulate development of the tracheal epithelium. Reports indicate that the tracheal epithelium in *Sox9* mutants adopts a "distal" phenotype with greater numbers of club cells and reduced numbers of basal cells [17]. This change in epithelial phenotype is thought to be secondary to either (1) a loss of *Fgf10* expression in the *Sox9* mutants or (2) a loss in mechanical support [17]. Cartilaginous rings are theoretically necessary to prevent collapse of any engineered tracheal transplant; however, cartilage has not been yet shown to regenerate in orthotopic [1] or heterotopic [34] models of tracheal transplantation.

### 2.1.3.3 Connective tissue and vascular function

Branches of the inferior thyroidal artery and bronchiolar arteries provide segmental perfusion to the trachea. In both mice and humans, microvessels anastomose along the lateral aspect of the trachea and penetrate the spaces in between each cartilaginous ring [4]. These vessels penetrate to the *lamina propria*, a layer of loose connective tissue which underlies the

epithelium [2]. Arterioles and venules run circumferentially in the mucosa between each cartilaginous ring, whereas capillaries cross each ring in a longitudinal fashion [5]. Superficial regions of the lamina propria are populated by lymphocytes which act as a component of the mucosal-associated lymphoid tissue. Connective tissue fibers condense and become elastic fibers in deeper layers of the lamina propria. Thus, the lamina propria provides nutritional, mechanical, and immunological support to the respiratory epithelium [2].

### 2.1.4   Pathology

Tracheal injuries and defects are rare. This low incidence has hampered the development of definitive surgical protocols for tracheal repair [35].

### 2.1.4.1 Types of tracheal insufficiency

Tracheomalacia describes the condition of having "collapsible" trachea which does not maintain its patency, particularly during expiration [36]. In children, it is typically caused by prematurity or congenital defects associated with cartilage development. In adults it is often a consequence of prolonged intubation, external compression (for instance, from a tumor), or chronic severe infection and inflammation. Surgical stenting is indicated in situations where the defect is not intrinsic to the trachea itself. In other situations, no appropriate surgical solution is known. *Tracheal stenosis* describes the condition of having a narrow (yet patent) trachea. "Complete" (that is, O-shaped, rather than C-shaped) tracheal rings are the most common congenital cause this condition [37]. In adults, stenosis can be iatrogenic, secondary to removal of a long-standing tracheostomy tube. In these cases, scar tissue forms over the anterior opening, which contracts and narrows the trachea. Alternatively, iatrogenic tracheal stenosis can result from prolonged

intubation: high-pressure cuffs (designed to form an airtight seal) can cause ischemia, necrosis, fibrosis, and contraction of tracheal tissue [35].

## 2.1.4.2 Surgical treatment of short- and long-segment tracheal insufficiency

When the insufficient tracheal segment is less than a few centimeters, it can be surgically corrected via *resection and anastomosis*. The applicability of this technique has been limited by the fact that the trachea is under intrinsic tension *in vivo*. Significantly shortening the trachea adds to this tension, which (1) raises the risk of tissue ischemia and (2) can potentially lead to separation of the anastomosis. For these reasons, no more than 25-30% of the trachea's length can be removed [38, 39]. When the stenotic region exceeds this length, surgeons have attempted to widen the trachea with an anterior incision closed with a pericardial patch [39]. However, these patched tracheas are particularly susceptible to obstruction via granulation tissue formation, and must be frequently cleared by bronchoscopy [39]. Further, resection and pericardial patching can disrupt the continuity of the epithelium, which can affects the mucociliary elevator [40] and the segmental blood supply [4].

*Slide tracheoplasty*, depicted in Figure 1, is the preferred treatment for long-segment tracheal stenosis [38, 39, 41]. In this technique, a transverse cut is made across the stenotic segment of the trachea. The caudal and cranial segments are opened with an anterior longitudinal cut and a posterior longitudinal cut, respectively. Finally, the two segments are "slid" against each other and are sutured together. The resulting segment has twice the original diameter, about four times the cross sectional area, and half the original length [38, 39]. In pediatric patients, the resulting segment has been shown to grow over several years [39].
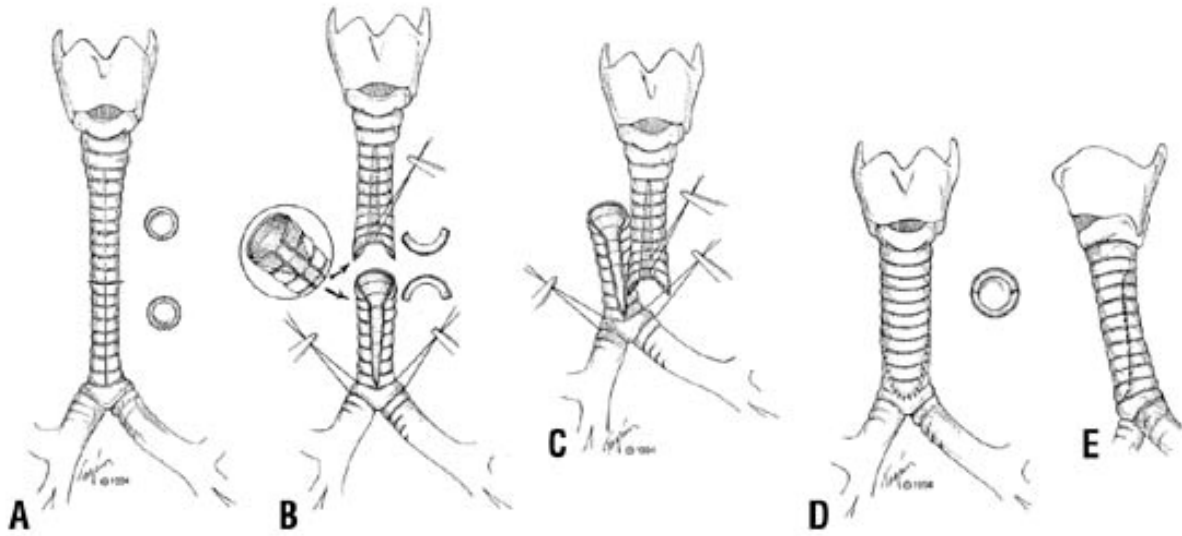
**Figure 1. Technique of slide tracheoplasty, as diagrammed by HC Grillo [39].** (A) A transverse cut is made at the midpoint of the stenotic segment. (B) Anterior and posterior longitudinal cuts are made to widen the caudal and cranial segments. (C) The two ends are anastomosed to each other. (D, E). The widened trachea.

### 2.1.4.3 Severe tracheal defects lack an effective surgical solution

Despite these advances in tracheal surgery, there remains a cohort of patients for which neither resection nor slide tracheoplasty is possible. These include pediatric patients with congenital tracheal agenesis (with or without an esophageal fistula), and adults with tracheal tumors. In these patients, tracheal transplantation or prosthetic replacement would be a life-saving therapy.

Tracheal agenesis is rare, occurring in about 1:50,000 births [42]. It may be managed temporarily with the insertion of an esophageal tube to provide ventilation to the lungs through what remains of the trachea [43]; however, given its low incidence there is no established treatment protocol. Mortality approaches 100% and in fact the condition has been described as incompatible with life [42].

Cancer of the trachea is also rare, occurring in 0.1 per 100,000 person-years. They represent about 0.2% of all respiratory tract tumors [44]. These are typically malignant tumors, 30-40% of which are squamous cell carcinomas associated with smoking. Another 30-40% are adenoid cystic carcinomas of unknown etiology [44, 45]. The ten-year survival rate following a diagnosis of tracheal cancer is estimated to be between six and seven percent. For patients afflicted with these severe tracheal defects, tracheal transplantation could be a curative therapy. However, the low incidence of these conditions and the lack of available donor tissues have prevented the development of appropriate transplantation protocols.

## 2.2     ENGINEERED GRAFTS FOR AIRWAY TRANSPLANTATION

Given the lack of suitable native tissues, the trachea represents a desirable candidate for repair using a tissue-engineered graft. Historically, tracheal transplants have been prepared from synthetic or natural materials, using polymeric or decellularized constructs. Polymeric materials have the advantage of being relatively easy to produce in large numbers, and their composition is easily controlled. Extracellular matrix is both biomimetic and biocompatible, and in theory should be an ideal substrate for tissue repair. However, neither type of construct in clinical cases has been able been able to sustain a cell population which can fulfill the varied design requirements of the trachea.

Over the last decade and a half, several published reports have described tracheal transplantation using decellularized and synthetic grafts. In recent years, many of these reports (especially several reports by Maccchiarini and colleagues) have been difficult to interpret  due to concerns about data completeness and  integrity and institutional approval and oversight

approval [46]. This has left the field of tracheal repair in an uncertain state. The following is a brief overview of human bioengineered airway repair, with a focus on decellularized grafts in particular.

### 2.2.1   Indications for Tracheal Transplant

Tracheal transplantation is indicated for non-resectable causes of airway insufficiency. In adults, any lesion less than one-half the length of the trachea can be safely resected; in children, this threshold drops to one-third [47]. For patients with smaller defects, slide tracheoplasty can be employed to restore the airway [39]. Few options are available for patients with larger defects, which can result from congenital causes (long segment tracheal stenosis, tracheal agenesis), trauma, or malignancy.

### 2.2.2   Decellularized Tracheal Grafts

A tracheal graft must support a ciliated epithelium and maintain its patency under negative pressure. Epithelial cells show improved survival on vascularized surfaces [48], but adequate perfusion also remains a challenge in all tissue-engineered constructs (even cell seeded ones). The lack of effective perfusion severely limits the size of grafts. Cartilage regeneration is particularly important to maintain the patency of implanted grafts. In the human trachea, segmental perfusion is provided by microvessels which penetrate the lamina propria, beneath the respiratory epithelium [2].

Bioengineered tracheal transplants have recently been created by seeding decellularized native tracheal scaffolds with primary airway cells, mesenchymal stem cells, or some

combination of both [49, 50]. The extracellular matrix it thought to provide cells with a three-dimensional substrate for migration and growth while its molecular composition likely influences cell behavior. Molecular signals contained within the decellularized matrix may affect rates of engraftment and revascularization, and therefore can be beneficial or deleterious for the process of *in vivo* cellularization.

### 2.2.3  Preclinical Research Models for Tracheal Transplantation

A recent review identified 85 preclinical studies on tracheal repair and regeneration [51]. These have been performed in a variety of animal models (mouse, rabbit, sheep, pig and dog), and use a number of graft types (decellularized, synthetic, and hybrid). Of these, the rabbit appears to be the most popular animal model due to its favorable size (for ease of surgery) and cost. Common to all models is the observation that airway repithelialization is a relatively straightforward process; however, re-establishment of cartilaginous and vascular cell populations remains difficult [51, 52].

Decellularized tracheal grafts are prepared using a variety of chemical and physical means to remove cellular and immunogenic material from a harvested tissue [51, 53]. Decellularization protocols vary in length from three days to six months, and typically use cycles of detergents, enzymes, and hypertonic/hypotonic solutions to lyse cells and remove them from the extracellular matrix. Our published method makes use of a series of vacuum cycles in order to increase the ability of these solutions to penetrate the scaffold [1], a version of this approach being then adopted by others [54]. Acellular grafts are frequently terminally sterilized via gamma irradiation [51]. Many grafts are implanted in the acellular state, but others are seeded

with epithelial cells, cartilaginous cells, vascular cells, or some combination thereof and incubated in a bioreactor to promote cell adhesion [51].

We have elected to use the murine, orthoptoic, acellular tracheal graft model due to the commercial availability of global mouse knockouts. This technology will allow us to study the role of specific genes in airway repair and regeneration. Our experience with decellularized mouse tracheal transplants (published in [1], and reproduced in 3.0 on page 34) has demonstrated that cell seeding is unnecessary for the establishment of a ciliated epithelium within eight weeks of orthotopic transplantation.

### 2.2.4   Clinical Use of Tissue Engineered Tracheal Grafts

A number of research groups have attempted to create engineered tracheal transplants using decellularized, synthetic, and hybrid grafts [51, 52]. Despite the publication of clinical case reports and subsequent considerable media coverage [55], these engineered tracheas have shown limited success in humans, and complication rates remain very high. Published reports have also made concurrent use of an omental soft tissue flap to wrap the engineered transplant with to (1) provide a source of angiogenic-driven vascularization and (2) create a barrier between the non-sterile tracheal lumen and the surrounding sterile tissues of the mediastinum [19]. Epithelial repair in such decellularized grafts can be described as healing by "secondary intention" -- the process by which the surface of the graft is covered with granulation tissue, which is then re-epithelialized [19].  Indeed, this is the healing process which has been observed in polymeric tracheal grafts [20].  While this process generates a functional epithelium, it significantly lowers the lumen's cross-sectional area and the resultant trachea is stenotic. It is thought that re-epithelialization can prevent iatrogenic stenosis due to scar tissue formation  [20]. Methods to

promote rapid re-epithelialization of the luminal surface of the decellularized scaffolds must be developed, in order to limit the overgrowth of scar tissue which narrows the tracheal lumen.

## 2.3  HUMAN BIOENGINEERED TRACHEAL TRANSPLANTATION

As mentioned, several groups have attempted to bioengineer human tracheal transplants over the last three decades, with the majority of these reports arising from Macchiarini et. al.. Based on the currently available data within the public domain, this group reported  17 tracheal transplants using decellularized and synthetic grafts between 2008 and 2013 [56].  A review of the current state of the field of tracheal tissue engineering would be incomplete without a discussion of the preliminary attempts at human bioengineered tracheal transplants, the difficulties associated with them, and the implications for the field.

### 2.3.1  Catalog of Patients

Macchiarini et. al. have been involved with at least 17 trachea transplants in the US, Europe and Russia between 2008 and 2013. These are briefly summarized in a 2014 article by Jungebluth [56], hereafter referred to as the 2014 Review. A full accounting of these patients is difficult, as few of these cases generated individual peer-reviewed articles. That this is the case was further highlighted in a 2014 news article in *Science* that also noted the absence of published case reports regarding many of these patients and a lack of long-term follow up data [57]. However, a review of the literature and popular media reports can be used to provide some albeit limited information to begin to catalog these patients and assess their clinical outcomes. A summary of

these findings based entirely upon sources within the public domain is represented in Table 1, and to the best of our knowledge this is the most complete review of these patients currently available.

The 2014 Review [56] provides only limited information regarding the 17 patients. For each, only the graft type, the indications for surgery, and the status at the time of publication are available (in Table 3 on page 104 of that article). To generate Table 1 below, these patients were enumerated (1 to 17) and details in the original table were cross-referenced with available literature and media reports. In particular, papers authored by Macchiarini and colleagues describing their experience with airway repair and regeneration were used to corroborate and expand upon the information in the 2014 Review. The patients were re-sorted by surgical date where known. In some cases (in particular, the Russian cases) granting agency databases and translated institutional press releases were consulted.

Given the novel nature of this treatment, these surgeries were frequently accompanied by reports in mass media outlets. In some cases, these sources were consulted to provide context and identifying information which could be cross-referenced with the information provided in the 2014 Review [56]. Of particular note were the following media sources (1) a 82-minute long documentary released in 2014 by NBC News regarding the case of Patient 15 [55] (2) a three-part question raising documentary investigating Dr. Macchiarini and his work at Karolinska, aired by the Swedish television network SVT in early 2016 [58], and (3) a series of news articles published in the journal *Science* [57, 59, 60]. While the SVT documentary is only available in Swedish, certain associated articles and videos could be found in English (or in Swedish with English subtitles), and these online media items were used as sources to generate Table 1.

The three Russian cases were a particular challenge, as they did not generate any peer-reviewed case reports, and therefore their clinical outcomes are difficult to determine.  Reports in European media and Russian government websites indicate that three tracheal transplants using synthetic grafts were performed at Kuban State Medical University in Krasnodar during 2012 and 2013. The 2014 Review [56] states that the authors were the recipients of a "megagrant" from the Russian Ministry of Education and Science (identified by its grant agreement number, 11.G34.31.0065) to perform surgeries in Russia. These three  patients are apparently among the 17 briefly described in the 2014 Review [56] and correspond to patients 12, 13, and 16 in Table 1.  Data from two of these patients was presented at a scientific conference in the United Kingdom in May 2013 [61].Their identities have been inferred from various Russian and Swedish media sources. Of the three, Patient 12 (is the individual whose identity is known with the most certainty, as she was closely followed in the SVT documentary [58] (and appeared briefly in the NBC documentary [55] describing the case of Patient 15).

In August 2014, four colleagues at the Karolinska Institutet[1] prepared a document analyzing six of Macchiarini et. al. articles on tracheal repair, as part of a complaint filed at the Karolinska Institutet [62]. This document was subsequently leaked to the public via the science blog RetractionWatch.com in December 2014 [63]. This document describes a number of inconsistencies between the patient records of the three individuals treated at Karolinska University Hospital and the descriptions of their clinical outcomes in the published literature reports. The clinical findings included in the complaint could be used to clarify the outcomes of the three Karolinska patients from Eritea, the United States, and Turkey, who are enumerated as

[1] In the literature and in media reports, the name of this institution is typically written with its Swedish spelling ("Institutet") rather than the English spelling ("Institute").  This convention has been maintained herein.

Patients 10, 11, and 14 in the table below. It should be noted that the leaked complaint [62] also enumerates the Karolinska patients in chronological order using an independent numbering system. Within that document, 10, 11, and 14 are denoted as Case 1, Case 2, and Case 3 respectively.

The results of these preliminary cases of human bioengineered tracheal transplantation have generated significant debate, with implications for the field of tracheal bioengineering. A number of recent review articles on tracheal tissue engineering have taken an uncritical approach toward these cases, however the reasons for this ae not clear given the substantial perioperative morbidity and mortality and long-term complications in these cases [51, 53]. The following is a synthesis of peer-reviewed literature and media reports on the controversial surgeries, with a focus on a subset of the seventeen patients. The next section will discuss the consequences and implications of the incident for this field (and more generally, clinical translation of tissue engineering).

**Table 1. Trachea Transplants by Macchiarini et al, 2008-2013**

|  | Nationality | Age | Indication | Type | Site of surgery | Date MM/YY | Status and date | Ref. |
|---|---|---|---|---|---|---|---|---|
| 1 | Columbia | 30 | Malacia secondary to tuberculosis | Decell. | Hospital Clinic, Barcelona, Spain | 06/08 | Alive as of 2014 | [56, 57, 64-66] |
| 2 | UK | 11 | Long segment congenital stenosis | Decell. | Great Ormond Street Hospital, UK | 03/10 | Alive as of 2014 | [56, 57, 67, 68] |
| 3 | Unknown Child | <18 | T-E fistula | Decell. | ? | ? | Died of massive bleeding (chest/GI?) | [56, 57] |
| 4 | Unknown Child | <18 | Malignancy | Decell. | ? | ? | Died, tumor recurrence months later | [56, 57] |
| 5 | Unknown. | ? | Malacia | Decell. | ? | ? | Alive as of 2014 | [56] |
| 6 | Unknown. | ? | Malacia | Decell. | ? | ? | Alive as of 2014 | [56] |
| 7 | Unknown. | ? | Malacia | Decell. | ? | ? | Alive as of 2014 | [56] |
| 8 | Unknown. | ? | Malignancy | Decell. | ? | ? | Died, tumor recurrence | [56] |
| 9 | Unknown. | ? | Malignancy | Decell. | ? | ? | Died, tumor recurrence | [56] |

| | Nationality | Age | Indication | Type | Site of surgery | Date MM/YY | Status and date | Ref. |
|---|---|---|---|---|---|---|---|---|
| 10 | Eritea | 36 | Malignancy | Synth. [2] | Karolinska Inst., Sweden | 06/11 | Died Jan. 2014. | [56, 62, 69-75] |
| 11 | USA | 30 | Malignancy | Synth. | Karolinska Inst., Sweden | 11/11 | Died Mar. 2012, pneumonia? fistula? | [56, 57, 62, 70] |
| 12 | Russia | 33 | "Malacia" (Trauma) | Synth. | Kuban State Medical University, Russia | 06/12 | Died Sept. 2014 | [56, 70, 76-79]. |
| 13 | Russia | 28 | "Malacia" (Trauma) | Synth. | Kuban State Medical University, Russia | 06/12 | Died in bicycle accident. | [56, 70, 79] |
| 14 | Turkey | 22 | Iatrogenic malacia | Synth. | Karolinska Inst., Sweden | 08/12, 07/13[3] | Remains hospitalized as of Jan. 2016 | [56, 62, 80, 81] |

[2] The material in this patient's synthetic graft was polyhedral oligomeric silsesquioxane/poly(carbonate-urea) urethane (POSS/PCU) [69]. Other patients receiving synthetic grafts received grafts comprised of polyethylene terephthalate/polyurethane (PET/PU) [62].

[3] This patient required a re-transplantation.

| | Nationality | Age | Indication | Type | Site of surgery | Date MM/YY | Status and date | Ref. |
|---|---|---|---|---|---|---|---|---|
| 15 | Canada | 2 | Congenital agenesis | Synth. | Children's Hospital, Ill., USA | 04/13 | Died July 2013. | [55-57, 82] |
| 16 | Jordan | 42 | "Malacia" (Trauma) | Synth. | Kuban State Medical University, Russia | 08/13 | ? | [56, 83] |
| 17 | Unknown. | ? | Long segment congenital stenosis | Synth. | ? | ? | ? | [56] |

### 2.3.2 Patient Narratives: Decellularized Grafts

In 2004, Patient 1 presented to the Hospital Clinic in Barcelona, Spain with a tuberculosis infection. The infection was successfully treated with antibiotics over the next six months, but she continued to have breathing difficulties. She was diagnosed with post-tuberculosis chronic tracheitis, tracheal stenosis, and severe malacia of the left main bronchus. A three-centimeter stenotic region of her trachea was resected, and a stent was placed to maintain the patency of her bronchus. While the resection was successful, the stent was poorly tolerated and removed. By 2008 her condition had worsened and to the point where she was unable to perform basic activities of daily living: the diameter of her left main bronchus had been reduced to four millimeters by a fixed airway stenosis, and she experienced complete expiratory collapse due to her progressing bronchiomalacia [64].

Patient 1 received a tracheal transplant in June 2008 [57, 64]. Her graft was harvested from a human donor and underwent a six week decellularization process referred to as the "detergent-enzymatic method." Twenty-five cycles were performed. During each cycle the trachea was washed with distilled water, sodium deoxychoalate, deoxyribonuclease I, and sodium chloride solutions to remove cellular material. Bone marrow stem cells (BMSCs) and bronchiolar epithelial cells were harvested from the patient and expanded *in vitro*. BMSCs were differentiated into chondrocytes. The epithelial cells and the chondrocytes were seeded onto the graft in a bioreactor and were allowed 24 hours to adhere. An air-liquid interface was established by rotating the graft within the bioreactor for three days, after which the graft was transplanted into the patient.

Over the next several years she would receive a series of stents to maintain the patency of her graft [57, 84]. In April 2013, independent journalists seeking to contact the patient were unable to do so [57], but at the time of the 2014 Review she was reported to be alive and well [56]. Unfortunately her status as of July 2016 is unknown, as no peer-reviewed reports have been published about her case since the five-year follow-up in early 2014 [66].

In early April 2013, Macchiarini et. al. reported to *Science* that three children had received bioengineered tracheal transplants [57]. This count excludes fourth child, Patient 15, who had not yet received her transplant at the time of publication. Peer-reviewed reports could only be found for one, the first, of these children: Patient 2, an Irish boy born with long-segment tracheal stenosis. He received a decellularized transplant in March 2010 [56, 67, 68].

The second of these children was said to have died due to hemorrhage into her chest after receiving a decellularized transplant [57]. This could only correspond to the patient in the 2014 Review who received a transplant due to a tracheoesophageal fistula and died due to "fulminant GI bleeding" [56]. She is enumerated as Patient 3 in Table 1.

Another child was said to have died due to recurrence of a tumor [57]. The article does not specify whether she received a decellularized or synthetic transplant but cross-referencing this report with the 2014 Review [56] suggests that she was one of the three patients who received a decellularized transplant and died due to "systemic tumor recurrence." She is enumerated as Patient 4.

Decellularized tracheal transplants were ultimately performed by this group on nine patients between 2008 and 2011, including Patient 1 and the three children described above. Five of these patients were reported to be alive as of 2014 [51]. This cohort included three males and six females. The patients ranged in age from 11 to 72 years. At some time during this

process a change in the nature of the transplant was made. Jungebluth and Macchiarni indicate that the choice to switch to polymeric grafts as opposed to decellularized natural tracheal tissue was driven by concerns over the cost and availability of decellularized tissues of appropriate shape, size, and quality [56, 71], and an inability of the decellularized tissues to maintain their mechanical integrity when stored or after implantation [57].

### 2.3.3   Patient Narratives: Synthetic Grafts

Patient 10, a 36-year old man, became the first individual to receive a polymeric tracheal graft [69, 73]. Patients 11 and 14 followed soon afterwards. All three were treated at Karolinska University Hospital between 2011 and 2013. Several patients were also treated at Kuban State Medical University in Krasnodar, Russia, but very few details could be obtained on these patients.

Patient 10 was a graduate student at the University of Iceland at the time of his surgery [85]. He presented to Karolinska University Hospital with a recurrent primary tracheal mucoepidermoid carcinoma which had been unsuccessfully treated at another institution with tumor debulking and radiotherapy [69]. He was deemed eligible for a polymeric graft for two reasons: first, staging of his tumor [86] indicated that the tumor had not metastasized to distal sites [69]; and second, the shape and size of his tumor made resection impossible according to existing standards [87]. His graft was comprised of POSS-PCU (that is, polyhedral oligomeric silsesquioxane covalently bonded to poly[carbonate-urea] urethane) [69], seeded with bone marrow stem cells incubated in a bioreactor for 36 hours. He was also given granulocyte colony stimulating factor, filgrastim and epoetin beta following surgery. His surgery was performed in June 2011.

The Lancet case report published following his surgery is uniformly positive, stating the following:

> There were no major complications, and the patient was asymptomatic and
> tumour free 5 months after transplantation. The bioartificial nanocomposite has
> patent anastomoses, lined with a vascularised neomucosa, and was partly covered
> by nearly healthy epithelium. [69]

On further review this statement and others were found to be unsupported by clinical records. An investigation by the Karolinska University Hospital found several major inconsistencies in the 2011 Lancet report and other articles associated with this case [62]. These included clinical findings and assessments which could not be corroborated (or were contradicted) by existing patient records, a lack of institutional ethical approval, and an informed consent form dated over two weeks after the surgery [62]. Patient 10 was readmitted to the hospital 5.5 months following transplantation and several days before manuscript publication by *Lancet*. He would ultimately require multiple re-hospitalizations, and was admitted to Karolinska University Hospital for a final time in September 2013. Doctors performed 32 additional surgical interventions before his death in January 2014 [62]. For unknown reasons none of these clinical details were neither disclosed in the original 2011 article [69] nor the follow-up article which was published in April 2014 [71].

Patient 11 was a 30-year-old American from Baltimore, MD. Like Patient 10, he suffered from cancer which had infiltrated his trachea and received a synthetic tracheal transplant. Unlike Patient 10, his transplant was prepared from PET/PU (polyethylene terephthalate/polyurethane). His surgery was performed in November 2011 [56, 62, 70]. Very few details are known about his

case, as the patient returned to the U.S. from Sweden after his surgery and was apparently lost to follow-up until his death in March 2012 [57]. No autopsy was performed. The 2014 Review [56] states that he died at home "due to unrelated causes" however the sources of the information upon which this conclusion is based cannot be found. When asked about this case, Macchiarini speculated that the patient contracted pneumonia [57]. Others suggested that Patient 11 likely died due to post-surgical complications [57], and in fact claim that this information was relayed to the authors Jungebluth and Macchiarini before the 2014 Review was published [62]. The case generated no peer-reviewed case reports.

Patient 14 was a 21-year old University student in 2011 when her trachea was damaged during a surgical procedure in her home country, Turkey [80, 81]. As with many other patients described herein, the use of bioengineered tracheal transplants was justified under the so-called "compassionate use" concept (what Karolinska University Hospital calls a "vital indication" [88]). In such cases a patient's grave condition justifies emergency experimental treatment for humanitarian reasons [57]. The article which describes her case states the following as a reason for her transplant:

> A 21-year-old female patient suffered from an iatrogenic induced severe tracheal damage that affected the entire organ. An immediate transplantation was necessary to replace the entire trachea with a synthetic based TE tracheal graft [81].

However, reviewers of her clinical record discovered that she was in no immediate distress. She had been released from Istanbul Hospital in October 2011, and was offered a transplant in March 2012 -- a full four months before her surgery in August of that year [62]. At the time of her

surgery, she had been living at home and was stable. The original iatrogenic injury to her airway led to coughing fits every few hours, and a Heimlich drain had been placed to drain fluids from her right pleural cavity, but she managed her condition from home [62].

The peer-reviewed article describing her case states the following about the weeks and months after her transplant:

> The early clinical evaluation revealed an initial graft epithelialization as judged from the 1-week post-operative brushing. The intermediate post-operative outcome (5 months) has shown a patent and non-contaminated graft without any signs of inflammation. [81]

Here also the review of the patient's records could not confirm these statements. The reviewers could not locate clinical reports corresponding to a five-month post-operative time point. Bronchoscopies taken three months after surgery describe bacterial infection, and similar bronchoscopies 4.5 months after surgery describe granulations and stenting [62]. The patient was diagnosed with an iatrogenic tracheo-esophageal fistula 17 days after the first transplantation in August 2012. By the time the article was submitted on February 5, 2013 the patient had undergone 55 surgical interventions to mitigate complications following her transplant in August 2012, none of this information appearing in any publications [62].

As of August 2014, 139 surgical interventions had been performed on Patient 14. These include 72 total days of extracorporeal membranous oxygenation (ECMO), seven weeks of hemodialysis, 305 total days of ventilator dependency, and re-transplantation using a second polymeric graft in July 2013. Bronchoscopies were scheduled every fourth hours, every day, to

clear mucus from her airway [62]. By mid-2015, the cost of her continuing care was estimated to have reached 60 million SEK, or just under $7 million [80].

Public reports available in May 2015 indicated that her quality of life has been diminished substantially relative to the period after her injury but before her first transplant [80], and it remains unclear that her transplant could be justified under the principles of "compassionate use" (Karolinska's "vital indication" standard) [62, 88]. Nearly three years later, she remained hospitalized in the intensive care unit at Karolinska University Hospital, awaiting a third transplant which she hoped would provide a partial recovery and grant her the opportunity to leave the hospital [62, 80]. Her status as of July 2016 is unknown.

In both the cases of Patient 10 and 14, it appears that the complications associated with airway repair using polymeric artificial grafts were known within the first few months after surgery. Many of these complications and important surgical details (such as the use of an omental wrap) are not forthcoming in the case reports submitted to peer-reviewed journals. Nonetheless additional transplants were completed including a notable case in the United States: Patient 15 was a Korean-Canadian girl born with congenital tracheal agenesis in August 2010 [82]. She received a synthetic tracheal transplant in April 2013. She died three months after her surgery, on July 6, 2013, just before her third birthday. Her case was the subject of a NBC News documentary in the summer of 2014 [55], which was pulled by NBC following allegations of academic fraud and impropriety [89].

### 2.3.4   Post-transplant results

In late 2014, a complaint [62] filed by four colleagues of P. Macchiarini led to a formal investigation. The Karolinska Institutet turned over the complaint to Dr. Bengt Gerdin, a

professor of surgery at another university in Sweden. Dr. Gerdin completed his investigation in May 2015 and described "a systemic misrepresentation of the truth that leads the reader to have a completely false impression of the success of the technique" [59]. He judged Dr. Macchairini guilty of scientific misconduct.

By August 2015, the Karolinska Institutet had received the complaints by Corbascio et al. [62], reviewed the "Statement of opinion" from Dr. Gerdin regarding the complaints, and considered the non-public responses from Dr. Macchiarini -- and came to the opposite conclusion, declaring Dr. Macchiarini "not guilty" of scientific misconduct [90, 91].

In January 2016, the television network SVT aired a three-part documentary [58] about the surgeries, and the American publication *Vanity Fair* published an article [89] alleging academic fraud by Macchiarini (among other charges). The Karolinska Institutet reopened their investigation soon afterward [60, 88]. Multiple Karolinska officials involved in the initial investigation resigned from their posts in the wake of the renewed public focus on the surgeries, including Vice Chancellor Anders Hamsten, secretary-general of the Nobel Assembly Urban Lendahl, and Dean of Research Hans-Gustaf Ljunggren [88]. In April 2016, *The Lancet* published a "statement of concern" from the Royal Swedish Academy of Sciences regarding the paper which describes Patient 10 [74]. Four authors have asked to be disassociated from the article [92, 93].

In June 2016, Dr. Paolo Maccharini was charged with involuntary manslaughter in the deaths of two of the Karolinska patients [94].

The long-term consequences of the matter are unknowable. The European Union and the NIH continue to fund several tracheal repair projects and trials [95]. Despite global media attention, these cases remain generally unknown in the US. The worst-case scenario would likely

resemble the fallout following the death of Jesse Gelsinger, which had a chilling effect on gene therapy research in the US for a generation [96]. These cases and the subsequent manuscripts derived from them, similar to the so-called "STAP" papers of 2014 [97], demonstrate a weakness in our scientific method: while peer review can capture errors in logic and data interpretation, even the most experienced reviewers are incapable of detecting omitted or fabricated data. Thorough and complete documentation and reproducibility of results by multiple separate and independent research groups are therefore important in the continued development of bioengineered tracheal transplants.

## 2.4    CONCLUSIONS

Tracheal repair and bioengineering of tracheal transplants is a complex undertaking. It is not surprising that the preliminary attempts have been frustrated by complications. At this time it is not possible to perform a complete, accurate analysis of the existent clinical experience with bioengineered tracheal transplantations given the paucity of detailed publications of the known cases in refereed scientific journals. However, based on the information found in the public domain it is legitimate to conclude that the procedure remains associated with very high morbidity and mortality. It is also clear that the field of tracheal bioengineering is in an evolving state. Indeed the case has been made that it may be premature to implant tissue-engineered tracheas into people. Pierre Delaere and Dirk Van Raemdonck, of University Hospital Leuven (Belgium), have been strong critics of the field.  They came to the following conclusion in March 2016:

31

The engineered trachea was represented as a regenerated trachea after applying

bone marrow cells to a decellularized or synthetic scaffold. There is no scientific

foundation whatsoever to assume why stem cells would support airway tissue

regeneration in this setting. In addition, even if a trachea-like organ would be

generated, it would irrefutably fail after implantation if adequate blood supply had

not been restored. As expected, the implantation of decellularized and synthetic

scaffolds resulted in extremely high morbidity and mortality rates. At this point in

time, this form of airway regeneration should be regarded as hypothetical and

scientifically unfounded [98].

This view represents an extreme interpretation of the science. Nonetheless, it is prudent to

reassess the dominant paradigm within the field and given the difficulties encountered with

present techniques, further basic and translational research is appropriate. The current and

accepted view has been to provide super-physiologic growth stimulating agents/factors and

pluripotent and non-pluripotent cell types in huge numbers, the "more-is-better" idea, to enhance

the healing of engineered transplants, but to no avail. It is reasonable then to re-examine specific

molecular cues including matrix-cell (matricellular) interactions which inhibit the cellular re-

population and survival of tissue-engineered grafts. Such matricellular interactions may regulate

angiogenesis and vascularization, cell proliferation, cell survival, or cell turnover.

Leveraging the power of genetics, our group has developed and published a murine

model to assess decellularized tracheal grafts to test in mutant mice the role of key matricellular

signals in tracheal transplantation [1]. Further, I propose that a stress-induced matricellular

interaction between the secreted protein thrombospondin-1 (TSP1) and its cognate receptor

CD47 is maladaptively induced during transplantation and functions as a natural, but as of yet

unappreciated, barrier to the healing of engineered tracheal transplants. The deleterious effects of the TSP1-CD47 signaling axis on cell and tissue survival and angiogenesis under a wide range of stress including hypoxia, ischemia/reperfusion, transplant, burn, radiation and heart failure have been well characterized by our lab and others [99-112]. The next chapter will describe the murine tracheal transplant model. Successive chapters will summarize some of the research on TSP1-CD47 signaling in wound healing and regeneration, in order to provide a rationale for the work described in this dissertation. I will also describe our efforts to develop a novel floxed CD47 mouse line, for future studies examining the effects of this signaling pathway on specific cell populations within a given tissue.

# 3.0    DECELLULARIZED TRACHEAL EXTRACELLULAR MATRIX SUPPORTS EPITHELIAL MIGRATION, DIFFERENTIATION AND FUNCTION

(This chapter has been heavily adapted from our published work, cited here: [1].)

Tracheal defects or stenosis can result from congenital defects, trauma, or various pathologies such as cancer or infection. Partial tracheal loss in patients is debilitating and life-threatening [113]. In pediatric patients surgical approaches, including slide tracheoplasty, have been employed with some success [114]. In adults trachea mobilization has enabled post-resection repair in select cases. Long-term stenting, dilation, and tracheostomy have also been employed as palliative care. However, regardless of the approach complication rates remain very high and long term morbidity is common [115, 116]. Also, there remains a cohort of patients for which none of the standard approaches can be employed. Therefore, a functional tracheal replacement graft is still desirable.

Initially, engineered tracheal grafts consisted of purified collagen sponges around a stent or synthetic scaffold [20, 117]. Although widely studied in pre-clinical models, these have had multiple deficiencies. Failure of the first engineered tracheas resulted from several causes including infection, stenosis, and complete tissue disintegration [115]. Current engineered tracheal grafts and patches are considerably more complex and employ both multiple graft modifications and recipient treatments. Common to many is a foundation built upon a decellularized tracheal allograft [64, 118]  or a synthetic polymer/nanofiber scaffold [119]  In at

least one case, an aortic allograft was employed as the tubular scaffold [120] to provide similar structural support. These scaffolds are then seeded with various cell types in order to provide functionality, as the size of these grafts limits the degree to which cellular invasion can occur. A number of cell populations have been suggested for reseeding, including basal cells of the lower trachea and induced pluripotent stem cells [33]. Scaffolds used in clinical case reports have typically been reseeded with autologous airway cells isolated via bronchoscopic biopsy and/or chondrocytes differentiated from bone marrow mesenchymal stem cells [49, 50, 64, 84, 118]. Finally pedicle soft tissue flaps from the abdomen or chest are then wrapped around the engineered tracheal transplant to promote angiogenesis, and to sequester the transplant from the mediastinum [117]. Recipients may in some cases be treated pre- and post-transplant with growth factors in order to maintain the cell population. Current strategies have shown modest success based upon mortality rates, arguably more so with the decellularized allografts than with the synthetic scaffolds.

Despite the publication of clinical reports of transplantation of bioengineered tracheas [64, 65, 121-125], the molecular and cellular processes controlling the survival of the tracheal grafts remain incompletely defined. We tested the hypothesis that decellularized tracheal scaffolds allow cellular invasion/repopulation and functional epithelialization following orthotopic transplantation. Employing a murine tracheal transplant model, we report evidence that decellularized tracheal scaffolds allow rapid functional cellular restoration and provide a rationale for continued development of this technology.

# 3.1    MATERIALS AND METHODS

## 3.1.1   Animals

All animal experiments were reviewed and approved by the University of Pittsburgh Institutional Animal Care and Use Committee and were performed in compliance with the Guide for the Care and Use of Laboratory Animals as published by the NIH [126]. Age-matched female C57BL6 mice (approximately 12 weeks old and 20 g in weight) were used in the study, half as donors and half as recipients.  Donor tracheas were either immediately transplanted into a recipient or were decellularized (with and without vacuum-assistance) and sterilized for subsequent implantation as a tracheal graft.  In the first cohort, mice receiving fresh (n=7) or non-vacuum decellularized (n=17) tracheal grafts were weighed at regular intervals over four weeks to assess failure to thrive in animals during the post-operative period.  Surgeries were performed in groups of two or three animals over several sessions. At the end of the study period, specimens were harvested for histological analysis and high-quality slides were selected for quantification. Tracheas in the second cohort were decellularized with vacuum assistance before transplantation, and surviving mice were sacrificed after one or eight weeks. Histologic examination was performed on at least four tracheas in each treatment group at both the one- and eight-week time points. At eight weeks, three additional specimens underwent fresh video microscopy to examine ciliary beat frequency. In three other tracheas microcomputed tomography (microCT) analysis was performed.

### 3.1.2 Tracheal Harvest

Donor animals were anesthetized with an intraperitoneal injection of ketamine (80 mg/kg) and xylazine (8 mg/kg), and euthanized by exsanguination. The trachea was exposed through a midline neck incision with extension through the proximal sternum. The trachea was harvested from the carina to proximal to the larynx. The larynx was included to facilitate determination of proximal to distal orientation of the tracheal graft, which was important for the fresh transplants. All tracheas were immediately placed in chilled saline and stored on ice. The fresh transplants were prepared for implantation within 15 minutes of harvest.

### 3.1.3 Decellularization

Tracheas were trimmed of excess tissue under a dissecting microscope (Zeiss StemiDV4) and were then frozen at -80°C until time for further processing in preparation for surgery. The tracheas were thawed in deionized water at room temperature. Tracheas were then decellularized with fourteen 90-minute cycles each consisting of deionized water, 3% Triton X-100, and 3M NaCl treatments, leaving a decellularized tracheal scaffold. Tracheas in late cohorts were subjected to cyclical pressure changes between room atmosphere and 94% vacuum (6.325 KPa absolute pressure) during these washes in a custom apparatus. Vacuum initially degasses the scaffold, removing any microbubbles that might serve as a barrier to interactions between cells and the decellularization reagents. The cyclical pressure changes are hypothesized to provide superior infiltration of detergents and removal of cellular debris. Following decellularization scaffolds were disinfected through agitation on a shaker in a 0.1% peracetic acid (PAA)/ 4% ethanol solution for 90 minutes at room temperature followed by three 30 minute rinses in

phosphate buffered saline (PBS). Scaffolds were then individually packaged in physiologic saline, and terminally sterilized by exposure to 20 kGy gamma irradiation.

### 3.1.4 Orthotopic Tracheal Transplantation

Recipient animals were anesthetized with an intraperitoneal injection of ketamine (80 mg/kg) and xylazine (8 mg/kg). Animals were placed in a supine position and maintained on a heating pad throughout the surgery. The tracheal reconstruction was performed with microscopic assistance as described previously [127-130]. The ventral cervical trachea was exposed through a midline incision. The graft was then prepared by removing any loose connective tissue from the surface and liquid from the lumen, and was cut to a length of five cartilaginous rings from the proximal end of the graft. Care was taken to maintain the proximal-distal orientation of the grafts, particularly for the fresh transplants. A segment of three recipient tracheal rings was dissected from the surrounding connective tissue circumferentially starting approximately four rings below the larynx, with care not to damage the recurrent laryngeal nerves. Once the tracheal segment was freed, a transverse cut was made in the intracartilaginous tissue until a complete transection was performed. A second transection was performed to remove two complete rings of the trachea. Meticulous hemostasis was performed through the process. The distal anastomosis was performed first followed by the proximal anastomosis. In both cases, the anastomosis was performed with two interrupted 10-0 Prolene sutures placed near the dorsal ends of the cartilage rings and one or two sutures placed on the ventral aspect of the tracheal repair. The strap muscles were approximated, and the skin incision was then closed with interrupted 7-0 PDS sutures. Animals were kept under a warming light and monitored until fully recovered from anesthesia. The operative time averaged 20 minutes.

### 3.1.5   Post-operative care

After surgery, mice were housed in groups of four to five in standard cages, and food and water was supplied ad libitum. The following medications were administered as subcutaneous injections for five days following surgery: buprenorphine (0.1 mg/kg) twice daily for pain relief, gentamicin (8 mg/kg) once daily for infection prophylaxis. At one, four, and eight weeks following surgery animals were humanely euthanized with intraperitoneal injections of ketamine/xylazine followed by immediate exsanguination, and the tracheas were harvested for analysis. For ciliary beat frequency evaluation, animals were euthanized by exposure to carbon dioxide and cervical dislocation.

### 3.1.6   Histology

Hematoxylin and eosin staining was performed on decellularized grafts before implantation using standard techniques. Briefly, deparaffinization of tissue sections was performed with two changes of xylene for three minutes each followed by rehydration in an ethanol series.  Sections were exposed to hemotoxylin for two minutes, rinsed with water, exposed to eosin, and rinsed with water a second time. Finally, slides were dehydrated with an ethanol series, exposed to xylene, and sealed with a cover slip.  Explants selected for immunofluorescence were embedded in wax and likewise deparaffinized in two xylene washes, followed by rehydration in an ethanol series. Antigen retrieval was performed using 10 mM citrate buffer in double distilled water. 5% bovine serum albumin in PBS was used as a blocking reagent.  For the keratin-5 (K5)/keratin-14 (K14) dual stains, the following primary antibodies were applied: mouse anti-K14 (1:500 in blocking reagent) (Thermo/Neomarkers MS-115-P0) and rabbit anti-K5 (1:1000) (Covance

PRB-160P). The following secondary antibodies were employed: AlexaFluor 488-conjugated goat anti-mouse IgG$_3$ (1:500) (Invitrogen A21151), AlexaFluor 594-conjugated donkey anti-rabbit (1:500) (Invitrogen A21207). For acetylated tubulin (ACT)/club cell secretory protein (CCSP) dual stains, the following antibodies were applied: mouse anti-ACT IgG$_{2b}$ (diluted 1:20000) (Sigma T6793) and goat anti-CCSP (1:1000) (kindly provided by Dr. Peter Di, University of Pittsburgh). These were detected with: donkey anti-mouse IgG (H+L) 594 (1:500) (Jackson Immuno 715-485-150), and donkey anti-goat IgG (H+L) 488 (1:500) (Jackson Immuno 715-515-150). All slides were counterstained with VectaShield Mounting Medium with DAPI (Vector Laboratories H-1200). Completed slides were examined with an Olympus IX71 florescence microscope (Nikon) and the images were captured with Nikon cellSens Dimension (version 1.5). A single section from each explant was selected for imaging and quantification. Sections were selected for quality based on the orientation of the cutting plane and the integrity of the epithelium. Multiple overlapping images were taken of each explant and Adobe Photoshop CS5 was used to prepare a photomosaic of all the images from a given slide which allowed visualization of the entire trachea. Multiple measurements were taken from each photomosaic for quantification.

### 3.1.7   Quantification

ImageJ (NIH, Bethesda, MD) was used to measure the length of several basement membrane segments along each explanted tracheal lumen. For each measured segment, DAPI-stained and antibody-immunolabeled cells along the segment were hand-counted in order to determine cell densities (cells/µm). Mean cell densities were calculated for each explanted trachea at each time point.

40

### 3.1.8 Ciliary beat frequency evaluation

Three tracheas from each treatment group were harvested eight weeks after surgery. Strips of tracheal tissue were secured luminal side down on a 35-mm glass-bottomed culture dish (Willco Wells, Amsterdam, The Netherlands) using a glass coverslip covered with a silicone sheet (0.5mm thick, AAA Acme Rubber Co.) from which a small window had been cut to form a shallow chamber. Cilia dynamics were captured at room temperature with a ×100 differential interference contrast (DIC) oil objective and a Leica inverted microscope (Leica DMIRE2). Movies were captured at 200 frames/s (fps) with a Phantom v4.2 camera (Vision Research). To quantify ciliary beat frequency (CBF), ImageJ was used to examine cyclic variations in pixel intensities corresponding to the ciliary stroke. More than three randomly selected areas were imaged from each trachea in order to calculate mean native and graft CBF for each treatment group.

### 3.1.9 Ciliary beat axis evaluation

To quantify variance in ciliary beat axis (CBA), an average of 35 cells were selected in each available *en face* video. ImageJ was used to determine a beat axis for each selected cell, with zero degrees representing an axis parallel to the left-right axis of the frame, and 90 degrees representing the perpendicular axis. The mean beat axis (between zero and 90 degrees) was determined for each video. The degree to which each cell's beat axis deviated from the video mean was calculated. These deviations were pooled for each animal, and plotted as a histogram.

### 3.1.10 Micro computed tomography

Three-dimensional image acquisition of explanted tracheas was carried out using a high resolution micro-CT (Siemens, Inveon Multimodality, Munich, Germany) at 12 μm image resolution at 80 kVe and 500 μm X-ray. 3D surface volume renderings were reconstructed using OsiriX software.

### 3.1.11 Statistics

Statistical analysis was performed using GraphPad Prism 6 (GraphPad, La Jolla, CA). Data are presented as mean ± one standard deviation (SD) for each group. For weight change and survival analysis, Student's t-tests and log-rank (Mantel-Cox) tests were performed, respectively. Differences in cell counts and ciliary beat frequencies between untreated controls, fresh transplants, and decellularized transplants were assessed with two-way analysis of variance (ANOVA) with Tukey's multiple comparisons test. For ciliary beat axis, differences in the variance of each distribution were quantified by F-test. Statistical significance was defined as $p < 0.05$.

## 3.2    RESULTS

### 3.2.1    Orthotopic tracheal transplantation and decellularized tracheal reconstruction rescues mice following tracheal loss.

Tracheal loss is often fatal, whereas lack of robustly phenotyped pre-clinical models has hindered tracheal replacement development  [18]. We tested the hypothesis that orthotopic decellularized tracheal transplant alone would rescue mice following full thickness tracheal loss. We performed orthotopic transplantation using fresh or decellularized grafts in age matched female mice as described (Figure 2a). A summary of the harvested tracheas and analyses performed on them is provided in Table 1.  Representative images show excellent healing of the fresh tracheal transplant rescuing mice from full thickness tracheal loss (Figure 2b, c). Although mortality rates were initially higher for animals receiving the decellularized grafts, particularly in the model development phase, they approached those for fresh transplants as experience with the model increased. Mortality typically occurred within the first week post-transplant, and was generally associated with obstruction secondary to damage to the recurrent laryngeal nerves, stenosis, or mucous build-up in the tracheal lumen. Mean weight gain was determined as a physiologic relevant marker of overall health. Importantly, surviving animals receiving fresh transplants were found to have a $15.1 \pm 3.4\%$ increase in weight over the 28-day period following surgery (Figure 2c). In contrast to animals receiving fresh transplants, surviving animals receiving decellularized grafts experienced an approximate 11% decrease in weight ($89.2 \pm 16.0\%$ of pre-operative weight) during the post-operative interval.
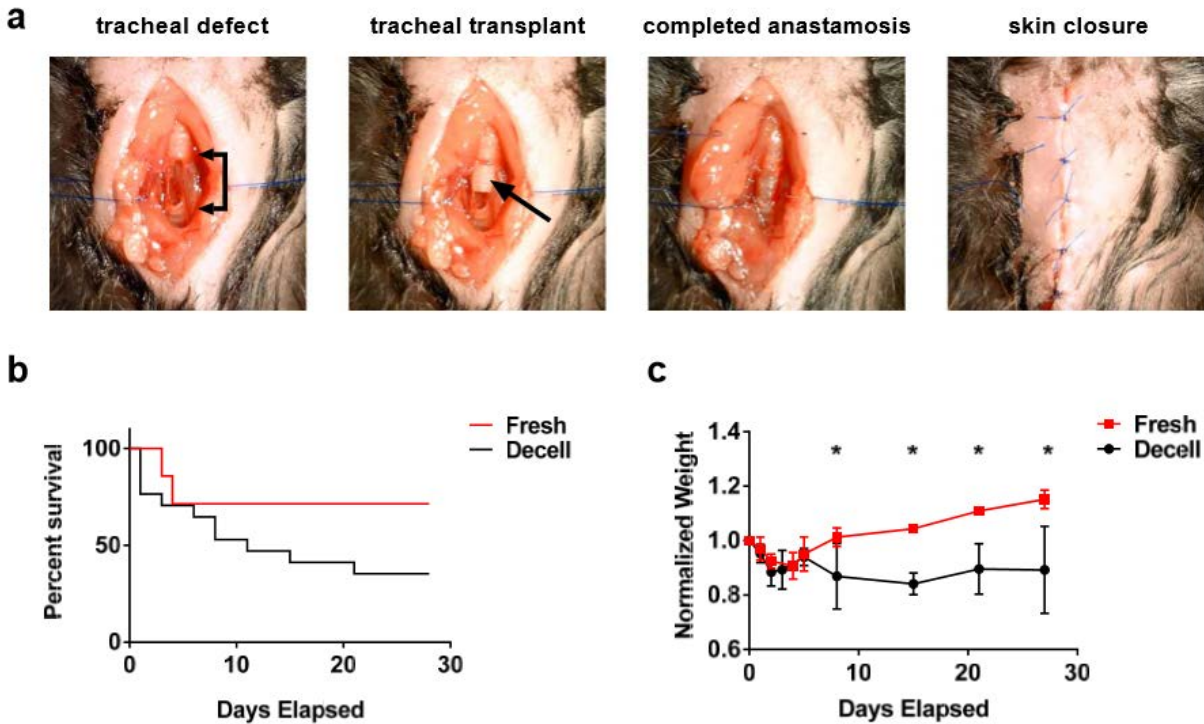
**Figure 2. Orthotopic transplantation of fresh tracheal grafts is associated with superior recovery post-operatively.** Orthotopic transplants of fresh and decellularized tracheal grafts were performed on wild-type female C57BL6 mice. (a) Still frames from video recording of tracheal transplant performed in a wild-type mouse. Arrows denote the site of the tracheal defect (in the first panel) and the transplanted graft (in the second). (b) Survival (fresh: n = 7, decellularized: n = 17, p = 0.165) and (c) weight gain (n > 3 at each time point, p < 0.001 at time points denoted with asterisks) over four weeks following surgery shown, for early model development studies.

### 3.2.2 Vacuum assisted tracheal decellularization effectively eliminates cells

We subjected fresh murine tracheas to a range of decellularization cycles (as detailed in the methods) during the model development phase. Interestingly tracheas treated with fewer cycles displayed the same degree of decellularization as tracheas treated with higher number of cycles. Hematoxylin and eosin stains demonstrated total removal of the epithelial layer and no nuclei in

44

the intercartilagenous segments of the tracheal wall, though some nuclear material was maintained within chondrocyte lacunae of the cartilaginous rings themselves (Figure 3).
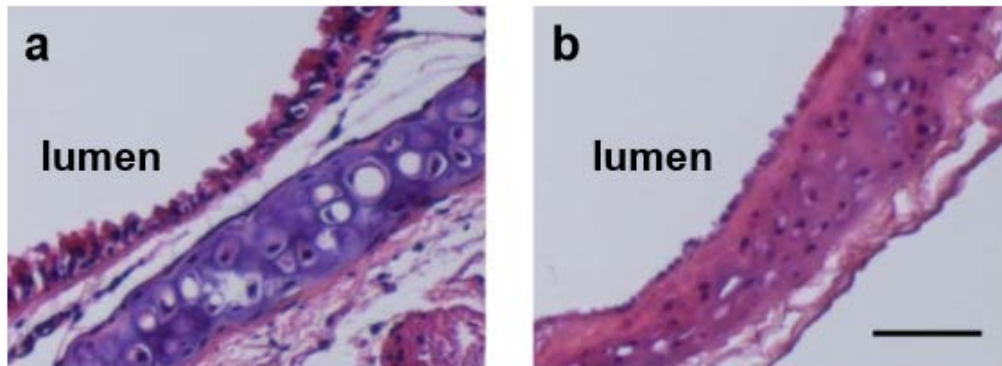


**Figure 3.   Decellularization effectively removes cells from explanted tracheal tissue.**   Representative hematoxylin and eosin stains from native (a) and decellularized (b) tracheas following 14 cycles of detergent osmotic-shock treatment with cyclic pressure changes, as described in this study. Magnification = 20X.  Scale bar = 50 μm.

### 3.2.3   Decellularized tracheal scaffolds display epithelial restoration following orthotopic transplantation

Our finding that decellularized tracheal scaffolds rescued mice from full thickness tracheal defects suggested that the decellularized scaffolds facilitated reconstitution of the cellular population. Immunofluorescent labeling of fresh and decellularized grafts post-transplantation showed complete resurfacing of the internal surface of decellularized grafts by one week post-

operatively (Figure 4, Figure 5). Time course quantification of cell specific repopulation of the tracheal scaffold was performed. Within the first week following surgery, we observed rapid repopulation of the luminal surface with a large number of dual-expressing keratin-5/keratin-14 (K5+/K14+) cells (Figure 4d, h, i). There was no evidence of secretory cells or ciliated cells by one week (Figure 5). Over successive time-points the population of K5+/K14+ cells declined while the proportion of K5+/K14- and ACT+ cells increased (Figure 4n, o; Figure 5n).

This same pattern was observed at the anastomotic site in animals receiving the fresh tracheal transplant (Figure 4a, e, i). The middle of the fresh transplants showed increased numbers of K5+/K14- and ACT+ cells compared with the repopulated decellularized graft. At eight weeks post-transplant the repopulated decellularized grafts contained equivalent numbers of K5+/K14+, and K5+/K14+ cells compared to fresh orthotopic tracheal transplants (Figure 4n, o). Total numbers of secretory cells per micrometer though initially not significantly different from numbers in fresh transplants were decreased in decellularized grafts after eight weeks (Fig. Figure 5o). The cartilaginous rings of the decellularized tracheal grafts did not repopulate with chondrocytes over the course of the study period (Figure 4, Figure 5, rightmost columns).
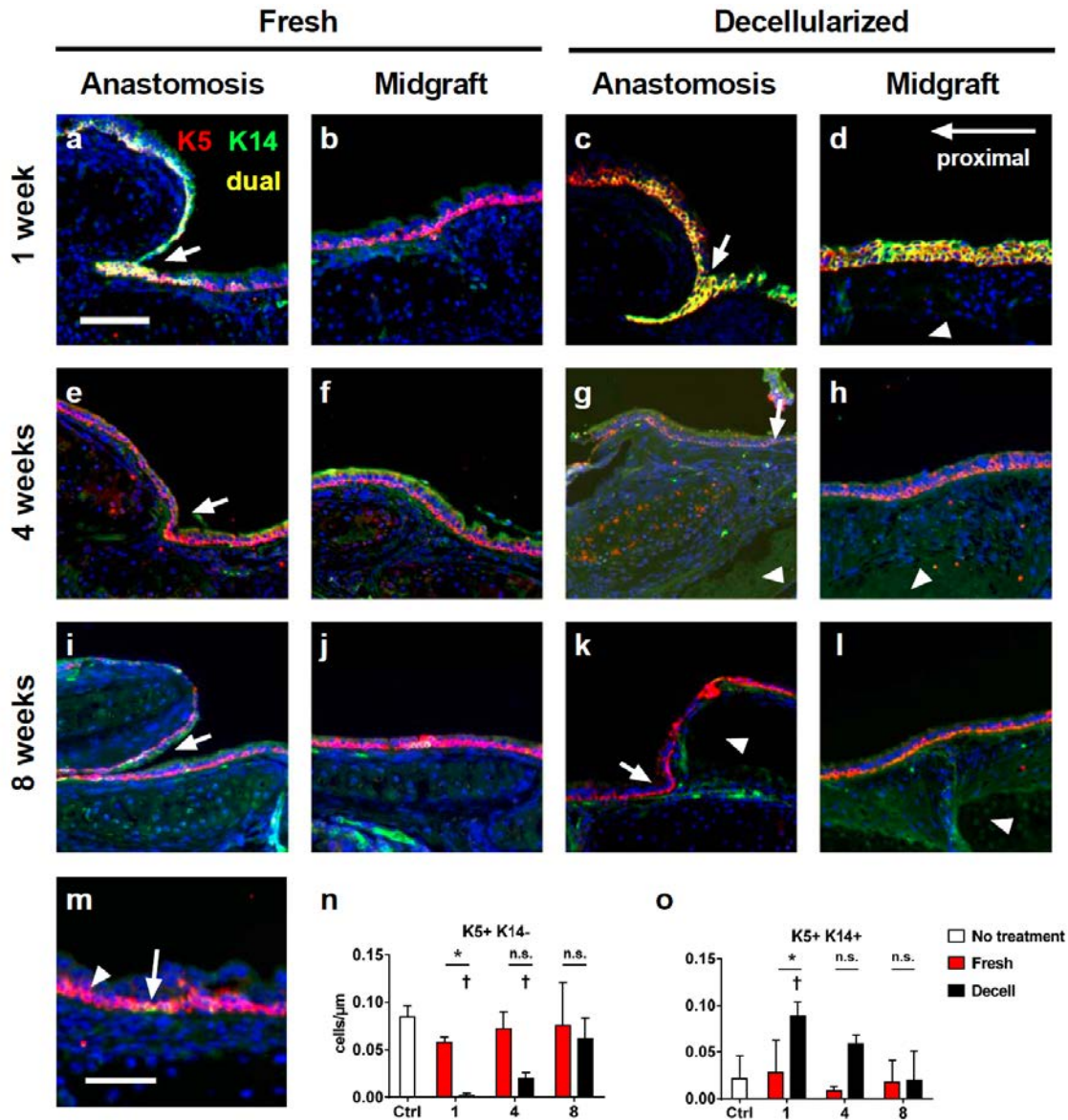
**Figure 4. Histologic quantification of basal cell protein expression in mouse trachea transplants.** (a-l) Mice receiving fresh (a, b, e, f, i, j) or decellularized (c, d, g, h, k, l) transplants were sacrificed one (a-d), four (e-i), or eight (i-l) weeks following surgery. Immunofluorescent labeling for basal cell markers keratin-5 (K5, red) and keratin-14 (K14, green) was performed, followed by DAPI-staining (blue). Dual-expressing (K5+/K14+) cells are indicated in yellow. Images are shown at a site of anastomosis (a, e, i, c, g, k) or at a mid-graft region (b, f, j, d, h l). Arrows denote interface between graft and native tissue; arrowheads denote decellularized graft rings (where visible). Scale bar in panel (a) = 100 μm. (m) Higher resolution image demonstrates prototypical K5+/K14-(arrowhead) and K5+/K14+ dual-expressing (arrow) cells. Scale bar = 50 μm. (n, o) Single-positive K5+/K14- (n) and dual-expressing K5+/K14+ (o) cells along the basement membrane were counted in order to determine cell densities (cells/μm). Columns labeled "Ctrl" denote cell densities for untreated, native trachea from C57BL6 mice. Columns with error bars represent mean ± one standard deviation with n ≥ 3 mice in each group. Pairs of columns denoted with an asterisk (*) indicate statistically significant differences (p < 0.05). Columns denoted with a dagger (†) are statistically different relative to the untreated control. Multiple photomicrographs were captured, merged, and adjusted for ease of counting. Magnification = 10X. Orientation mark given in (d) applies to all images.
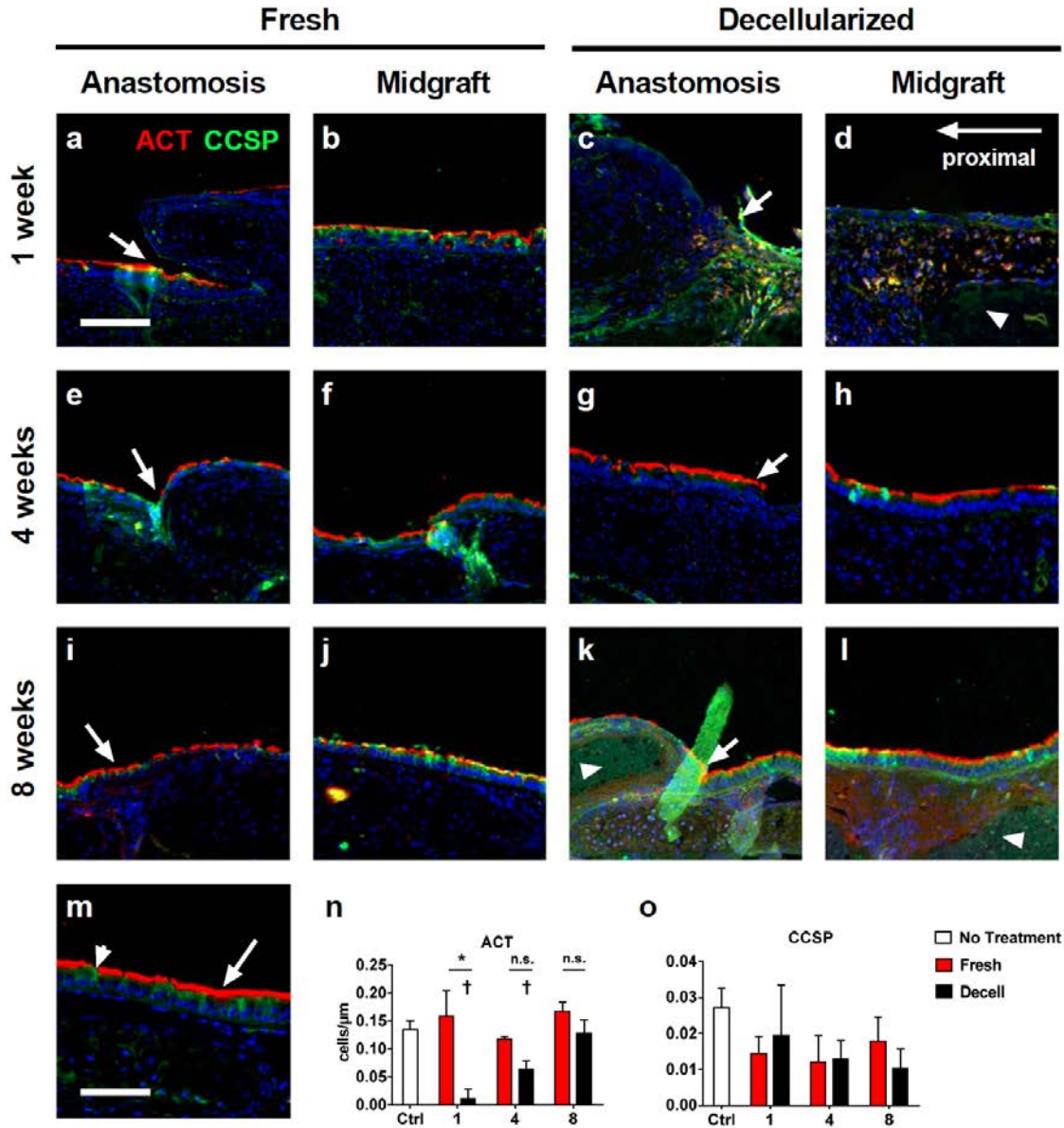
**Figure 5. Histologic quantification of ciliated and secretory cell maturation in mouse trachea transplants.** (a-l) Mice receiving fresh (a, b, e, f, i, j) or decellularized (c, d, g, h, k, l) transplants were sacrificed one (a-d), four (e-i), or eight (i-l) weeks following surgery and immunofluorescent labeling for mature epithelial cell markers acetylated tubulin (ACT, red) and club cell secretory protein (CCSP, green) was performed, followed by DAPI-staining (blue). Images are shown at a site of anastomosis (a, e, i, c, g, k) or at a mid-graft location (b, f, j, d, h l). Arrows denote interface between graft and native tissue; arrows denote decellularized graft rings (where visible). Scale bar in panel (a) = 100 μm. Orientation mark given in panel (d) applies to all images. (m) Higher resolution image demonstrates prototypical ACT+ (arrowhead) and CCSP+ (arrow) cells. Scale bar = 50 μm. (n, o) Cells expressing acetylated tubulin (n) and club cell secretory protein (o) along the basement membrane were counted in order to determine cell densities (cells/μm). Columns labeled "Ctrl" denote cell densities for untreated, native trachea from C57BL6 mice. Columns with error bars represent mean ± one standard deviation with n ≥ 3 mice in each group. Pairs of columns denoted with an asterisk (*) indicate statistically significant differences ($p < 0.05$). Columns denoted with a dagger (†) are statistically different relative to the untreated control. Multiple photomicrographs were captured, merged, and adjusted for ease of counting. Magnification = 10X.

### 3.2.4 Cilia function is diminished in decellularized tracheal transplants

An important feature of the healthy trachea is the ability to handle secretory load and a robust coordinate ciliated cell response is a requirement for engineered tracheal transplants. We used state-of-the-art real-time microscopic imaging to assess cilia function in our decellularized and fresh tracheal transplants and calculate ciliary beat frequency (CBF). We observed the presence of functional cilia in both decellularized and fresh orthotopic tracheal grafts. In both fresh and decellularized transplant groups, CBF for cells along the graft was not significantly different from adjacent native tissue. However, ciliary beat frequency in both fresh and decellularized grafts was significantly lower than that of native, untreated trachea (Figure 6b).

We observed that the ciliary movement in repopulated decellularized transplants appeared less uniformly-oriented than in the native tissue. A mean beat axis was calculated for each *en face* video, and an analysis of the deviations from the mean was performed for each of three animals. We observed significantly greater variability in the decellularized graft's repopulated epithelium compared to the adjacent native tissue (Figure 6c).
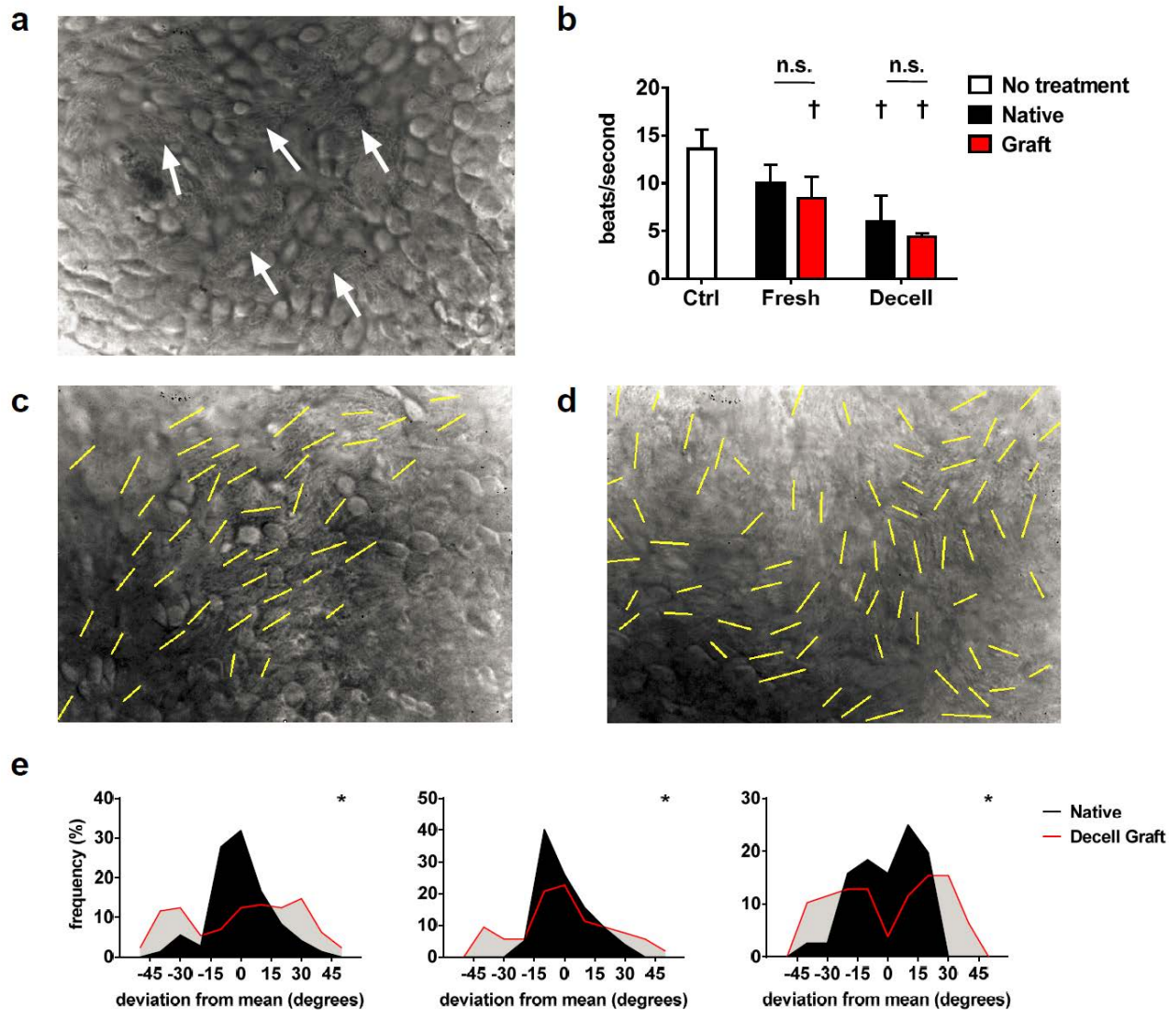
**Figure 6. Ciliated cell function of orthotopic fresh and decellularized tracheal transplants.** Real time video microscopy was employed to quantify ciliary activity eight weeks after transplantation. (a) A contrast-adjusted still frame depicting beating cilia within a decellularized graft is shown; arrowheads denote ciliated cells. (b) Calculated ciliary beat frequencies are shown, with n = 3 mice in each group. Column labeled "Ctrl" denotes ciliary beat frequency for untreated, native trachea from C57BL6 mice, based on historical data (n = 41). Columns denoted with a typographical dagger (†) indicate statistically significant differences (p < 0.05) relative to the control column. (c, d) ImageJ was used to examine variability in ciliary beat axis within the epithelium of repopulated decellularized grafts. Shown are contrast-adjusted still frames of decellularized (d) and adjacent native (c) tissue. (e) Distributions of ciliary beat axis (relative to mean beat axis) in three mice receiving decellularized grafts. (*) indicates a statistically significant difference between the native and graft variances, (p < 0.0001).

### 3.2.5 Tracheal patency is maintained in orthotopic tracheal transplants.

The current generation of engineered tracheal transplants has been complicated by loss of structural integrity and an inability to maintain tracheal diameter [114]. We assessed tracheal morphology using micro-computed tomography (Figure 7). Cartilaginous rings were visible as radiopaque structures in fresh transplants (Figure 7b), as they were in wild-type untreated controls (Figure 7a), but could not be visualized in decellularized transplants (Figure 7c). Both the fresh and decellularized transplants experienced a moderate degree of concentric narrowing at eight weeks post-surgery. The time course of this narrowing was not immediately clear.

**Native**

**Fresh**

**Decell**
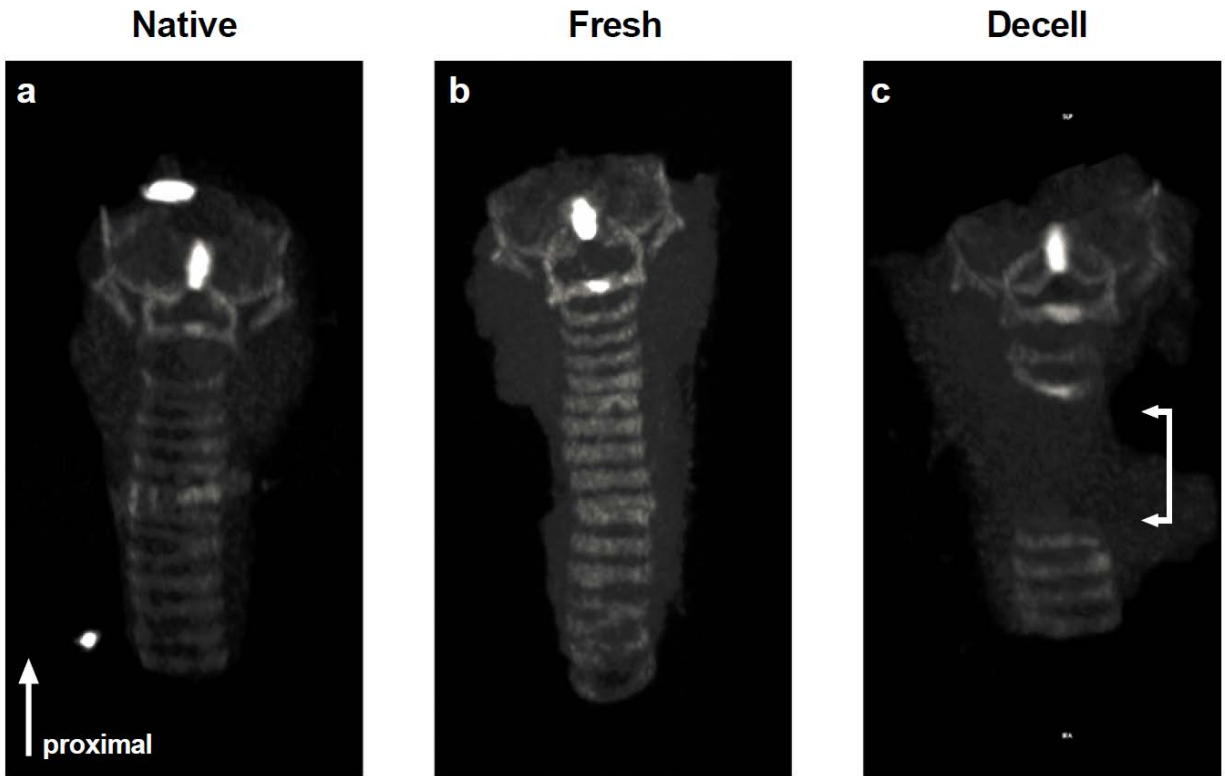
**Figure 7. Micro-computed tomography analysis of fresh orthotopic tracheal transplants.** Representative images shown from computed tomography performed on explanted trachea from wild type, untreated C57BL6 mice (a), mice receiving fresh transplants (b), and mice receiving decellularized transplant (c). Orientation in (a) applies to all images. Arrows in (c) denote the boundaries of the decellularized graft.

## 3.3    DISCUSSION

The present study showed quantification and functional assessment of the first ever murine model of orthotopic decellularized tracheal transplant. Although more technically challenging than established the heterotopic transplantation models, the orthotopic model carries a reduced risk of luminal obliteration [127]. Further, orthotopic transplantation provides the opportunity to observe physiologic healing via epithelial migration and proliferation from native tissue adjacent

to the anastomosis site. Most important, it mimics the clinical situation and demands functional responses from the transplant if the animal is to both survive and thrive.

A wide variety of techniques have been proposed to decellularize tissues and organs, including chemical, enzymatic, and mechanical [49, 131]. In this study, decellularized trachea processed with Triton X-100, 3M NaCl, deionized water, and 0.1% peracetic acid supported rapid cellularization with epithelial cells on the lumen of the graft and mesenchymal cells within the parenchyma of the scaffold. By eight weeks, the lumen was covered with a site-appropriate pseudostratified epithelium with ciliated cells and secretory cells present. By eight weeks, the epithelium showed motile cilia, although the ciliary beat frequency was less than a native mouse trachea, and showed variations in the orientation of ciliary movement as compared to the normal synchronized beating found in the native trachea. Analysis of longer time points will determine if ciliary function normalizes in transplanted grafts.

The trachea is potentially an ideal candidate for repair using a decellularized graft. A mature epithelium in particular is a necessary component of any tracheal graft, in order to (1) act as a barrier defense and (2) to provide mucociliary clearance. It has been reported that a confluent epithelial layer can reduce or even prevent fibrosis and subsequent stenosis of a tracheal graft [20, 117]. To promote the development of an epithelial layer, decellularized tracheas are frequently seeded with epithelial cells, and cartilaginous rings are repopulated with chondrocytes derived from bone marrow stem cells. Such grafts have been shown to maintain some cell population during the recovery period [84, 118, 132]. Further, decellularized matrix derived from porcine tracheal tissue promotes re-epithelialization in a canine model of patch tracheoplasty [133, 134]. Porcine decellularized tracheal tissue grafted into pigs and mice in heterotopic models showed no immune rejection [135]. These findings suggest that the

53

decellularized matrix provides an appropriate substrate for epithelial migration, differentiation, and function.

The native tracheal epithelium is complex and is composed of heterogeneous cell populations, some of which act as progenitor cells [30, 136, 137]. Although multiple studies have included histologic evaluation of tracheal allografts following transplantation, none have examined invasion, proliferation and regression of various populations of basal cells over time. Herein, we examined the kinetics of epithelial healing and quantified the spatiotemporal rate of epithelial repopulation via immunofluorescent labeling. We observed complete resurfacing of the decellularized tracheal lumen by the end of the first week post-transplant, following early proliferation of K5+/K14+ basal cells. Previous studies have demonstrated that K5+/K14+ basal cells represent a precursor cell population with the capacity to develop into ciliated (ACT+) and secretory (CCSP+) cells [24, 136]. This finding is supported by our histological data, which shows a correlation between the depletion of the K5+/K14+ cell population and the generation of a mature differentiated epithelium (Figure 4, Figure 5). Similarly, in animals receiving fresh transplants, the presence of K5+/K14+ cells near sites of anastomosis suggests that this cell population plays a role in epithelial healing (Figure 4a).

Histologically, we observed that cartilaginous portions of the decellularized trachea remain acellular throughout the course of the 8 week healing period, while chondrocytes within the fresh tracheal transplants appear to be maintained. Computed tomography (Figure 7) did not demonstrate radiopaque cartilaginous rings within decellularized grafts after eight weeks, in contrast to fresh transplants. Scans performed on decellularized grafts before transplantation similarly demonstrated a lack of visible radiopaque cartilage (data not shown). These findings suggest that cartilaginous rings lose their molecular structure during the process of

decellularization, and are not repopulated after transplantation. Despite the presumptive loss of mechanical structure associated with the degradation of the cartilaginous rings, decellularized tracheal grafts maintained their patency over eight weeks. Additional studies will assess chondrocyte viability and repopulation in orthotopic transplants.

The present study had a several limitations. First, the murine orthotopic tracheal transplant is technically challenging, and these challenges contributed to the decreased post-operative survival observed in the early model development studies. The technical challenges involved in the surgery were mitigated with experience, as demonstrated by the improved survival seen in later cohorts. Second, histologic analysis was limited by the selection of time-points. Rapid re-population of the luminal surface of each tracheal graft prevented observation of basal cell behavior within the first week, during the period of initial proliferation. This will be addressed by the addition of early time points in future studies. Third, the diameter and cross sectional area of the decellularized tracheal grafts could not be assessed via computed tomography, as originally predicted. We hypothesize that exposure to peracetic acid and/or gamma irradiation during the decellularization process disrupts the molecular structure of the cartilaginous rings, making it difficult to identify the lumen of each graft via microCT. Given that the cartilaginous rings maintain the structural integrity of the trachea and patency is an absolute requirement for a tracheal graft, the functional consequences of this loss of cartilage must be further investigated. Further, we observed moderate narrowing of the decellularized tracheal explants which could be secondary to this loss of cartilage.

## 3.4    CONCLUSIONS

These data demonstrate the potential for an orthotopic murine tracheal transplant model to be performed for the evaluation of decellularized grafts. The data presented suggest this model is a reliable pre-clinical platform for research. The use of mice will allow for the procedure to be economic and efficient. This model will also allow for harnessing the power of mutant murine models to test the role of specific genes (in knock out or over-expressing strains) in the process of matrix restoration and tracheal transplant healing. The role of innate and acquired immunity in the setting of tracheal transplantation may also be investigated by applying this technique to several well characterized murine systems of immunologic activation.

## 4.0 THROMBOSPONDIN-1 (TSP1) AND CD47 IN HEALTH AND DISEASE

The thrombospondin-1 (TSP1)-CD47 signaling axis represents a key cell-matrix interaction which may regulate repopulation of decellularized grafts through its effects on cell survival, self-renewal, and angiogenesis. TSP1 is a secreted protein upregulated after injury and in response to hypoxia and tissue stress. Prior research has demonstrated that TSP1 binding to and activation of receptor CD47 hinders the survival of cells and whole tissues under stress [138].

The role of TSP1-CD47 signaling in direct regulation of the airway epithelium is unclear. Literature reports indicate that TSP1 is highly expressed by humans airway basal cells in *in vitro* culture conditions [21]. At least one study also demonstrates that TSP1 null mice have greater club cell repopulation after naphthalene injury [139]. These findings support the role of matricellular proteins in regulating cell behavior, and highlight the potential role matricellular proteins may play in decellularized grafts. **This informs my hypothesis that TSP1, via interactions through cell-surface receptor CD47, inhibits cellular survival, engraftment, and revascularization of decellularized tracheal grafts.**

The following sections will provide some background on TSP1 and CD47, will describe the TSP1 null and CD47 null phenotypes, and will give some details on TSP1-CD47 signaling in health and disease. Finally, this chapter will describe our efforts to develop a floxed CD47 mouse line for future studies examining the role of CD47 signaling in specific cell populations within tissues.

## 4.1 THROMBOSPONDIN-1 (TSP1)

The thrombospondins are founding members of a class of molecules known as matricellular proteins [140]. These molecules reside in the extracellular matrix, but provide no structural support. Thrombospondin-1 (TSP1) in particular is a 420 kDa protein which is assembled from three identical polypetides. Each polypetide is 1152 amino acids in length, which is cleaved from an 1170 amino acid precursor. The three peptides are joined via disulfide linkages near their N-terminal end.

The structure of TSP1 is highly conserved in the mammalian genome, with 95% homology between mouse and man in terms of sequence and exon distribution [141, 142]. Murine *Thbs1* and human *THBS1* are both about 16 kilobases in length, with about 6 kilobases of exons [141, 142]. Many literature reports prefer the shorter acronym, TSP1, to refer to the protein itself.

### 4.1.1 Structure

Each of the three TSP1 peptides is modular, and contains sequences which are named for their resemblance to other known proteins [141]. These regions include an N-terminal domain, a procollagen-like domain, three sets of "repeat" motifs (termed type 1, 2 and 3), and finally the carboxy-terminal domain. A schematic is shown in Figure 8. Like other matricellular proteins, TSP1 functions through binding to multiple molecules including matrix such as collagen and cell membrane proteins [143]; a study of the TSP1 interactome identified 83 interacting partners [144], a number of which are described below. It is important to emphasize however, that ligand

binding affinities for these interactions have only been published in a few specific cases, and thus use of the term 'binds' implies interacts with.

The N-terminal domain binds to a number of extracellular matrix proteins including aggrecan and heparin [144] and the calcium binding protein calreticulin [145]. Three "Type-1" repeats bind TGF-β, MMP2, MMP9, laminin, and fibronectin in the matrix and to CD36 and β1 integrins on cells [141, 144]. TGF-β in particular is activated by TSP1, while TGF-β signaling can stimulate the production of TSP1 [146, 147]. TSP1 binding to β1 integrins inhibits cell migration [148]. Three Type-2 ("EGF-like") repeats bind β1 integrins [141, 144]. Seven "Type 3" repeats are noted for their interactions with calcium ions [141]; the last of these contains an RGD sequence which binds readily to αvβ3 integrins [141]. Finally, the carboxy-terminal domain is primarily notable for its high-affinity interactions with the cell membrane receptor CD47. Of all its binding partners, TSP1 appears to have the most affinity for CD47, which it activates at picomolar concentrations [141, 144].
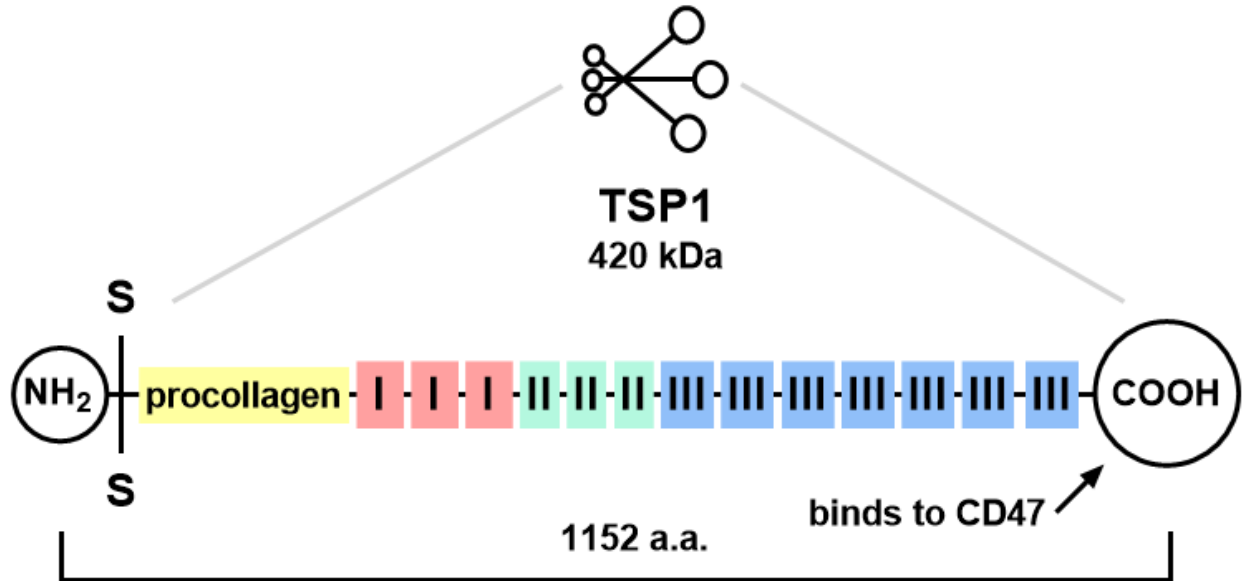
**Figure 8. Schematic of the secreted glycoprotein thrombospondin 1 (TSP1).** TSP1 is a homotrimer, with three identical monomers linked together via a disulfide knot. Figure demonstrates the locations of the type 1 (I), type 2 (II) and type (III) repeats within the chain. CD47 binds to the carboxyterminus. A nearby VVM sequence may be important for TSP1 binding to occur. Original figure created by author, adapted from [141].

### 4.1.2    TSP1 in Development and Adult Tissues

TSP1 is expressed highly in a variety of developing tissues, including the lung, bone, brain, heart, liver, and kidney [149, 150]. Its expression is often associated with specific cell populations within a tissue. For instance, TSP1 is highly expressed in mesenchymal cells as they differentiate into osteoblasts [151], and low levels of expression are associated with chondrogenesis [149]. During lung development, TSP1 is observed along the basement membrane in the columnar epithelium of the large airways [151].

Within the adult, TSP1 is most well-known for its localization within the alpha-granules of platelets, and is released upon platelet activation [112, 141]. The remainder decorates the

extracellular matrix of various tissues. It is produced by a variety of cell populations (epithelial, stromal, and endothelial) under stress [112].

### 4.1.3    TSP1 in Clinical Disease

In systemic sclerosis, tissue levels of TSP1 are correlated with fibrosis and disease severity [140, 146, 152]. This is thought to be due to TSP1 activation of TGF-β. TSP1 has also been investigated as a biomarker for metabolic syndrome [153, 154], stroke severity [155, 156], and peripheral artery disease [157]. TSP1 has also been found to be upregulated in sickle cells disease and associated with some vasculopathic changes in these individuals (cite Novelli et al, PMID: 22318901 and Rogers et al, PMID: 25006410)

TSP1 has been implicated in the pathological vascular remodeling process which occurs in pulmonary arterial hypertension [158]. Hypoxia induces TSP1 production via HIF2α [159]. TSP1 has also been implicated in kidney disease (specifically, renal epithelial cell self-renewal [100, 103, 160] and kidney fibrosis [161, 162]). Many, if not all, of these effects are mediated through TSP1 ligation of CD47, which is described in more detail below.

## 4.2    CD47

### 4.2.1    Structure and Localization

CD47 is a widely-expressed 50 kDa transmembrane protein, once known as integrin associated protein (IAP) due to its tendency to co-precipitate with placental αvβ3 integrin [163].  Its N-

terminal extracellular domain is an immunoglobulin-like loop. It has five transmembrane sequences and a short cytoplasmic tail [163]. The structure of CD47 is well-conserved. Murine CD47 is 71% identical (and 87% "similar") to its human counterpart [163].

Intracellularly, four CD47 isoforms have been described, which differ only in their localization and the length of their cytoplasmic tail [164]. The shortest, Form 1, is four amino acids in length; the longest (Form 4) is 34 amino acids in length. Of these, Form 2 is the most widely expressed. The sequences of the four isoforms are highly conserved between mouse and man, but their significance remains unknown [164]. CD47 has been observed to associate with a variety of other cell-surface proteins to form a supra-molecular complexes in different cell populations, and it is possible that these splice isoforms are partially responsible for this phenomenon [111].

### 4.2.2 Signaling and Function

Historically, CD47 has been considered a marker of self which ligates with SIRPα on macrophages and prevents phagocytosis, termed a "don't-eat-me" signal [111, 165]. In this regard, CD47 has been investigated as a target for anti-cancer [166-168] and anti-atherosclerotic [169] immunotherapy. This finding has further encouraged the development of CD47-functinonalized biomaterials and xenografts to modulate immune responses [170, 171]. However, the relevance of this is called into question by studies that found that CD47 null tissue transplants survived and flourished when transplanted into wild type animals, outperforming wild type transplants into wild type recipients [107]. Others have suggested immune responses attributed to CD47 recognition of self are non-specific [172, 173]. Thus, the implications of the so-called "don't-eat-me" signal in relation to human disease are not clear. Far from being a

passive protein, CD47 is in fact a component of a number of signaling pathways involved in tissue survival. These signaling pathways are reviewed briefly below.

Although CD47 has been shown to interact with TSP2 and TSP4 at lower affinity, TSP1 is its only known soluble high-affinity ligand [174]. A VVM sequence on the C-terminal end of TSP1 is thought to be important for its ability to bind to CD47 and modification of this sequence abolishes the interaction between these two proteins [175], even though the VVM motif itself does not appear to be directly involved in binding [111]. Heparin sulfate glycosylation of the extracellular domain of CD47 at $Ser^{64}$ seems to be necessary for TSP1-CD47 signaling to occur in certain cell types such as T-cells [111, 176].

CD47 is thought to signal through a variety of pathways which vary depending on cell type [111]. It has been observed to associate with the cytoskeleton via PLIC-1 (also known as ubiquilin) [177], and, in doing so, signals through a non-canonical G-protein pathway [178, 179]. Its extracellular IgV domain has been shown to laterally associate with a number of integrin populations, but most specifically αvβ3 [180]. CD47 has also been shown to laterally associate with VEGFR2 in endothelial cells. TSP1 ligation disrupts this association, and in doing so, inhibits VEGFR2 signaling and several downstream pathways including putatively nitric oxide (NO) signaling [112, 181]. Independent of its interaction with VEGFR2, the TSP1-CD47 axis is a redundant limiter of nitric oxide. In endothelial cells TSP1 signaling inhibits the activation of endothelial nitic oxide synthase and thus limits NO production (Bauer et al, PMID: 20610415). In multiple vascular cell types the TSP1-CD47 axis also inhibits NO activation of soluble guanylate cyclase [182-184]. Given the critical role of nitric oxide signaling in cardiovascular health, TSP1 ligation of CD47 has broad implications [112, 184, 185].

## 4.3     TSP1-CD47 SIGNALING IN TISSUE SURVIVAL

We and colleagues have reported that the TSP1-CD47 axis is a redundant inhibitor of multiple angiogenic and survival signals including the biogas nitric oxide (NO) and vascular endothelial growth factor (VEGF) [181, 186]. Upregulation of the TSP1-CD47 axis impairs healing of skin grafts in mice [107] and ischemic soft tissue flaps in pigs [106]. Lack of CD47 activation by TSP1 in null mice significantly reduces necrosis/apoptosis after ischemia-reperfusion injury in the liver, kidney, and brain [99-105] and limits radiation-induced cell death [108-110]. Targeting the TSP1-CD47 interaction with CD47 specific antibodies or morpholino oligonucleotides, to suppress protein production, improves tissue healing to ischemia, ischemia reperfusion and organ transplantation. Significantly, CD47 activation has also been shown to inhibit protein and mRNA levels of c-Myc and other key self-renewal factors including Klf4, Sox2 and Oct4 [187].  This observation has been identified as a likely mechanism for improved healing after kidney ischemia reperfusion injury [103].

## 4.4     TSP1 NULL VERSUS CD47 NULL PHENOTYPE

CD47 null mice, like TSP1 null mice, are available from the Jackson Laboratory [188, 189].  The CD47 null mouse was created via elimination of exon 2 [190].  It is known to be susceptible to certain infections such as *E. coli* due to deficits in neutrophil trafficking [190].  Phenotypic differences between the TSP1 null mouse and the CD47 null mouse are likely secondary to their interactions with different binding partners [111].  CD47 null and TSP1 null mice show greater numbers of healthy mitochondria and lower levels of reactive oxygen species relative to wild-

type mice [191]. Mice of both genotypes also show resistance to radiation injury [108, 110], and both show improved skin graft survival relative to wild type recipients [107]. Both also show similar cardiovascular physiology and increased sensitivity to isolflurane anesthesia due to the effects of TSP1-CD47 on nitric oxide signaling and blood pressure regulation [192].

Hemotologically, TSP1 null mice have greater white cell counts than their wild-type counterparts [149]. There is some dispute as to whether or not TSP1 null mice and wild type mice have similar platelet counts; early literature reports suggested that the two populations have comparable counts [149] whereas later reports indicate suggest that TSP1 null mice have about 22% more platelets [147]. As expected, platelet α-granules do not release TSP1 upon activation. TSP1 null mice have an increased lordotic curvature of the spine [149] and increased bone mass [193]. In contrast, CD47 null mice show decreased bone mass and lower numbers of osteoclasts and osteoblasts, a phenotype which is thought to be due to a lack of SIRPα signaling [194], while other have found the opposite (cite Uluckan et al, PMID: 19276363). The TSP1 null mouse is an accepted model of Sjorgen's Syndrome [189, 195].

Histologically, the adult TSP1 null mouse is very similar to the wild-type mouse, suggesting that other signaling pathways can compensate for its role during development [149]. There are a few notable exceptions: TSP1 null mice have normally-developed lungs, but show increased susceptibility to pneumonia and hyperplasia of the airway epithelium, largely due to a greater number of club cells [149].

## 4.5    DEVELOPMENT OF A FLOXED CD47 MOUSE LINE

Global knockouts are of some utility in cell signaling studies. They can be employed to characterize systemic phenotypic differences, but studies of organ-specific, tissue-specific, and cell specific differences require a more precise approach.   An induced knockout could be employed to identify phenotypic differences which are independent of development. The ubiquitous expression of CD47, and its wide range of downstream effects, make it an interesting scientific and therapeutic target. A cell-specific knockout may therefore useful to examine consequences of cell-specific CD47 therapy. Further, cell-specific knockouts could be used to determine exactly which cells within a given tissue are responsible for TSP1-CD47 signaling.

To this end, we have sought to derive a mouse line in which critical CD47 exons are flanked by *lox*P sites. This mouse, when bred with a *Cre* expressing mouse, wound undergo recombination which leads to production of incomplete CD47 protein. *Cre*-expression can be constitutive or inducible, cell-specific or global. Each of these expression patterns correlates with a different pattern of recombination, and each would elucidate of different aspects of CD47 signaling.  A floxed CD47 mouse would therefore be an invaluable resource to scientists which aim to study the role of TSP1-CD47 signaling in specific cell types within tissues after development.

To complete this task we have exploited the resources of the Knockout Mouse Project (KOMP), an NIH-funded, nationwide effort to develop mouse knockout strains and make them available to scientists in the United States and worldwide [196].  KOMP collaborates closely with the International Knockout Mouse Consortium (IKMC), which coordinates publicly- and privately-funded projects worldwide. The following is a summary of the history of the IKMC and its aims.

### 4.5.1 Background

A large-scale, genome-wide knockout mouse project was first proposed in 2003 with the aim of developing knockout mouse resources for laboratory investigators. Curated databases at the time only described global knockout mice in about one-tenth of 25,000 estimated mouse genes [197]. Many of these resources were unavailable for public use. In light of this a worldwide, systematic, centrally-curated initiative to mass-produce knockout mouse lines could provide investigators with a vital resource. These mice could be used to generate previously-unavailable experimental models and, in doing so, advance biomedical research.

The 2003 working group (whose proceedings are summarized in a 2004 publication [197]) promulgated the following guidelines for the initiation of such a project: (1) a variety of methods (e.g., both gene trapping and gene targeting [198, 199]) should be employed in order to mass-produce null alleles, (2) null alleles should include reporter sequences in order to expedite the process of cell and tissue phenotyping for end-users, and (3) at a minimum, the project should produce, bank, and make available mutant ES cells to researchers across the country and around the world [197]. The authors recommended against the use of *cis*-elements (such as *lox*P or FRT sites) which could be used to generate conditional knockouts, due to the nascent state of the technology at the time.

Austin et al. [197] further described several tiers of phenotyping which could be centrally provided by the project. Once the absence of a particular gene in a particular mouse line has been firmly established, Tier 1 phenotyping would be employed to elucidate certain aspects of the mutant mouse's physiology (for instance, blood chemistry and hematological profiles). Microarray transcriptome analysis would identify a subset of mice for deeper, system-specific examination. At the time, it was estimated that a majority of mouse genes could be knocked out

within five years, at a total cost of about $50 million (about $10 million per year). Production of 500 new mouse lines from the mutant ES lines was estimated to cost $12.5-15 million annually. Tissue of these 500 lines was expected to cost up to another $5 million (for tissue phenotyping), with another $2.5 million for Tier 1 phenotyping and another $18,000 for each mouse line selected for transcriptome analysis.

Critics of such large-scale projects raised concerns about the scope and scale of the project, citing insufficient demand for many of the commercially available knockout lines which were available at the time [200]. Further, given that many phenotypes are driven by multiple genes and redundant signaling pathways, single-gene knockouts may not alter physiology in a clinically meaningful way.

In spite of this, not one but *four* genone-wide knockout mouse projects have arisen in the years since the 2003 working group [199]: one in Europe (EUCOMM), one in Canada (NorCOMM), and two in the United States (the NIH-funded Knockout Mouse Project [196] and the state-funded Texas Institute for Genomic Medicine). The International Knockout Mouse Consortium (IKMC) was established in 2006 in order to limit redundancy and encourage data sharing between these four groups and any others willing to undertake the task [196, 199, 201].

### 4.5.1.1 Allele Types and Allele Conversion

Austin et al. [197] describe several deliverables for the knockout mouse project, including gene trapping constructs, frozen zygotes, frozen embryos, live mice, and phenotypic data. Critical to all is the development of an allele which can be easily modified via recombination using Cre-lox or FLP-FRT recombination.

KOMP has developed a generic allele design for this purpose known as the *tm1a* allele [201]. It is based on the "knockout-first" allele design described by Testa et al [202]. A *tm1a*

homozygote is a complete knockout (due to the presence of two SV40 polyadenylation sequences which prevent transcription of the entire gene). A *tm1a* mouse is the "first" step in a breeding strategy to derive a floxed allele (hence the name, "knockout first"). Recombination of the *tm1a* allele using *Cre* or FLP-FRT technology yields further alleles. The *tm1a* allele and its derivatives are diagrammed in Figure 9.
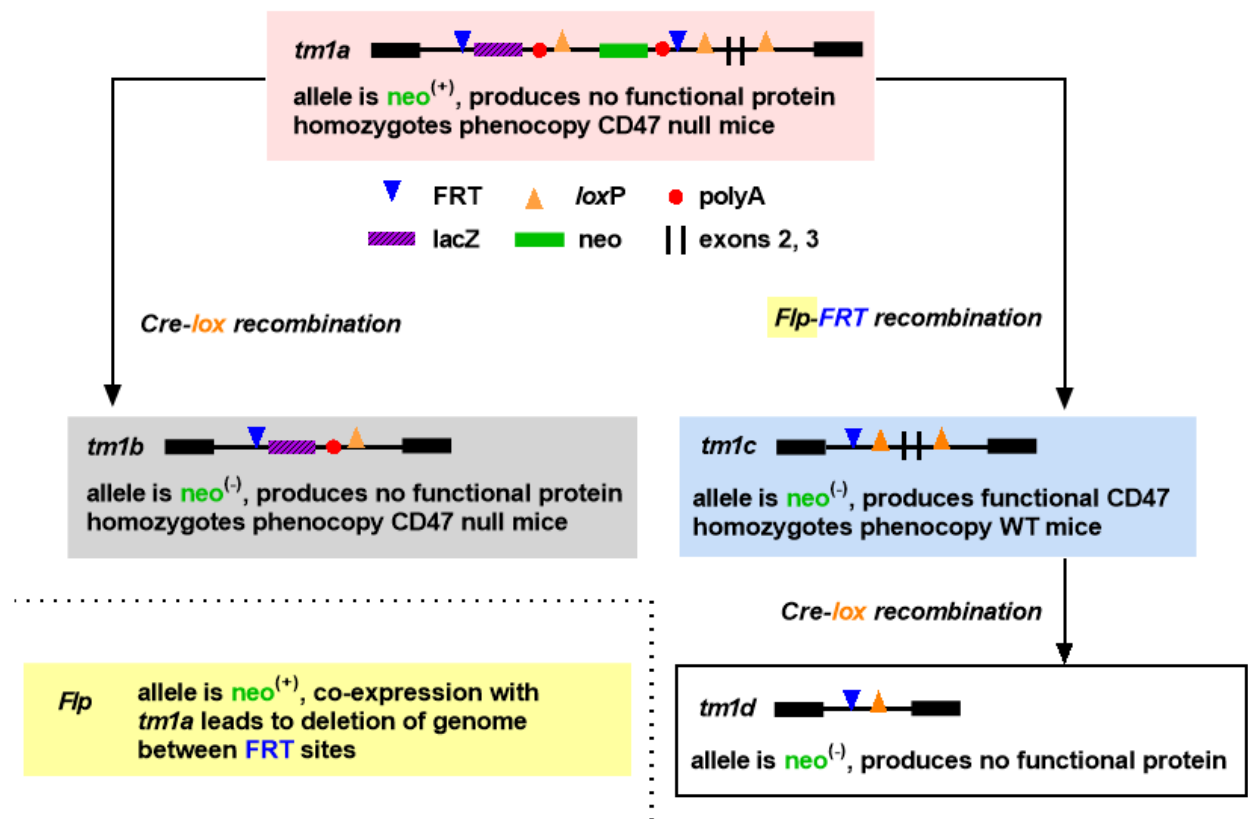


**Figure 9.** **Allele maps and recombination strategy for the *tm1a* allele.** Figure made by author, adapted from [203].

69

The *tm1b* lacZ-tagged allele is generated when the *tm1a* allele undergoes *Cre* recombination [201]. Ideally, this process removes all genetic material between the most 3' and 5' *lox*P sites in the *tm1a* sequence, including the *neo* sequence, both poly-adenylating sequences, one or more targeted exons, and one of the FRT sites. Mice which are homologous for *tm1b* should also be complete knockouts. (In practice, *Cre* recombination can remove genetic material between any two of the three *lox*P sites in the allele – not just the most 3' and 5' sites. This means that two additional alleles can be generated in addition to the desired *tm1b* allele: one which lacks the *neo* sequence only, and the other lacks targeted exons only. In these cases, the allele is designed so that the recombination process creates a frameshift mutation which phenotypically resembles a knockout [201].)

The *tm1c* allele is generated when the *tm1a* allele undergoes FLP/FRT recombination, which excises all genetic material between the two FRT sites, including both polyadenylation sequences [201]. This recombination reverts the cell to a wild-type phenotype, and it should generate a normal protein. In particular, it should be noted that this recombination leaves two *lox*P sites on either side of the target sequence which can be targeted with Cre recombination; thus, a mouse homozygous for *tm1c* is a traditional "floxed mouse."

Finally, Cre recombination of the *tm1c* allele yields the *tm1d* allele, which should not express normal protein. Like the *tm1a* and *tm1b* alleles, and the *tm1d* allele represents a "knockout" genotype and phenotype.

The *tm1a* allele for the CD47 gene was originally developed by the Knockout Mouse Project [203]. It should be noted that the target sequence of the CD47 *tm1a* allele includes exons 2 and 3 [203], whereas the commercially available CD47 null mouse was generated via the

removal of exon 2 only [188, 190]. The physiological implications of this difference are not completely known, however cell-specific analysis suggest the lack of exons 2 and 3 phenocopies gene expression patterns found in cells from the commercial CD47 null mice.

### 4.5.2 Methods

We aimed to generate a mouse line which (1) is homozygous for a floxed CD47 allele and (2) expressed CD47 in the absence of Cre. A $tm1a^{+/+}$ mouse population would not fulfill these criteria. (Once again, even though the $tm1a$ allele contains $lox$P sites, the allele *does not* express CD47 due to the polyadenylation sites within its sequence – hence the term, "knockout-first" [201]). We genotyped mice at every step of the process, and in early generations, assessed for the expression of CD47. Genotyping was initially performed using in-house protocols based on information provided by KOMP; however, as litter sizes increased we elected to outsource this task to Genetyper (NY) which specializes in this work.

### 4.5.2.1 Breeding Strategy

The breeding strategy we developed was designed to derive a $tm1c^{+/+}$ mouse line from tm1a$^{+/-}$ breeding pairs.

It is summarized immediately below, diagrammed in Figure 10a on page 77, and is described in detail in section 4.5.3. It should be noted that the $tm1a$ and *Flp* alleles both contain a *neo* sequence, as indicated in Figure 9. Mice were assayed for the *neo* sequence during later generations to establish that both the $tm1a$ and *Flp* alleles had been cleared from the $tm1c$ mouse line. This is discussed in more detail in the extended description of the breeding strategy below (see 4.5.3.3).

1. Founder Generation: $tm1a^{+/-}$ x $tm1a^{+/-}$, which yields $tm1a^{+/-}$ mice

2. Generation 1: $tm1a^{+/-}$ x $tm1a^{+/-}$ sibling mating, which yields $tm1a^{+/-}$ mice

3. Generation 2: $tm1a^{+/-}$ x $Flp^{+/+}$, which yields ($tm1a^{+/-}$ $Flp^{+/-}$) mice. These undergo recombination to become ($tm1c^{+/-}$ $Flp^{+/-}$) mice.

4. Generation 3: ($tm1c^{+/-}$ $Flp^{+/-}$) x C57BL6J, which clears the *Flp* allele

5. Generation 4: $tm1c^{+/-}$ x $tm1c^{+/-}$, which produces the floxed mouse ($tm1c^{+/+}$)

### 4.5.2.2 Genotyping

We obtained primer sequences from KOMP (via our collaborator Dr. William Fazier) and the Jackson Laboratory to genotype each litter. For our in-house genotyping, these primers were synthesized by Integrated DNA Technologies (Coralville, IA).

In-house genotyping was found to be inefficient. Large litter sizes necessitated extended downtime (about one week every month). To increase efficiency, we employed the resources of Genetyper, a dedicated genotyping service. Genetyper synthesized their primers based on our provided sequences. The primer sequences provided to us are listed in Table 2. The primer pairs used to genotype each allele are summarized in Table 3. Cycling parameters for *Flp* and *tm1a* genotyping are provided in Table 4 and Table 5, respectively.

### 4.5.2.3 Western Blot Analysis

Western blots were employed as an assay of CD47 phenotype. Detailed descriptions of the standard Western blotting protocol used are available in 6.1.10, on page 100. Briefly, protein lysates were centrifuged at 17000 x g and supernatants were kept frozen until analysis. Samples were prepared under nonreducing/denaturing conditions, were run on acrylamide gels, and

transferred onto nitrocellulose membranes. A rat-anti-mouse CD47 antibody (clone MIAP301, Santa Cruz sc-12731, 1:500) in LiCor Odyssey Blocking buffer was used to detect CD47. Detection of CD47 required that the blots be incubated for 48 hours in the primary antibody, on a rocker, at 4 $^{\circ}$C. Rabbit anti-beta actin 1:5000 (Cell Signaling 4967) was used as a loading control. These were coupled with appropriate secondary antibodies.

**Table 2. Primer sequences**

| Name | Sequence | Ref. |
|---|---|---|
| CSD-lacF | GCTACCATTACCAGTTGGTCTGGTGTC | [204] |
| CSD-neoF | GGGATCTCATGCTGGAGTTCTTCG | [204] |
| CSD-loxF | GAGATGGCGCAACGCAATTAATG | [204] |
| CSD-Cd47-R | TAATTCAGCAGTCCTGATCCCACCC | [204] |
| CSD-Cd47-ttR | CTGTCTCTGTGCTCTCTGGCTAAGG | [204] |
| CSD-Cd47-F | TCTACACTAAACTCAGCTGGCCTGG | [204] |
| FLP-F (oIMR1348) | CACTGATATTGTAAGTAGTTTGC | [205] |
| FLP-R (oIMR1349) | CTAGTGCGAAGTAGTGATCAGG | [205] |
| neoF | Proprietary | N/A |
| neoR | Proprietary | N/A |

**Table 3. Primer pairs.**

| Allele | "Genotype" | Forward Primer | Reverse Primer | Size (bp) | Ref. |
|---|---|---|---|---|---|
| *tm1a, tm1c* | Floxed | CSD-loxF | CSD-Cd47-R | 312 | [204] |
| *tm1a* | PreCre | CSD-neoF | CSD-Cd47-ttR | 603 | [204] |
| *tm1b* | PostCre | CSD-lacF | CSD-Cd47-R | 610 | [204] |
| *Cd47* (wt) | Wild type CD47 | CSD-Cd47-F | CSD-Cd47-ttR | 445 | [204] |
| *tm1c* | PostFlp | CSD-Cd47-F | CSD-Cd47-ttR | 658 | [204] |
| *tm1d* | PostFlp&Cre | CSD-Cd47-F | CSD-Cd47-R | 660 | [204] |
| *Flp* | Flp-expressing | FLP-F (oIMR1348) | FLP-R (oIMR1349) | 725 | [205] |
| *tm1a, Flp* | neo-expressing | neoF | neoR | 280 | N/A |

**Table 4. Cycling parameters for *Flp* genotyping.**

| Step | Temp ($^{\circ}$C) | Time (s) | Cycling/Ramp parameters |
|---|---|---|---|
| 1 | 94 | 120 | |
| 2 | 94 | 20 | Repeat: Steps 2-4 for 10 cycles. |
| 3 | 65 | 15 | Ramp: Decrease temperature in Step 3 1.5 $^{\circ}$C each cycle |
| 4 | 68 | 10 | |
| 5 | 94 | 15 | Repeat: Steps 5-7 for 28 cycles. |
| 6 | 50 | 15 | Ramp: None |
| 7 | 72 | 10 | |
| 8 | 72 | 120 | |
| 9 | 4 | Hold | |

**Table 5. Cycling parameters for *tm1a* genotyping.**

| Step | Temp ($^{\circ}$C) | Time (s) | Cycling/Ramp parameters |
|---|---|---|---|
| 1 | 94 | 30 | |
| 2 | 94 | 15 | Repeat: Steps 2-4 for 10 cycles. |
| 3 | 65 | 30 | Ramp: Decrease temperature in Step 3 1.0 $^{\circ}$C each cycle |
| 4 | 72 | 40 | |
| 5 | 94 | 15 | Repeat: Steps 5-7 for 30 cycles. |
| 6 | 55 | 30 | Ramp: None |
| 7 | 72 | 40 | |
| 8 | 72 | 300 | |
| 9 | 4 | Hold | |

**4.5.3   Results**

The first $tm1a^{+/-}$ x  $tm1a^{+/-}$ breeding pairs were set up in May 2015. The following is a summary of our results at each generation.  These results are visualized in Figure 10.

**4.5.3.1 Founder Generation (Generation Zero): Generation 1: $tm1a^{+/-}$ x $tm1a^{+/-}$**

The Jackson Laboratory obtained cryopreserved $tm1a^{+}$ sperm from our collaborator Dr. William Frazier at Washington University. This sperm was used for *in vitro* fertilization of wild type (C57BL6J) oocytes.  These heterozygote ($tm1a^{+/-}$) embryos were then implanted into wild-type C57BL6J females (Jackson Labs, Statement of Work Q015966).  Four mice (two male, two female) were selected from this litter and became the founding members of our *tm1a* colony (Generation Zero in Figure 10). The founding members of our colony and their progeny were genotyped in-house as described in documents provided by KOMP, and representative results are shown in Figure 10b. Lung tissue was isolated from $tm1a^{-/-}$, $tm1a^{+/-}$, and $tm1a^{+/-}$ progeny, and protein immunoblot demonstrated that these mice phenocopy WT, CD47 heterozygote, and CD47 null mice respectively (in terms of their expression of CD47) (Figure 10c).

**4.5.3.2 Generation 1: $tm1a^{+/-}$ x $tm1a^{+/-}$**

Per [206], Generation 1 consisted of breeding pairs of heterozygote siblings (sibling intercross).  Once again, these mice produced a population of $tm1a^{-/-}$, $tm1a^{+/-}$, and $tm1a^{+/-}$ mice, which were genotyped as above. Heterozygotes were saved for future breeding. (The decision to use heterozygote mice rather than homozygote mice was made based on consultation with a colleague who was familiar with the technology and found greater success when breeding heterozygote mice).
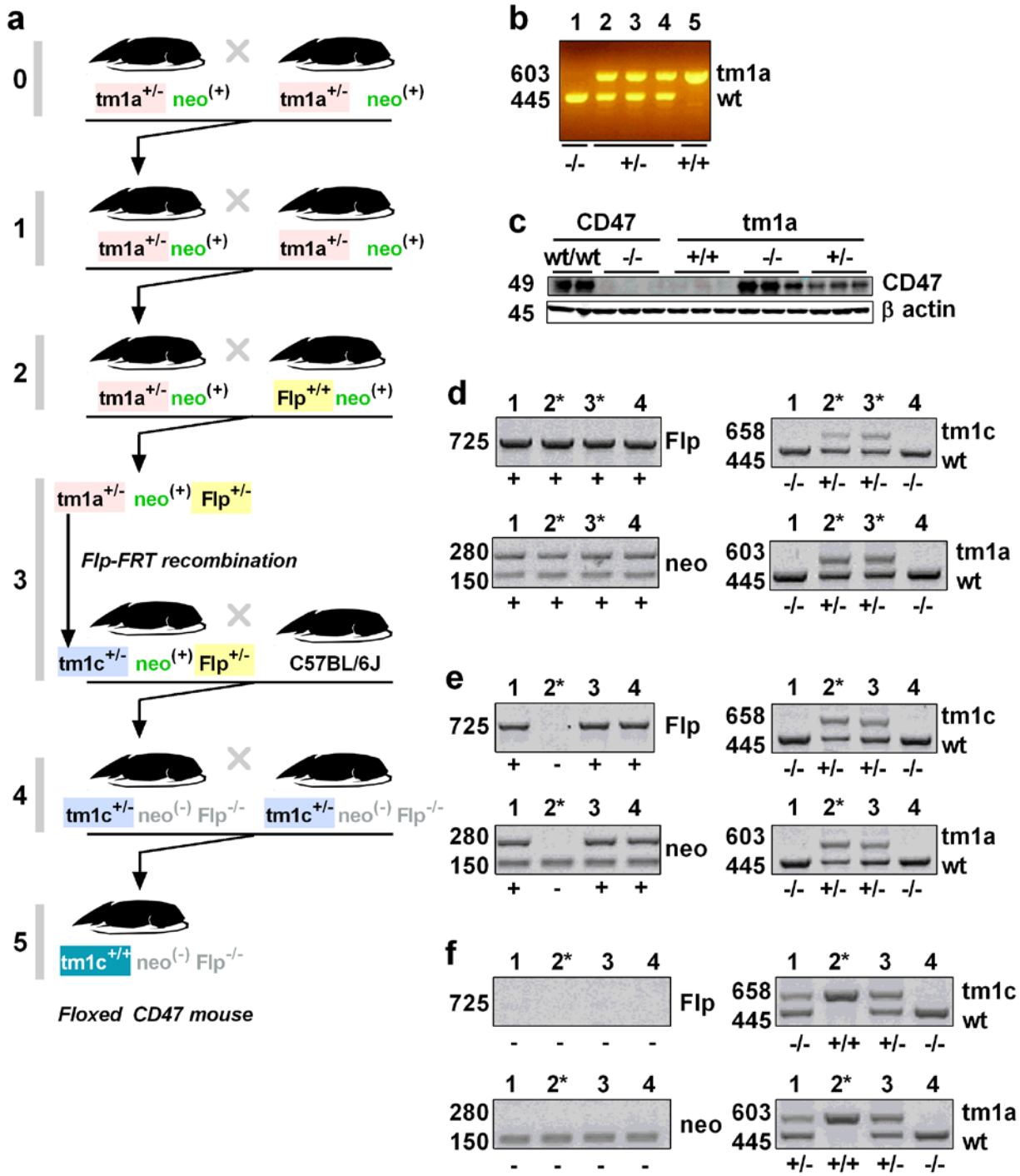
**Figure 10. Breeding strategy and results.** (a) Breeding strategy. (b, c) Representative genotyping (b) and phenotyping (c) results from generations zero, 1, and 2. (b) In-house genotyping results using samples from generation zero. Heterozygotes in lanes 2, 3, 4 were saved for future breeding. Amplicon sizes are reported at left, in basepairs. (c) Protein sizes are reported at left, in kilodaltons. (d, e, f). Representative genotyping results from generations 3 (d), 4 (e) and 5 (f). An asterisk (*) indicates mice which were saved for future breeding. Masses are reported in base-pairs.

### 4.5.3.3 Generation 2: *tm1a$^{+/-}$* x Flp$^{+/+}$

Generation 2 breeding pairs were prepared by mating *tm1a* heterozygotes (*tm1a$^{+/-}$*) with *Flp* deleter mice purchased from the Jackson Laboratory (stock number 009086). These mice were genotyped for *tm1a*, *tm1c,* and *Flp*. All progeny were expected to express *Flp* (and were found to do so), having inherited one allele from the *Flp* expressing parent. A subset of progeny experienced Flp-FRT recombination which converted the *tm1a* allele to *tm1c*.

Curiously, we observed that all *tm1c$^{+/-}$ Flp$^{+/-}$* mice also appeared to express *tm1a* as well (Figure 10d, lanes 2 and 3). This seemed to suggest either (1) incomplete conversion of the *tm1a* allele to the *tm1c* allele, yielding *tm1c$^{+/-}$ tm1a$^{+/-}$* mosaics or (2) nonspecific binding of the *tm1c* primer pair, yielding a "false positive" *tm1c* band.

We hypothesized that the presence or absence of *neo* would allow us to discriminate *tm1a* "true positives" from "false positives," since that the *tm1a* allele contains a *neo* sequence (and the *tm1c* allele does not). However, we discovered that the *Flp* allele contains a *neo* sequence as well, and therefore all Generation 2 progeny were expected to be *neo*-positive. With this finding, it was clear that we would not be able to use *neo* to determine whether we had generated (1) *tm1c$^{+/-}$ tm1a$^{+/-}$* mosaics or (2) *tm1c$^{+/-}$* mice with a "false positive" *tm1a* signal at this point.

We elected to wait another generation to resolve this question. We set up Generation 3 breeding pairs as originally planned: the *tm1c$^{+/-}$ Flp$^{+/-}$* mice (which unexpectedly expressed *tm1a*) would be crossed with wild-type mice. We were aware of the possibility that our *tm1c$^{+/-}$* mice were in fact mosaics (*tm1a$^{+/-}$ tm1c$^{+/-}$*). However, given that *tm1c* and *tm1a* alleles reside at the same locus, we reasoned that zygotes from mosaic mice would contain either one allele or the other, but not both. All future generations of mice were therefore genotyped for *neo* in addition to *tm1a, tm1c,* and *Flp*.

**4.5.3.4 Generation 3: ($tm1c^{+/-}$ $Flp^{+/-}$) x C57BL6J**

Our $tm1c^{+/-}$ $Flp^{+/-}$ mice were crossed with wild-type mice in order to yield a subpopulation of $tm1c$ heterozygotes which did not express Flp (e.g., $tm1c^{+/-}$ $Flp^{-/-}$). This step is necessary to prevent unexpected genomic recombination due to cryptic FRT sites which may be present in the mouse genome [207].

These mice were genotyped for $tm1a$, $tm1c$, $Flp$, and $neo$. A mouse carrying a $tm1a$ allele or $Flp$ allele should always carry a $neo$ sequence, due to the way these synthetic alleles are constructed. The absence of a $neo$ sequence would tell us definitively whether or not a particular mouse was expressing $tm1a$ or $Flp$.

We observed a subpopulaton of mice which were $Flp$-negative and $neo$-negative, but apparently positive for both $tm1c$ and $tm1a$ (Figure 10e, lane 2). Given that the $neo$ sequence is included in the $tm1a$ allele, we could safely conclude that any mice which expressed a $tm1a$ signal but no $neo$ signal represented a false positive. Mice which were negative for $neo$ were therefore assumed to be negative for $Flp$ and $tm1a$ as well. We would continue to assay for all four genes ($tm1a$, $tm1c$, $Flp$, and $neo$). Mice which were heterozygous for $tm1c$ but were negative for $neo$ ($tm1c^{+/-}$ $neo^{(-)}$) were kept for future breeding.

**4.5.3.5 Generation 4: ($tm1c^{+/-}$ $neo^{(-)}$) x ($tm1c^{+/-}$ $neo^{(-)}$)**

In the final generation of breeding, mice which were heterozygous for $tm1c$ but negative for $neo$ were bred together to generate a subpopulation of $tm1c^{+/+}$ $neo^{(-)}$ mice (Figure 10f). The first $tm1c^{+/+}$ $neo^{(-)}$ mouse was born on June 3, 2016 and was discovered in the June 21, 2016. Mice which are homozygous for $tm1c$ can be crossed with $Cre$ expressing mice to generate progeny which are homozygous for the $tm1d$ allele. These mice should be complete CD47 knockouts, and should phenocopy the original CD47 null.

### 4.5.4 Ongoing Work

The first *tm1c*$^{+/+}$ (floxed CD47 mouse) breeding pair has been set up in our colony. Progeny of this pairing will be crossed with global *Cre* mice in order to generate global CD47 knockouts (*tm1d*$^{+/+}$). *tm1a*$^{+/+}$ and eventually *tm1d*$^{+/+}$ mice, both of which should be CD47 knockouts, will undergo kidney ischemia reperfusion injury to demonstrate that they phenocopy the resistance to injury that our lab has demonstrated in the CD47 null mouse [103].

### 4.5.5 Conclusions

This chapter has provided a brief review of the literature on TSP1, CD47, and TSP1-CD47 signaling. It has summarized the beneficial effects of CD47 blockade which provide a rationale for my dissertation project. It also describes the development of a floxed CD47 mouse line which will be used to establish a unique colony here at the University of Pittsburgh for future studies examine the role on CD47 signaling in specific cell types in an *in situ* environment.

The floxed CD47 mouse will be bred with *Cre* mice to generate a global knockout. Future studies will establish that the floxed mouse phenocopies the wild-type mice (and the Cre mouse phenocopies the CD47 null).

The specific role of TSP1-CD47 signaling in the airway is unknown. Preliminary data suggested that differences in the proportions of various cell population within the airway epithelium. The next chapter will therefore examine the global CD47 null phenotype in the tracheal epithelium.

# 5.0 QUANTIFICATION OF AIRWAY BASAL CELL POPULATIONS USING AUTOMATED IMAGE ANALYSIS

CD47 null tissues show improved healing capacity and survival under stress relative to wild-type tissues. This was first demonstrated in studies examining full-thickness skin grafts [106, 107] and has been substantiated using ischemia-reperfusion in multiple organ systems [99, 101, 102, 208] and radiation models of injury [108-110]. Of note the study of skin graft healing among wild type and null mice also found that CD47 null skin grafts healed better on wounds in wild type mice than wild type grafts, calling into question the so-called "don't eat me" signal presumed to be mediated by macrophage SIRP-α-mediated phagocytosis of cell not expressing CD47. The superior survival of CD47 null tissues has been attributed to the effects of thrombospondin-1 (TSP1)-CD47 signaling on the vasculature [181, 186]. TSP1 is secreted under conditions of stress, and its ligation of CD47 on endothelial cells redundantly inhibits nitric oxide signaling through multiple mechanisms. In doing so, CD47 reduces vasodilation and limits angiogenesis. Thus, TSP1-CD47 signaling inhibits tissue perfusion over short- and long- time scales, and has a deleterious on tissue survival after injury.

There is increasing evidence that the TSP1-CD47 signaling axis has effects on tissue survival which are independent of its known effects on nitric oxide and the vascular system. TSP1 ligation of CD47 has been observed to induce apoptosis in hematopoetic cells through a caspase independent mechanism [209-211]. Perhaps more interestingly, TSP1 ligation of CD47

has been observed to reduce intracellular levels of multiple key transcription factors associated with self-renewal, such as c-Myc, Sox2, Oct3/4 and Klf4 (abbreviated OSKM) [103, 187].

The overarching aim of my dissertation project is to prepare a functional tissue-engineered trachea using a decellularized graft. Given the known effects of TSP1-CD47 signaling on tissue survival, I hypothesize that this signaling axis negatively affects the physiology of an engineered graft in a number of ways. It may lead to (1) reduced vascular density and perfusion, (2) decreased protein and genomic markers of self-renewal within seeded or migrating cells, and (3) decreased numbers of self-renewing progenitor cells within the epithelial and stromal tissues.

Within the tracheal epithelium, keratin 5-expressing basal cells are widely considered the progenitor cell population [7, 21-25]. In various injury models, basal cells differentiate into the various mature cell populations of the airway, including ciliated and club secretory cells. Basal cell self-renewal is driven by the transcription factors p63 and Sox2. Since Sox2 is to suppressed by activated CD47 [103, 187], I hypothesized that elimination of the CD47 signaling pathway will lead to increased numbers of proliferating basal cells. This hypothesis was informed by preliminary histological stains which seem to indicate increased keratin 14 levels within the CD47 null tracheal epithelium at baseline.

## 5.1    TECHNICAL RATIONALE

In previous studies [1], I have quantified the various cell populations within the airway epithelium by hand-counting cell nuclei associated with a particular marker. This method is tedious and subject to observer bias. Further, it was possible that the cellular distribution of the

trachea could be dependent on tissue geometry and orientation of tissue sections. In light of these concerns, a method was developed in order to quantify the cell populations of the airway epithelium. Isolation of epithelial cells before staining eliminates tissue geometry as a confounding variable, and digital image analysis allows observer-independent quantification. This method can be used to fully quantify the various basal cell types in the airway epithelium.

## 5.2    METHODS

### 5.2.1    Tracheal Harvest and Digestion

Primary murine tracheal epithelial cells (abbreviated MTECs) were isolated for quantification as described [212]. Briefly, tracheas were explanted from three wild-type (WT) and six CD47 null mice of a C57BL6 genetic lineage, all 12 weeks of age. Tracheas were further dissected in presence of Ham's F-12 supplemented with 1% penicillin-streptomycin (hereafter Ham's F-12/1%PS) to remove connective tissue, and were cut along the longitudinal axis to expose the lumen. Each dissected and opened trachea was placed in a 15 ml conical tube containing 0.15% Pronase from *Streptomyces griesus* (Roche Applied Science 10165921001) in Ham's F-12/1%PS. These tubes were placed on a rocker at 4 ºC for 18 hours to loosen epithelial cells attachment to the extracellular matrix. Subsequently, FBS was added to each tube to bring the final serum concentration to 10% and halt the digestion.

Epithelial cells were released from the tissue by mechanical agitation. Each tube containing one digested trachea was rapidly inverted 20 times in order to separate cells from the extracellular matrix. After agitation, each trachea was lifted into a second tube containing Ham's

F-12/1%PS/10% FBS, which was itself inverted 20 times. This process was repeated until the tracheas had passed through four tubes, and the remnant tracheal tissue was discarded. Supernatants were pooled in the final tube and centrifuged (500 x g, 5 minutes, 4 $^{\circ}$C).

Each pellet was resuspended in MTEC BASIC media (as described in literature [212]: DMEM/F12 supplemented with 15 mM HEPES, 1% Penicillin-Streptomycin, 4.0 mM L-glutamine, 7.5% sodium bicarbonate) further supplemented with 10% fetal bovine serum. The resuspended cells were incubated in a tissue culture dish at 37 $^{\circ}$C to remove fibroblasts via differential adherence to plastic. After four hours, the supernatant was removed from each dish and the adherent fibroblasts were discarded. The supernatant was centrifuged once again (500 x g, 5 mins, 4 $^{\circ}$C) to collect mouse tracheal epithelial cells.

Each pellet was resuspended in 200 microliters Ham's F-12/1%PS/10% FBS and cells were counted using a hemacytometer. Cells from each animal were spun onto two slides at 1000 RPM for 15 minutes and stored at -20 $^{\circ}$C until staining.

### 5.2.2 Keratin-5/Keratin-14 Cytospin Staining

The following was adapted from a collaborator's protocol (T. Gilbert):

Cytospun slides were incubated in PBS supplemented with 0.5% Triton X-100 for 30 minutes at room temperature in order to permeabilize cells. Blocking was performed with PBS/0.5% Triton X-100/5% bovine serum albumin for 45 minutes at room temperature. Slides were subsequently washed three times with PBS. The following antibodies were diluted in blocking buffer (PBS/0.5%Triton X-100/5% BSA) and were applied in sequence, with intervening PBS washes: (1) Rabbit anti-keratin 14 (Covance PRB-155P) (1:500) for 90 minutes at room temperature; (2) AlexaFluor-488 conjugated donkey anti-rabbit IgG (Life Technologies

A21206) (1:500) for 90 minutes at room temperature; (3) anti-Rabbit blocking antibody fragment (Jackson ImmunoResearch 111-007-003), overnight, at 4 ℃; (4) Rabbit anti-keratin 5 (Covance PRB-160P) (1:1000), for 90 minutes at room temperature; (5) AlexaFluor-594 conjugated donkey anti-rabbit (Life Technologies A21207) (1:500), for 90 minutes at room temperature. After three washes each in blocking buffer and PBS, all slides were mounted with a DAPI-containing mounting medium (Vector Laboratories H-1200) and imaged within 48 hours.

### 5.2.3 Imaging and Quantification

Each cytospun slide was imaged repeatedly (at between six and ten non-overlapping locations). At each location, three images were captured corresponding to each of the three stains: (1) DAPI-stained nuclei, (2) AlexaFluor 594-stained keratin 5, and (3) AlexaFluor 488-labeled keratin 14. A novel MATLAB script, titled "CytoAnalysis", was developed to correlate AF594- and AF488-labeled objects to DAPI-stained nuclei in order to determine the fluorescence intensity of each imaged cell. This program is summarized briefly below, but is reproduced in full in the Appendix (page 124).

The following lines of MATLAB code from the program `runcytoanaysis.m` summarize the core of the segmentation technique. This code has been greatly abbreviated and slightly modified for clarity.

```
    ...
% load the image file into memory
gray = imread(filename);
% create a binary mask
mask = im2bw(gray, graythresh(gray));
% identify objects, and calculate properties
```

85

```
imstats = regionprops(mask, gray, {'Area', 'PixelIdxList',
     'MeanIntensity'});
```

```
...
```

Each captured image is loaded into memory as a grayscale image, `gray`. The MATLAB `graythresh` function determines a pixel intensity threshold which discriminates brighter, positively-stained pixels from dark background pixels. A call to the MATLAB function `im2bw` converts the original grayscale image into a binary image `mask`, in which pixels with intensity values above this calculated threshold are white and pixels below this threshold are black (Figure 11a). The mask was used to generate a list of discrete "objects" and determine their properties. An area (`Area`) and mean pixel intensity (`MeanIntensity`) was calculated for each object, and a list of all pixels within the object's borders was generated (`PixelIdxList`). Objects smaller or larger than user-defined limits were discarded from further analysis.

To identify individual cells, DAPI was selected as a universal marker. Within each set of three images, objects in the keratin 5 image were associated with objects in the corresponding DAPI image on the basis of shared pixels. The same process was repeated for objects in the green (keratin 14) channel. In this way, the degree of keratin 5 or keratin 14 fluorescence (if any) could be quantified for each DAPI-stained object, and a histogram could be prepared showing the distribution of fluorescence intensities for all the cells within a given set. These results were plotted as shown (Figure 11b-d).

### 5.2.4   Cell Cataloguing

DAPI-labeled objects were sorted into four groups based on the degree of fluorescence intensity relative to a user-defined threshold: (1) K5-low/K14-low "double negative" cells (2), K5-high/K14-low cells, (3) K5-high/K14-high "double positive" cells and (4) K5-low/K14-high

cells.  The fraction of the total number of cells within each of the four groups was calculated
(Figure 11e).
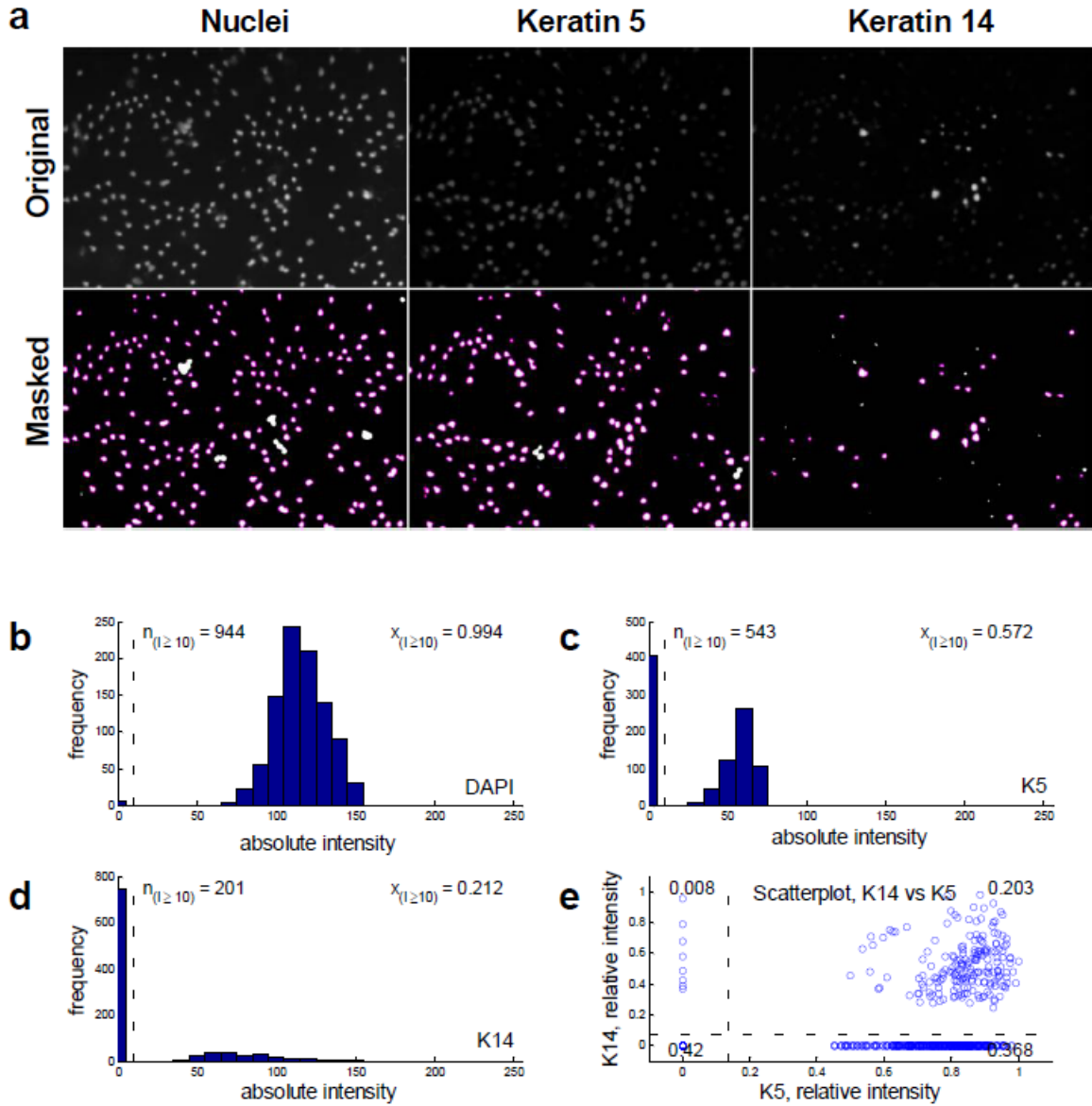


**Figure 11. CytoAnalysis automatically counts and characterizes fluorescent objects.**   Above is an example of
data output from a single animal. (a) Demonstration of the "masking" technique by which the program identifies
pixels corresponding to individual objects. Objects matching the proper inclusion criteria are highlighted in pink (b-
d) Histograms demonstrate the distribution of fluorescence intensity of all objects within a given set of images for a
particular slide. The dotted line marks the boundary between cells determined to have "high" and "low" expression
of a particular marker.  (e) Once the program has determined the keratin 5 and keratin 14 fluorescence intensity for
each cell, a scatter diagram can be prepared which shows four distinct groups of objects. On this particular slide, a
higher than normal number of cells showed a keratin-5 signal above the defined threshold.

## 5.3    RESULTS

### 5.3.1    CytoAnalysis identifies cells and quantifies fluorescence intensity

Cells were isolated from three wild type C57BL6 mice and six CD47 null male mice, 12 weeks of age, of the same genetic background. Two cytospin slides were prepared for each animal. One of the two was triple-stained for keratin 5, keratin 14, and DAPI as described above. Images were captured from between six and 10 non-overlapping locations in each slide.   The total number of cells analyzed for each slide averaged $n = 445.8 \pm 176.0$ cells.

### 5.3.2    CD47 null and wild-type tracheal tissues have equal distributions of basal cell populations

Keratin-5 is generally considered a universal airway basal cell marker, as it is expressed both in quiescent and proliferative states [24]. In the wild-type and CD47 null mice, keratin-5-expressing basal cells comprised $30.0 \pm 2.54\%$ and $30.1 \pm 3.9\%$ of the total number of isolated cells, respectively. These numbers match literature reports, which have indicated that keratin 5 expressing basal cells represent about 30% of the epithelial population within the trachea [24, 25].

Within this population, a subset of dual-positive (that is, keratin 5-positive and keratin 14-positive) cells represent a proliferative population. Dual expressing cells comprised $10.4 \pm 4.46\%$ of all cells isolated from three wild type mice, and $8.08 \pm 2.75\%$ of cells isolated from six CD47 null mice.  A full breakdown of basal cell subpopulations is given in Table 6 and

is summarized in Figure 12.  No statistically significant differences were observed in basal cell

populations.

**Table 6. Mean distribution of basal cell populations within the tracheal epithelium.**

|  | WT ($n = 3$) | | | CD47 null ($n = 6$) | | |
|---|---|---|---|---|---|---|
|  | mean | ± | sd | mean | ± | sd |
| Other | 68.9 | ± | 3.0 | 69.2 | ± | 4.1 |
| K5 only | 19.5 | ± | 2.1 | 22.0 | ± | 2.0 |
| K5 K14 dual | 10.4 | ± | 4.5 | 8.1 | ± | 2.8 |
| K14 only | 1.1 | ± | 9.8 | 7.0 | ± | 0.5 |
| K5 total | 30.0 | ± | 2.5 | 30.1 | ± | 3.9 |
| K14 total | 11.6 | ± | 4.6 | 8.8 | ± | 3.0 |
| Count | 399.3 | ± | 178.9 | 469.0 | ± | 186.6 |
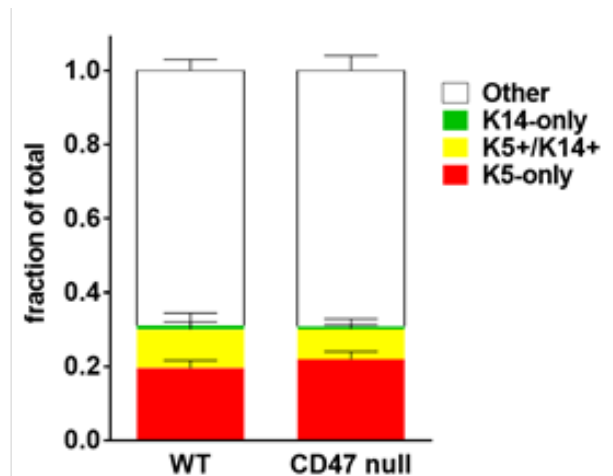


**Figure 12.  Distribution of basal cell populations within the tracheal epithelium.**
 No statistically significant differences were observed.

# 5.4    DISCUSSION

## 5.4.1   Limitations

There were a number of limitations to the method employed in this study. First, while it is a simple to compare relative fluorescence intensity between objects on a particular slide, fluorescence intensity could not be easily compared between slides. This is due to the fact that a given object's intensity is not solely a function of protein expression; rather it is also dependent on (1) antibody affinity, (2) incubation times, (3) exposure time at time of imaging, and (4) the length of the time interval between staining and imaging. Steps were taken to control these variables, but the exact relationship between fluorescence intensity and protein expression is not clear. Thus, while comparisons of fluorescence intensity could be made between objects within a particular slide, such comparisons may not be appropriate between objects on different slides. Despite this limitation, objects could be sorted into relative "high" and "low" intensity groups. Therefore, conclusions could be drawn based the proportion of cells within these categories. Another limitation is that the process of cell separation and harvest from the trachea may itself alter the relative expression levels of genes as compared to the *in vivo* setting.

## 5.4.2   Conclusion

The CD47 null genotype, though associated with elevated markers of self-renewal, does not appear to be associated with elevated numbers of keratin 5-expressing (or keratin 5/keratin 14 dual expressing) basal cells within the tracheal epithelium. This finding stands in contradiction to preliminary data which seemed to indicate greater keratin-14 expression in CD47 null mice

trachea airways, suggesting gene expression levels in these cells is context dependent. There may be any number of reasons for this. First, TSP1 and CD47 are both upregulated in stressed conditions including with cell isolation and culture, and TSP1 in particular is expressed at very low levels at baseline. Yet it is possible that there is not enough TSP1 in the native tracheal epithelium at rest in order to cause significant differences in the physiology of the airway epithelial cell population.

Second, while basal cells are considered the progenitor cell population of the airway epithelium, it has been suggested that not all basal cells are equally "multipotent" [23]. In light of this, keratins 5 and 14 may not be the best markers in order to quantify differences in progenitor cell number within CD47 null tissues, as they are universal markers for the entire basal cell pool. The transcription factors *p63* and *Sox2* may be more appropriate: both of these are expressed by self-renewing basal cells [13, 14], and as we and others have shown *Sox2* in particular is regulated by TSP1-CD47 signaling [103, 187]. However, the low quantities of these proteins (relative to a cytoskeletal molecule like keratin) makes them less-than-ideal targets for this technique.

The technique described in this study is a straightforward method by which airway epithelial cell populations can be analyzed, while eliminating observer bias and the potential effects of tissue geometry. Data gathered using the technique described in this study suggests that approximately 30% of the cells within a wild-type C57BL6 mouse trachea are basal cells. The fact that this proportion matches what has been previously reported in the literature [24, 25] lends credence to the idea that this is a reliable and scientifically valid method to quantify cell populations within the airway epithelium.

# 6.0 MALADAPTIVE TSP1-CD47 SIGNALING LIMITS AIRWAY RESTORATION AND HEALING OF DECELLULARIZED TRACHEAL TRANSPLANTS

(Portions of this chapter will be used in an upcoming manuscript: Kutten, J.C., et al., Maladaptive TSP1-CD47 Signaling Limits Airway Restoration and Healing of Decellularized Tracheal Transplants. *In preparation.*)

The trachea is a highly specialized structure composed of unique epithelial cellular types including basal cells, club cells, and ciliated cells. The stromal cell populations include chondrocytes arranged in a series of C-rings bridged by fibrous tissue and smooth muscle. The result is a structure that is both rigid enough to provide a patent and stable airway and yet can accommodate a wide range of motion. Unlike many other composite tissues in the body that are amenable to reconstruction with surrogate tissue types, there is nothing that can be enlisted to mimic the proximal airways. Thus, tracheal deficiency due to congenital causes [42] or malignancy [44, 45] represents is a life threatening problem without an effective surgical solution. Current approaches to address this include slide tracheoplasty [38, 39, 41], long-term stenting, intermittent dilation, tracheostomy and in a rare instances tracheal transplantation [51, 53]. Regardless of the approach the complication rates remain very high [56] and have provided inspiration for the development of a functional bioengineered tracheal transplant. Common to these efforts has been to begin with either a decellularized tracheal allograft or a synthetic polymer/nanofiber scaffold and then seed the three dimensional scaffold with cells and growth

factors [49, 50]. Some published reports have also indicated that regional pedicle soft tissue flaps, most commonly derived from the greater omentum, [19] are then employed to envelope the transplant and provide angiogenic stimuli and to render a sterile barrier between the chest cavity and the transplant. The clinical reports of bioengineered tracheal transplantation, although receiving significant media attention, remain hampered by very poor outcomes [98] including delayed healing and non-healing, transplant collapse and suffocation, infection, fistula formation between the trachea and other chest organs, respiratory ventilator dependency and in many cases death. However, the molecular and cellular processes controlling the survival and healing of the bioengineered tracheal transplants are incompletely defined.

Thrombospondin-1 (TSP1) is a matricellular protein upregulated with injury [138]. As a secreted protein it can alter cell activity through engagement of cell surface receptors. One such high affinity interaction occurs with CD47 [111, 112]. In this capacity TSP1 limits multiple restorative pathways including growth factors such as vascular endothelial growth factor (VEGF) and the biogas nitric oxide [181, 186]. Animals lacking CD47 show accelerated healing after skin graft transplantation [106, 107]. Conversely, therapeutically blocking the TSP1-CD47 interaction significantly improves the healing of hypoxic and ischemic tissues and organs [99, 106, 138, 213-215], and also limits radiation-induced cell death [108-110]. Perhaps more significantly, we and colleagues reported that key transcription factors known to control pluripotency and self-renewal were inhibited by TSP1-CD47 signaling [103, 187]. The specific role of TSP1 and CD47 in the trachea and proximal airway is unknown, but reports suggest that TSP1 ligation of CD47 may have a deleterious effect on airway healing. In asthma-induced inflammation TSP1 expression is increased [216], while TSP1 null mice show greater levels of club cell repopulation after chemical injury [139]. These results indicate that TSP1 is increased

in airway inflammation and impedes healing, and form a further basis for my hypothesis that maladaptive TSP1-CD47 signaling impedes airway healing and limits restoration of orthotopic decellularized tracheal transplants.

To test this hypothesis, we developed a unique murine syngeneic orthotopic tracheal transplant model and assessed healing *in vivo* and *in vitro* analyzed the restorative potential of tracheal epithelial cells. TSP1 and CD47 protein expression was essentially undetectable in healthy airways and tracheas but both were increased following short-term hypoxia. *In vitro*, human airway epithelial cell (HAEC) proliferation and response to wounding was inhibited by exogenous TSP1 and these responses were mitigated by treatment with a CD47 blocking antibody. CD47 null tracheal and airway epithelial cells (TECs) displayed increased proliferation and migration compared to wild type cells providing genetic confirmation of the signaling axis. Multiple key self-renewal transcription factors were increased in at the levels of message and protein in intact CD47 null airways and in CD47 null TECs compared to wild type airways and cells including octomer-binding transcription factor 4 (Oct4), sex determining region Y-box 2 (Sox2), Kruppel-like factor 4 (Klf4) and cellular homolog of the v-myc avian myelocytomatosis viral oncogene homolog (c-Myc), (abbreviated OSKM). Furthermore, CD47 null airways showed enhanced healing following chemical injury compared to wild type animals. Finally, decellularized tracheal transplants were more rapidly resurfaced when transplanted into orthotopic defects in CD47 null recipients versus similar decellularized tracheal transplants in wild type recipients. Together, these data indicate that maladaptive upregulation of the TSP1-CD47 axis in airway injury limits epithelial cell self-renewal and repair to suppresses restoration following both chemical injury and tracheal transplantation.

## 6.1    MATERIALS AND METHODS

### 6.1.1    Animal Studies

All studies were performed under protocols approved by the University of Pittsburgh Institutional Animal Care and Use Committee in accordance with NIH guidelines. Male C57BL6 wild-type (WT, CD47$^{+/+}$) and CD47 null mice (B6.129S7-$^{Cd47tm1Fpl/J}$), catalogue numbers 00664 and 003173 respectively, were obtained from the Jackson Laboratory (Bar Harbor, ME, USA).

### 6.1.2    Human Airway Epithelial Cell Isolation

Human airway epithelial cells (HAECs) were isolated employing a well-established technique at the University of Pittsburgh and under an approved IRB (protocol number: IRB970946). Briefly, approximately three centimeters of the proximal airway were cut from fresh human lungs and trimmed of excess parenchyma. Each section was cut open lengthwise and placed in sterile, cold EMEM/HEPES (Sigma M2645) with added sodium bicarbonate (Sigma S6297) solution (pH = 7.4), hereafter referred to as EMEM/HEPES media. The samples in media were placed on a rocker at 4$^{o}$ C overnight. After aspirating the media, the samples were trimmed a second time, rinsed in EMEM/HEPES media, and placed in cold protease solution (Sigma P5147, 1 mg/ml in EMEM/HEPES media) for 36 to 48 hours. 10X collagen coating solution was prepared by combining 5 mg collagen from human placenta (Sigma C7521) into 50 ml of 0.035 M acetic acid in water.  This 10X stock was incubated at 4 $^{o}$C overnight and filtered. To prepare a 1X working stock, 10X collagen coating solution was diluted 1:10 in 0.01M $Na_2CO_3$. Appropriate volumes of 1X collagen solution were pipetted into tissue culture flasks, dishes, and plates that were then

allowed to incubate for at least 30 minutes at 37 °C. After incubation the solution was removed and an appropriate number of cells were seeded for each application. HAECs were supported with BronchiaLife Complete Media (LifeLine Cell Technology, Frederick, MD) that was replenished every other day and were passaged at 80% confluence onto new collagen coated plates or flasks.

### 6.1.3 Human Airway Epithelial Cell Culture

Human airway samples were briefly digested with protease. The protease was collected in a 50 ml conical tube and sufficient fetal bovine serum (FBS) was added to bring the final concentration to 5% and halt digestion. Each section of tissue was placed into a sterile tissue culture dish and the luminal surface was scraped with a sterile scalpel to liberate cells. The tissue culture dish was washed in cold EMEM/HEPES to collect the cells. The cell-containing media was diluted in 200 ml of EMEM/HEPES and split into four conical tubes. All tubes were centrifuged (200 x g, 4 °C, 5 min). The supernatant in each tube was aspirated and replaced with 20 ml Accutase (Sigma 6964). The cells were incubated in Accuatase on a rocker at $4^o$ C for 10 min, and 1 mL FBS was added to stop the digestion. The cells were centrifuged a second time and were suspended in sterile, complete BronchaLife Complete Media with 1% penicillin-streptomycin. After counting, approximately $2 \times 10^6$ cells were seeded into collagen-coated T75 flasks.

### 6.1.4 Cell Proliferation Assays

MTS proliferation assays (Promega CellTiter 96 AQueous One Cell Proliferation Assays G3580) were performed according to the manufacturer's instructions. Cells were passaged and 2500 cells in 100 ul of media were seeded into wells of collagen-coated 96-well plates. The cells were allowed to adhere overnight and the media was replaced with 200 ul of media containing the indicated treatments. Combinatorial groups of the following were applied as described in the results section: mouse $IgG_1$ anti-human CD47 (clone B6H12, Santa Cruz sc-12730, 1 ug/ml), normal mouse $IgG_1$ (Santa Cruz sc-3877, 1 ug/ml), human thrombospondin-1 (TSP1, Athens Research 16-20-201319, at 2.2 nM, 5.0 nM, and 10 nM). In groups where blocking antibodies were combined with TSP1, cells were allowed to incubate in media containing the antibody alone for thirty minutes before it was replaced with media containing both the antibody and TSP1. After 72 hours of proliferation under each treatment condition 100 ul of media was removed and 20 ul MTS Reagent (Promega) was added to each well. The wells were allowed to incubate for 2-3 hours before absorbance was read at 490 nm on a spectrophotometer.

### 6.1.5 Cell Hypoxia

$1 \times 10^5$ HAECs were seeded onto collagen coated plates as above and grown to 80% confluence. On the day of treatment, the media was changed and cells containing flasks were placed in a normoxic incubator or a hypoxic incubator ($FiO_2$ 1%) for two or twelve hours. Afterward the media was collected, and plates were washed with PBS before cell collection and protein isolation.

### 6.1.6  Scratch Wound Healing Assays

Cells were seeded onto collagen-coated plates and grown to 80% confluence. At t = 0 hours, media was aspirated from each well and a single scratch was drawn across the surface using a p10 pipette. Each well was gently washed twice with PBS in order to remove debris before adding BronchiaLife Complete media. Three images were taken of each well at t = 0, 2, 6 and 10 h. There regions within each well were photographed at each time point. Care was taken to ensure that the same locations were photographed between time points. Images were de-identified during quantification in order to control for observer bias. For each image, ImageJ was used to identify contiguous regions containing no cells (or non-confluent cells). If multiple such areas were identified in a single image, the region with the largest area was used. The mean area of all three images from a given well at a given time point was taken to be representative of the area of the scratch. Wound areas from three scratches in three separate wells were averaged, and normalized to the wound area at time t = 0, in order to calculate "percent wound closure."

### 6.1.7  Human Airway Epithelial Cell Organoid Cultures

The sphere (organoid) culture protocol was adapted from the literature [24, 29, 217]. Briefly, human airway epithelial cells in BronchiaLife proliferation media were counted and resuspended in UNC/USG media [218] at a concentration of $2x10^5$ cells/ml. Where applicable, differentiation media contained the indicated treatments (2.0 μg/ml B6H12 and/or 20 nM TSP1). In cases where the two treatments where combined, the cells were incubated first in B6H12 for at least 30 minutes before adding TSP1. The mixture of cells in differentiation media was combined 1:1

98

with growth-factor reduced Matrigel (Corning 356230) to prepare a final cell- and treatment-loaded gel solution ($1x10^5$ cells/ml, ±1.0 μg/ml, ± 10 nM TSP1). 100 μl of the final gel solution were pipetted into the apical chambers of TransWell Clear membrane inserts (Corning 3740) placed in 24-well plates. Three wells were prepared for each of the four treatment groups. Plates were maintained at 37 °C to allow the gels to solidify before adding 800 μl of treatment-loaded differentiation media into the basolateral chamber of each well. Basolateral media was changed every two-to-three days. Four photographs were taken of each well on the day of seeding, plus every seven days thereafter. ImageJ was used to determine the cross-sectional area of objects within each photograph. An average cross sectional area was determined for each well, and the average cross sectional area was calculated for each treatment. At the final time point, gels were gently aspirated, pipetted into TissueTek cassettes, submerged in OCT media, and frozen for sectioning.

### 6.1.8 Porcine Tracheal Matrix (PTM) Scaffolds

Decellularization was performed in accordance with previously published protocols [1, 133] with some modifications. This process is summarized in Figure 15a. Briefly, porcine tracheas (kindly provided by Dr. Mauricio Rojas, University of Pittsburgh) were frozen overnight at -80 °C. Tracheas were then thawed in sterile MilliQ deionized water and exposed to a series of washes in freshly prepared 3.0 M NaCl, 3% Triton X-100, and sterile water. Each wash was performed at 200 RPM on a laboratory rocker for greater than eight hours. This was followed by sanitization in a 0.1% peracetic acid/4% ethanol solution in deionized water, followed by washes in sterile PBS and water. Once sanitized, the tracheas were cut into square sections (approximately 0.7 cm x 0.7 cm) under sterile conditions and stored in PBS + 1% antibiotic-antimycotic until use. PTM

scaffolds were held in place using Sigma Cell Crown 24 inserts in 24 well-dishes and were soaked in BronchiaLife media before cell seeding.

## 6.1.9    Airway Epithelial Cell Adhesion Assay

$1 \times 10^5$ HAECs were seeded onto each PTM scaffold in BronchiaLife media. The cells were allowed to adhere overnight and the scaffolds were rinsed in PBS. After rinsing, the scaffolds were moved to fresh plates and cells were allowed to proliferate for 3 days before further analysis.  For histological analysis, intact porcine tracheas, unseeded PTM scaffolds, and seeded PTM scaffolds were fixed in 4% paraformaldehyde/PBS for 24 hours before embedding and sectioning.

## 6.1.10  Western Blot Analysis

Western Blots were performed using standard protocols. Briefly, complete RIPA buffer was prepared from stock RIPA buffer (Cell Signaling 9806S) supplemented with PhosSTOP phosphatase inhibitor (Sigma 4906837001) and protease inhibitor (Sigma P8340). Cell-culture dishes were washed twice with PBS, frozen overnight, and incubated on ice for at least 45 minutes in complete RIPA buffer before lysates were collected. Likewise, whole tissues were submerged in complete RIPA buffer and were ground with a mortar and pestle over a 45-minute period interspersed with incubations on ice. Lysates were centrifuged at 17000 X g and supernatants were kept frozen at $-80^0$ until analysis. Protein concentration was determined via RC DC Protein Assay (BioRad, Berkley, CA). Samples were then run on acrylamide gels (8%) and transferred onto nitrocellulose membranes (BioRad). In most cases, samples were prepared

under reducing/denaturing conditions, with the exception of samples intended for CD47 protein detection (which were prepared under non-reducing/denaturing conditions). The following primary antibodies were used at the indicated dilutions in LiCor Odyssey Blocking Buffer: Rabbit anti-c-Myc IgG 1:1000 (Abcam ab69987), rabbit anti-Klf4 IgG 1:1000 (Abcam ab151733), rabbit anti-Oct4 IgG 1:1000 (Abcam ab18976), rabbit anti-Sox2 1:1000 (Abcam ab97959), rabbit anti-ΔNp63 (clone Poly6190, Biolegend 619002), rabbit anti-CC10 1:200 (clone FL96, Santa Cruz sc-25555), mouse anti-TSP1 IgG1 1:500 (clone A6.1, Abcam ab1823), rat anti-mouse CD47 1:500 (clone MIAP301, Santa Cruz sc-12731), mouse anti-human CD47 1:500 (clone B6H12, Santa Cruz sc-12731).  Rabbit anti-beta actin 1:5000 (Cell Signaling 4967) was used as a loading control.

### 6.1.11  qPCR analysis

RNA was isolated from tissues using a RNEasy Mini kit (Qiagen, Netherlands) and the manufacturers' instructions.  cDNA was prepared from total RNA using LAMDA Biotech G206 kit (St. Louis, MO, USA). Aliquots of cDNA were diluted to 10 ng/μL, and 4.5 μL cDNA was combined with 5.0 μL of ROX reaction mixture (Thermo Fisher 11745500) and 0.5 μL of the appropriate TaqMan primer (ThermoFisher) to make a reaction mixture of 10.0 μL per well. The following TaqMan Gene Expression Assay were employed: *Klf4* (Mm00516104_m1), *Pou5f1* (also known as Oct4) (Mm03053917_g1), *Sox2* (Mm03053810_s1), *Myc* (Mm00487804_m1), *Cd47* (Mm00495005_m1), *Thbs1* (also known as TSP1) (Mm01335418_m1), *Krt5* (Mm01305291_g1), *Krt14* (Mm00516876_m1), FoxJ1 (Mm01267279_m1), *Scgb1a1* (also known as CCSP) (Mm00442046_m1), *Hprt1* (Mm01545399_m1).

qPCR was performed according to the manufacturers' instructions. Briefly: each 20X assay was combined with appropriate volumes of cDNA and Platinum PCR SuperMix-UDG with ROX (Thermo Fisher 11743-500) within each well, and samples were run in triplicate. Fold-change was calculated using the $\Delta\Delta C_T$ method, with *Hprt1* as a housekeeping gene.

### 6.1.12 *Ex vivo* airway angiogenesis assay

Collagen type I-based gel solution was prepared as we published [184] using these ratios of the following reagents: 8.0 mL PureCol (stock: 3 mg collagen/mL, Fisher 50-350-230), 0.8 mL 10x M199 media (Sigma M0650), 74 μL L-glutamine (CellGro 25-005-CI), 74 μL penicillin/streptomycin (MediaTech MT30-002CIRF), and 1.0 mL of a pre-prepared 11.8 mg/mL sodium bicarbonate (Sigma S5761) solution in water. Sodium hydroxide (1.0 M) was added drop-wise to the solution to bring it to a pink color. 300 μL of the collagen gel solution was deposited into 16 wells of a 24-well plate, and the plate was incubated at 37 °C until the gel solution had solidified. Tracheas were harvested from male 12-14 week old wild-type C57BL6 and CD47 null mice and cleaned under a dissection microscope. These were then cut into one-ring sections using a scalpel. The rings were placed flat in one well of the prepared 24-well plate, and covered with an additional 400 μL collagen gel solution. The plates were allowed to incubate until the covering gel had solidified, and 400 μL of gowth media was added. Media was changed on the day immediately following gel placement and on every second day thereafter. Images were captured of each well on each day. In each photograph, the well was positioned such that a 90° arc of the explant ring's edge was contained in one quadrant of the image. This allowed the position of each well to be reproduced daily so that the degree of cell migration could be reliably quantified. To quantify cell migration, ImageJ was used to determine the pixel coordinates which

defined (1) the boundaries of the explant and (2) the locations of cells within each image. These results were exported to a data file, and a MATLAB script was designed to determine the shortest distance between each cell and the nearest explant border. Cell counts and mean cell migration distance could then be determined from analysis of this data.

### 6.1.13 *In vivo* Chemical Airway Injury

10- to 12- week old male wild type and CD47 null mice were obtained from the Jackson Laboratory or bred within our animal colony. Airway epithelial cell depletion was performed on these mice as previously described. Briefly, naphthalene (Sigma, St. Louis, MO, USA) was dissolved in corn oil (Sigma C8267) at a concentration of 0.275 mg/ml. Mice were weighed and then injected with naphthalene-corn oil solution to reach a dose of 275 mg/kg body mass. Mice were treated twice daily with subcutaneous 5% dextrose in normal saline for the first three days after the procedure. At indicated time points, mice were sacrificed via carbon dioxide exposure followed by exsanguination. Tracheas were cut open longitudinally along the trachealis muscle and embedded in OCT (TissueTek, Sakura Finetek USA, Torrence CA) for later tissue sectioning, and lung tissues were snap frozen for protein isolation.

### 6.1.14 Decellularization of Murine Tracheas

Mouse trachea decellularization was performed as previously published with slight modifications [1]. Briefly, fresh mouse tracheas are trimmed of excess tissue, frozen overnight, and thawed in MilliQ distilled water. They were then treated with washes of water, 3% Triton X-100, and 3 M NaCl while in a pressure chamber which cycles between normal atmospheric pressure and a

vacuum. After these washes, the tracheas were sanitized via a 0.1% peracetic acid/4% ethanol/water solution and were rinsed thoroughly with water and PBS before being stored in PBS supplemented with 1% antibiotic/antimycotic. In all cases, less than 24 hours passed between the completion of the final wash and the start of transplant surgery.

### 6.1.15 Murine Orthotopic Tracheal Transplantation Model

We conducted murine orthotopic tracheal transplantations of freshly decellularized tracheas obtained from wild type mice as we previously published [1] with minor variation. Briefly, mice were anesthetized with 80 mg/kg ketamine and 8 mg/kg xylazine and placed supine on a heating pad throughout the surgery. The cervical trachea was exposed via a midline incision. Two tracheal rings were dissected from the surrounding connective tissue and were resected, starting at four rings below the larynx. Care was taken to protect the recurrent laryngeal nerves throughout the procedure. The decellularized tracheal graft was positioned in the defect, and the anastomoses were made (first distal, then proximal) with interrupted 10-0 Prolene sutures (Ethicon). The skin incision was closed with 7-0 PDS sutures. Mice were monitored under a warming lamp until they had fully recovered from anesthesia and were ambulatory. The operative time averaged 30 minutes.

### 6.1.16 Decellularized Tracheal Transplantation Post-Operative Care

Mice were housed singly after surgery. Food and water were supplied ad libitum. Subcutaneous injections of the following were administered each day following surgery: buprenorphine (0.1 mg/kg) twice daily for pain relief, and gentamicin (8 mg/kg) once daily for infection prophylaxis.

Four days after surgery, mice were euthanized with an intraperitoneal injection of ketamine/xylazine and immediate exsanguination. The tracheal transplants were harvested, using the Prolene sutures as landmarks, for immediate processing.

### 6.1.17 Tissue Histology and Quantification

Tissue embedding and sectioning was performed by the Research Histology Services at the University of Pittsburgh. Multiple images were taken of each slide and the images were combined in Adobe PhotoShop CS6 in order to create a photomosaic which spanned the entire length of the trachea. In the naphthalene treated mice, keratin-5/keratin-14 dual staining cells could be observed in a patchy distribution along the luminal surface of the airway at the 4- and 7-day time points. The lengths of the entire trachea epithelium and the lengths of each dual-staining patch were measured, and the surface-coverage was calculated. After four days, mice receiving decellularized grafts showed a clear "migratory front" as keratin-5/keratin-14 cells migrated along the graft lumen. Measurement was taken along the epithelium from the far end of the native cartilaginous ring immediately adjacent to the anastomosis to the end of the migratory front. This measurement was averaged from up to four sites on a given slide.

### 6.1.18 Statistics

Statistical analysis was performed using GraphPad Prism 6 (GraphPad, La Jolla, CA). In general, data are presented as mean ± one standard deviation (SD) for each group. Intergroup differences were assessed with two-way analysis of variance (ANOVA). Statistical significance was defined as $p < 0.05$.

## 6.2 RESULTS

### 6.2.1 TSP1, via CD47, inhibits HAEC proliferation and growth in multiple *in vitro* models of healing.

Proliferation is an essential cell response to injury and necessary for healing. TSP1-CD47 has been noted to broadly regulate cellular differentiation and proliferation in response to stress HAEC cell cultures treated with exogenous TSP1 over 72 h displayed decreased proliferation in a dose-dependent manner (Figure 13a, on page 107). This inhibitory effect was abrogated by pre-treatment of cells with a CD47-blocking antibody (clone B6H12, 1.0 μg/ml) (Figure 13b). To further assess the role of TSP1 in epithelial healing, confluent HAEC layers were scratched and surface coverage was determined at several time points post-injury. Although exogenous TSP1 treatment (2.2 nM) did not significantly alter cell resurfacing of the scratch under these conditions, treatment with the CD47-blocking antibody accelerated wound closure in both the presence and absence of exogenous TSP1 (Figure 13c, d).

Finally, a sphere-forming assay [24, 29, 217], was employed to assess *ex vivo* the role of TSP1 on airway cell differentiation. Over the course of 20 days airway epithelial cells seeded in a 1:1 media:Matrigel mixture proliferated and formed "bronchospheres" which morphologically resembled the native airway epithelium (Figure 13e). By 14 days, bronchospheres in wells treated with TSP1 were hypoplastic (less developed) relative those in untreated wells. The inhibitory effect on bronchosphere size found in TSP1 treated systems was abrogated by treatment with the CD47 blocking antibody (clone B6H12) (Figure 13f).
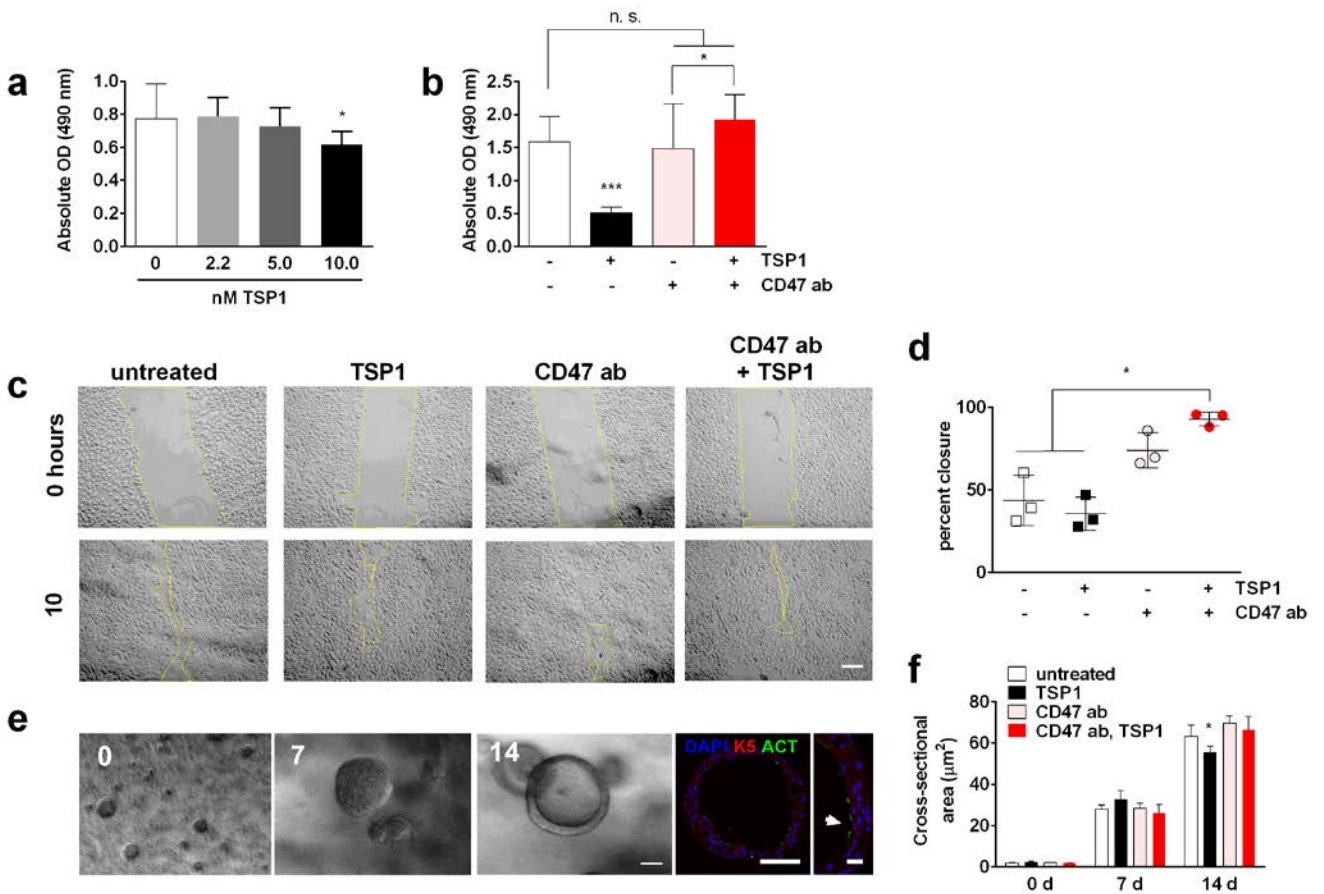
**Figure 13. TSP1, via CD47, inhibits HAEC proliferation and growth in multiple in vitro models of healing.** (a) MTS proliferation assay of HAECs, over 72 hours, using a number of TSP1 doses. (b) MTS proliferation assay of treated cells (±10 nm TSP1; ± CD47 antibody clone B6H12, 1 μg/ml). Results are the mean ± SD; * indicates p < 0.05. (c, d) Scratch assay wound closure after t = 10 hours (±10 nm TSP1; ± CD47 antibody clone B6H12, 1 μg/ml). Each symbol represents the mean of three measurements in a given experiment; n = 3 experiments. * indicates p < 0.05. (e) Cilliated bronchosphere-forming assay. Bronchospheres were photographed at 0, 7 and 14 days. Scale 100 μm. (e, far right) Bronchospheres contain keratin 5 (K5, red) positive basal cells and acetylated tubulin (ACT, green) positive ciliated cells and were counter stained with DAPI. Scales 100 μm and 20 μm (inset). (f) Bronchosphere cross-sectional area at the indicated time points. Results are the mean ± SD of n = 3 wells. * indicates p < 0.05 relative to each of the other groups, by ANOVA.

### 6.2.2 Airway TSP1 and CD47 are minimally detectable in health and upregulated in epithelial cells following hypoxia.

TSP1 protein is induced in lungs in response to bleomycin [219] and in airway neutrophils in human asthmatics [216]. Recent published reports have suggested that TSP1 can be a localizing signal which works in concert with BMP4 to drive differentiation toward an alveolar phenotype [139]. However, little is known about the homeostatic role of TSP1 in the proximal airway. Murine tracheas from healthy wild type mice did not display TSP1 on immunohistological staining of tissue sections (Figure 14a, on page 109). To more precisely explore this, we performed mass spectroscopy evaluation of tracheal samples. Platelet-derived human TSP1 protein, as a positive control, was identified on mass spectroscopy. Pre-digested murine tracheas were protein separated via Western blot and gel bands at the predicted molecular weight for TSP1 analyzed via mass spectroscopy. Consistent with results above, TSP1 was not among 974 proteins detected by mass spectroscopy in these preparations. Tissue injury through the disruption of normal perfusion induces hypoxia and ischemia, and these processes likely limit cellular restoration and healing of engineered tracheas [20]. As an *in vitro* mimic of injury we challenged HAECs to hypoxia ($FiO_2$ 1%, 2 and 12 hours). Both TSP1 and CD47 protein expression increased significantly in HAECs following hypoxia (Figure 14b). The finding of hypoxia-mediated induction of TSP1 and CD47 in HAECs is relevant as we reported CD47 is the cognate cell receptor for TSP1 [220].
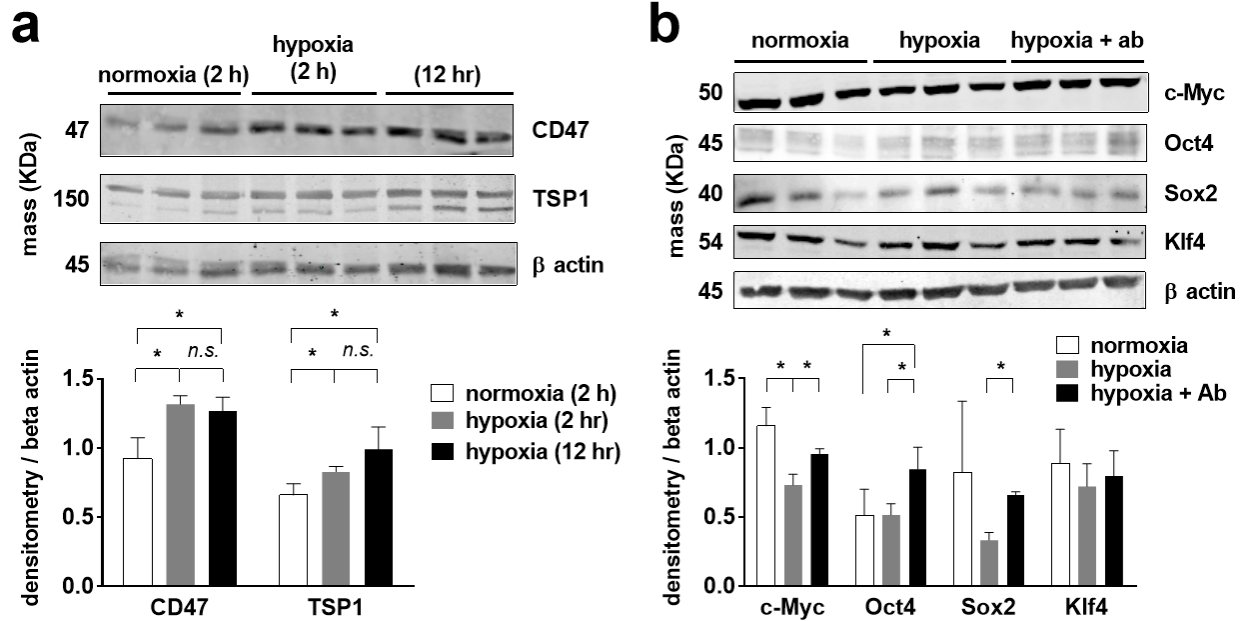
**Figure 14. Hypoxic challenge of human airway epithelial cells (HAECs)** (a) TSP1 and CD47 protein levels in HAECs exposed to hypoxia (FiO2 = 1%) for 2 and 12 hours. (b) Protein levels of multiple self-renewal transcription factors following 12-hour hypoxic challenge (FiO2 = 1%) of HAECs. Results are the mean ± SD of n=3 separate experiments. * indicates $p < 0.05$.

### 6.2.3 Maladaptive induction of TSP1-CD47 signaling in HAEC limits self-renewal gene expression.

We published that TSP1-CD47 signaling limited self-renewal gene expression in kidneys following ischemia reperfusion injury [103]. Consistent with these findings, the hypoxia-mediated upregulation of TSP1 and CD47 in HAEC correlated with a significant decrease in mRNA expression of several self-renewal genes including cellular homolog of the v-myc avian myelocytomatosis viral oncogene homolog (c-Myc) and sex determining region Y-box 2 (Sox2) (Figure 14b). Treating cells with a CD47 blocking antibody (clone B6H12, 1.0 μg/ml) restored c-

myc and Sox2 levels and increased octamer-binding transcription factor 4 (Oct4) levels beyond those found in normoxic control cells (Figure 14b).

### 6.2.4 Airway cell seeding on decellularized and synthetic tracheal scaffolds is associated with TSP1 expression.

To begin to investigate the role of TSP1-CD47 signaling in a tissue relevant setting we decellularized porcine tracheas and proximal airways as summarized in Figure 15a. Hematoxylin and eosin (H&E) staining demonstrated total cellular removal from the airway mucosal lining, although some cellular material was still present in cartilaginous rings (Figure 15b).

Control experiments found no detectable soluble TSP1 protein in stock HAEC media and matrix-conditioned HAEC media on ELISA (Figure 15c). However, immunoreactive TSP1 was histologically observed in intact porcine tracheas but was undetectable in decellularized porcine tracheal matrix (PTM) prior to cell seeding (Figure 15d). In contrast, immunoreactive TSP1 was detected in scaffolds (Figure 15d) 72 h following HAEC seeding. Interestingly, HAEC seeded onto both decellularized porcine trachea scaffolds and synthetic tracheal scaffolds as well as collagen coated cell culture wells all displayed TSP1 (Figure 15c) although absolute levels varied possible, in part, secondary to variation in cell adhesion and thus cell number.
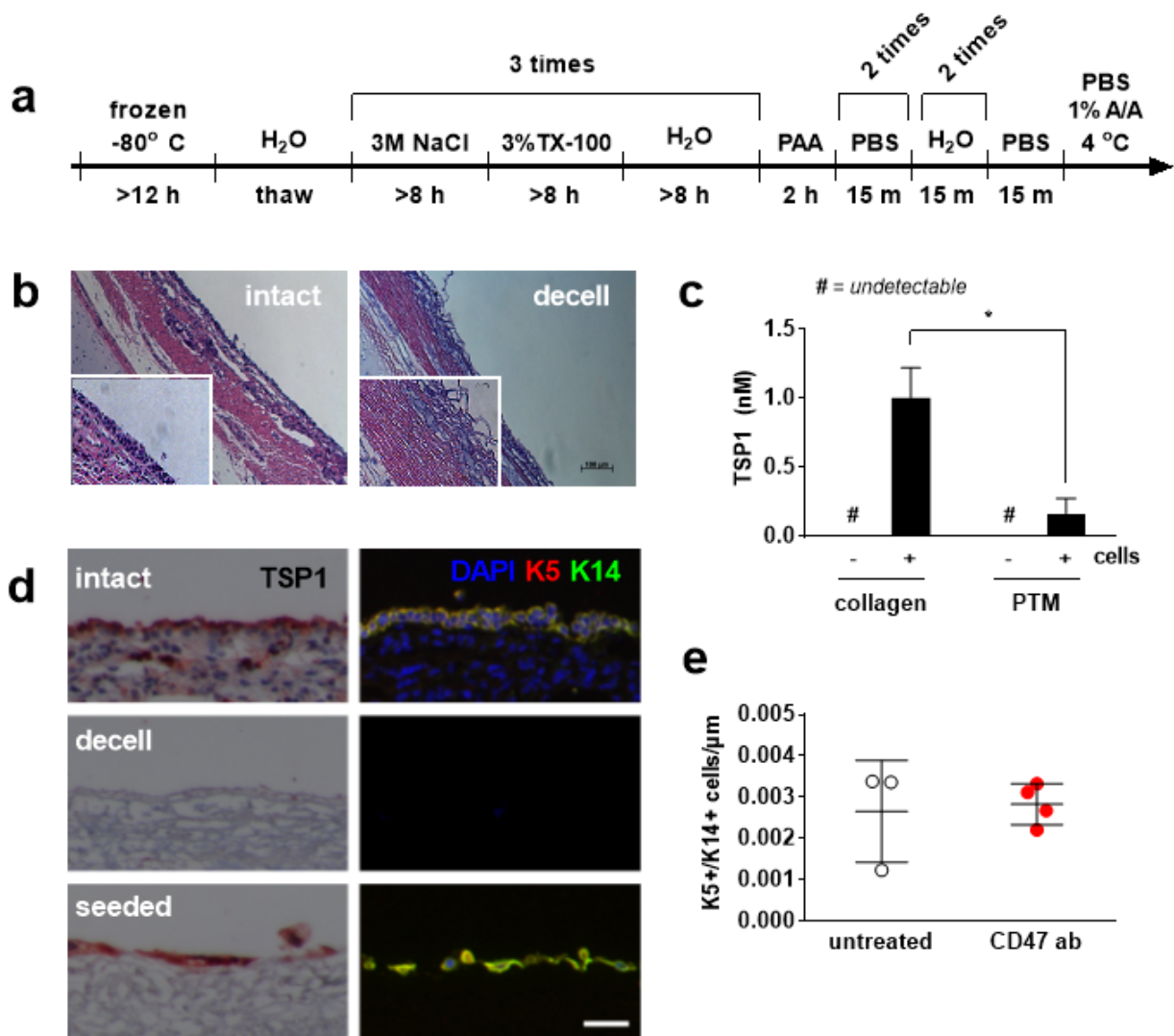
**Figure 15. Airway cell seeding on decellularized and synthetic tracheal scaffolds is associated with TSP1 expression.** (a) Serial washes under cyclic vacuum pressure effectively remove cellular material from porcine tracheas. (b) Hematoxylin and eosin stains of intact and decellularized tracheas. In both images, the lumen is at the upper right. Scale bar 100 microns (main image) and 20 microns (inset). (c) From left to right: TSP1 content in stock media, in media taken from cells seeded on collagen, in PTM-conditioned media, and media taken from cells seeded on PTM, after 72 hours. (d) Left, immunohistochemistry: TSP1 content in intact porcine trachea, porcine tracheal matrix, and HAEC seeded scaffolds. Right, immunofluorescence for keratin 5 (K5, red) keratin 14 (K14, green) and both (yellow), with a DAPI counterstain. (e) Quantification of dual-positive cells attached to PTM after seeding.

**6.2.5 Blockade of TSP1-CD47 signaling does not alter HAEC adhesion to porcine tracheal matrix.**

Lack of CD47 has been found to decrease adhesion in some cells [221]. Having found that TSP1 is expressed following airway cell seeding of decellularized airway scaffolds and that in cultured HAEC treatment with a CD47 blocking antibody increases self-renewal gene expression, we hypothesized that CD47 blockade might also alter HAEC adhesion to porcine airway scaffolds. HAEC ($1 \times 10^5$/scaffold) were seeded onto porcine decellularized airway scaffolds cut to fit within wells of 24-well plates. Cells were then treated with a CD47 blocking antibody (1.0 ug/ml). Histological stains showed no difference in nuclear counts in scaffolds treated with the CD47-blocking antibody versus the untreated controls (Figure 15e).

**6.2.6 Absence of CD47 is associated with increased expression of self-renewal genes in the trachea and proximal airway.**

New *in vitro* and *ex vivo* data suggests that TSP1-CD47 signaling limits airway healing. However, it was not clear if this signaling pathway was also suppressing airway restoration *in vivo*. We have previously reported that CD47 null mice display constitutive upregulation of the key self-renewal OSKM genes in tissues and isolated cells [103, 187]. Extending these studies, we characterized the expression profile of relevant genes in freshly harvested tracheas and proximal airways from male age-matched wild type and CD47 null mice. As expected, CD47 protein was not detected in tracheas from CD47 null mice (Figure 16a on page 114), although low levels of CD47 transcript were found (Figure 16b). In keeping with previously published reports [187], key genes associated with cellular self-renewal including Kl4 and Sox2 were

upregulated in airway tissue from CD47 null mice (Figure 16c). Coincident with this, tracheal and airway samples from CD47 null mice showed greater levels of the basal progenitor cell marker keratin 5 relative to samples from wild type controls (Figure 16d). Finally, tracheas and proximal airways from CD47 null mice displayed a greater number of cells expressing Ki67, a protein required for cell proliferation and increased during activation of the cell cycle [222], along the tracheal epithelium when compared to similar airway samples from wild type mice (Figure 16e).

### 6.2.7   CD47 null tracheas display enhanced angiogenic activity *ex vivo*

In the airway, it is thought that the rapid revascularization of a decellularized tracheal transplant, a process that likely involves both stromal and vascular cells [103], can promote re-epithelialization and prevent transplant loss [20]. Employing a model of tissue explantation we tested the angiogenic potential of tracheas and proximal airways *ex vivo*. The tissue explant outgrowth assay has been previously described in the literature and is recognized as a measure of angiogenic potential [184]. Explanted fresh tracheal segments from age-matched male wild type and CD47 null mice were embedded in type I collagen gels and cellular migration was quantified. After five days, cellular migration into the collagen gel was greater in CD47 null tracheal explants relative to wild type controls. (Figure 16g, h)  These results suggest increased wound healing capacity in CD47 null tracheas relative to those from wild-type mice.
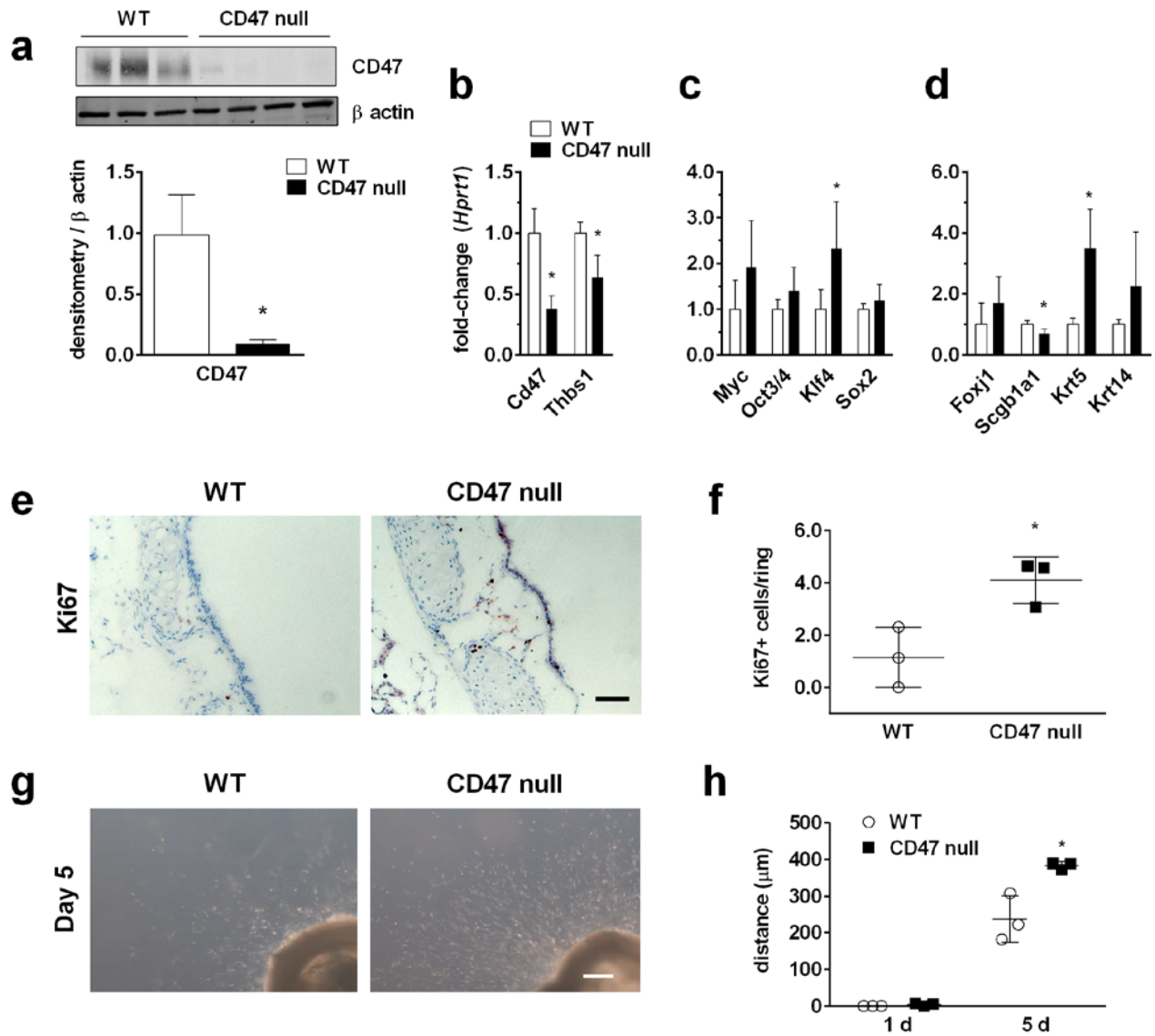
**Figure 16. Self-renewal, cell cycle activation and angiogenic responses are increased in CD47 null tracheas.**
(a) Western blot for CD47 protein. (b, c, d) Transcript levels of (b) *Cd47* and TSP1 gene *Thbs1*, (c) airway epithelial markers and (d) self-renewal markers (*n* = 5-7 tracheas, * indicates p < 0.05, error bars denote SD). (e, f) Quantification of Ki67+ nuclei along the airway epithelium at baseline (n = 3 animals, 9 rings counted per animal. * indicates p < 0.05, error bars denote SD, scale bar 50 μm.). (g) Explant outgrowth, is an *ex vivo* model of angiogenic capacity. (h) Explant outgrowth, quantified. Each symbol represents the mean distance traveled by the furthest 20 objects identified in each image captured of each ring. Each symbol represents one of *n* = 3 animals, error bars denote 1 SD, * indicates p < 0.05. Scale bar 200 μm.

### 6.2.8   Absence of CD47 provides for enhanced healing from chemical airway injury

Constitutive expression of increased proliferative and self-renewal genes in CD47 null airways might not correlate with improved healing after acute injury *in vivo*. To test this we employed intraperitoneal naphthalene, a commonly-used agent that provides for a reproducible degree of airway epithelial injury [22, 26-28]. Club cells within the airway epithelium convert naphthalene into a toxic metabolite which destroys these cells and adjacent non-club cells.  During the first week after naphthalene injury, keratin-5 (K5) expressing basal cells upregulate keratin-14 (K14), proliferate, and resurface the luminal surface of the trachea (Figure 17a) subsequently differentiating into the several cell types of the airway epithelium over the next several weeks. Given our *in vitro* results, we hypothesized that the early stages of this process (proliferation and resurfacing) would be accelerated in the trachea and proximal airways of CD47 null mice.

Age-matched male CD47 null and wild type mice received naphthalene (275 mg/kg, i.p.) and at the indicated time points tissue samples were acquired for analysis via immunohistology and Western blot. Immunofluorescent staining of tracheas collected four days after injury demonstrated patches of keratin-5/keratin-14 dual staining cells.  Four days after injury, a greater percentage of the luminal surface was covered with dual-staining cells in airways from CD47 null mice when compared to WT mice (Figure 17b). Approximately equal numbers of Ki67+ cells were observed at both time points (Figure 17c).

To further examine the observed differences in healing at four days, Western blots on were performed on bronchiolar tissue.  Wild type mice upregulated CD47 and TSP1 in response to injury. Airway samples from both WT and CD47 null mice demonstrated lower levels of CC10, a marker of club cells, however CD47 null samples nonetheless displayed greater levels than their WT counterparts (Figure 17d). We also examined the expression of OSKM markers of

self-renewal, in addition to the ΔN isoform of p63. In particular, Sox2 [15, 223], c-Myc [224], and ΔNp63 [225, 226] are associated with airway basal cell self-renewal and wound repair *in vivo.* After global chemical airway injury, CD47 null tissues showed greater levels of the transcription factor c-Myc and of ΔNp63 compared to wild-type mice (Figure 17e).

**6.2.9   Absence of CD47 is associated with accelerated resurfacing of decellularized orthotopic tracheal transplants.**

Data in mice indicates that the maladaptive TSP1-CD47 signal limits airway restoration following chemical injury. However, this is not exactly comparable to the complex healing of transplanted decellularized tracheal scaffolds. To integrate the role of the TSP1-CD47 axis in tracheal transplantation we conducted full orthotopic tracheal transplantation of decellularized tracheas obtained from wild type donor mice into both wild type and CD47 null recipient animals, as previously described [1]. After transplantation, keratin-5 expressing basal cells proliferate rapidly, upregulate keratin-14, and migrate into the graft to resurface the decellularized trachea in a manner reminiscent of wound healing after naphthalene injury [22, 26-28] (Figure 18a, b). Our previous study [1] has shown that the luminal surface of the decellularized tracheal transplant is completely re-surfaced with keratin-5/keratin-14 dual-expressing basal cells by post-transplant day seven.  Since new data demonstrated a difference in self-renewal gene expression between tracheas and airways from wild type and CD47 null mice four days after naphthalene injury, we hypothesized that an examination of K5+/K14+ expression after four days would demonstrate more rapid resurfacing of decellularized grafts transplanted into CD47 null mice.

Epithelial migration was measured from the far end of the native tracheal ring adjacent to the anastomosis to the leading edge of basal cell migration, as identified by keratin-5/keratin-14 dual staining (Figure 18b). As predicted, wild type decellularized tracheal transplants into orthotopic tracheal defects in CD47 null mice showed more rapid basal cell resurfacing than similar decellularized tracheal transplants into wild-type recipients (Figure 18c).
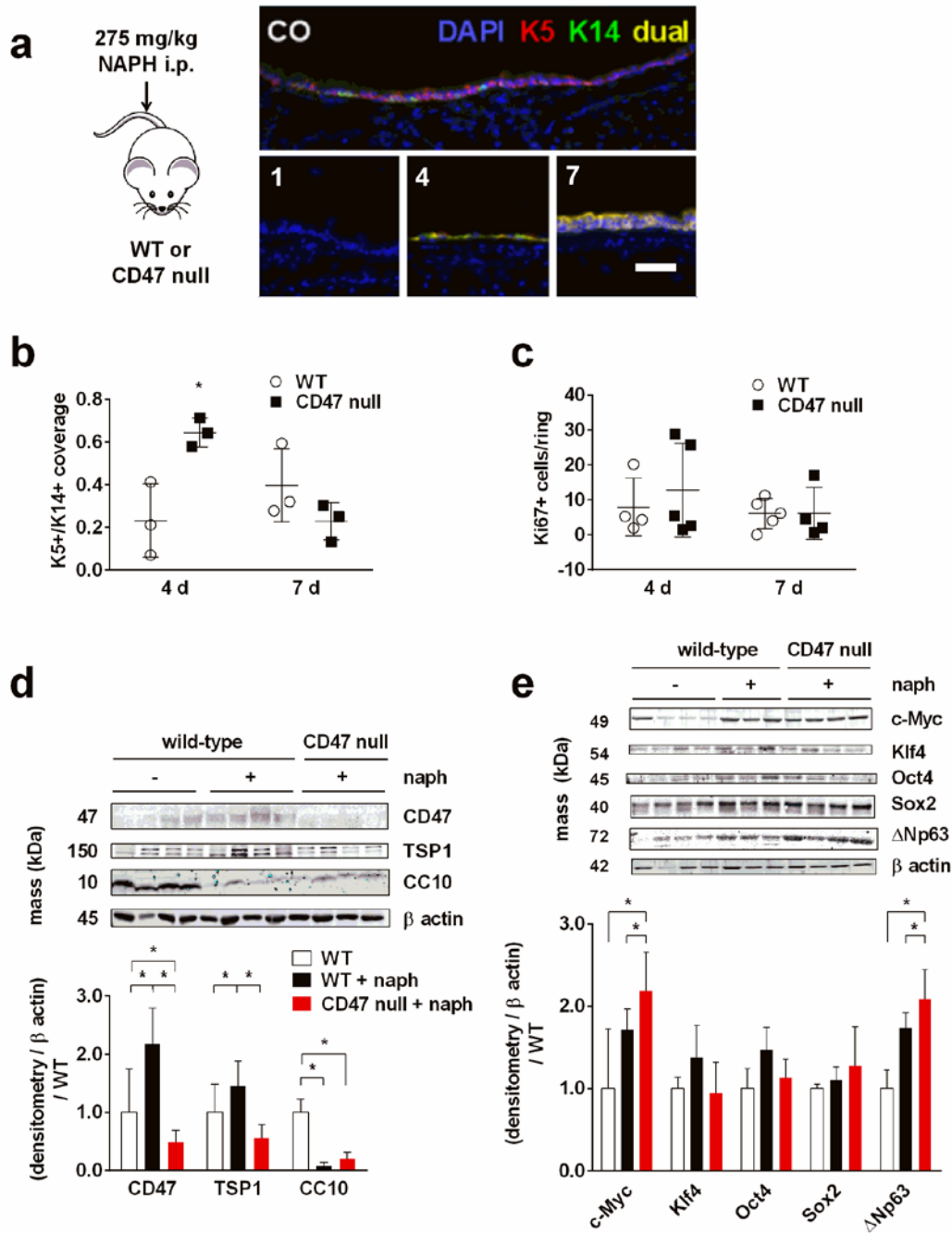
**Figure 17. CD47 null mice show greater expression of self-renewal markers 4 days after naphthalene airway injury.** (a) Male WT and CD47 null mice were treated with 275 mg/kg naphthalene in corn oil, i.p., and sacrificed after 4 or 7 days. A patchy distribution of squamoid epithelial cells was visible after 4 days. (b) Fraction of surface coverage at 4 and 7 days, calculated as (length of lumen covered with dual positive cells) / (total length of lumen measured). (c) Ki67+ cells along the airway lumen after naphthalene injury. (d) CD47 and TSP1 expression in WT and CD47 null mice after four days. (e) Transcription factor expression in WT and CD47 null mice after 4 days. (n = 3-4 tracheas, * indicates $p < 0.05$ by t-test, error bars denote SD).
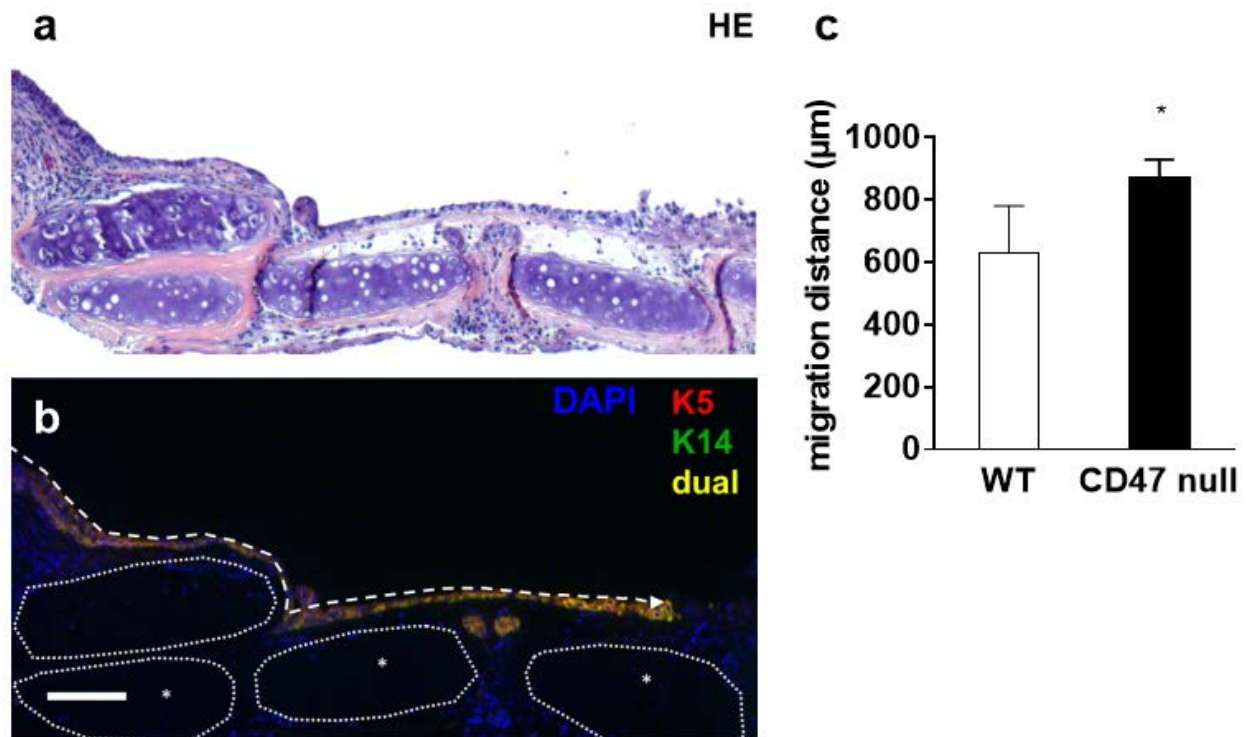
**Figure 18. Absence of CD47 accelerates resurfacing of decellularized orthotopic tracheal transplants.** (a) Hematoxylin and eosin staining of a representative slide at the site of anastomoses. (b) Immunolabeling demonstrates a clear migratory front. Dotted line indicates measured distance. In image, * = decellularized graft ring. Scale 100 μm and applies to (a, b). (c) Quantification of migration from n = 3 mice in each group. (* indicates $p < 0.05$, bars denote SD.)

## 6.3     DISCUSSION

Clinical human bioengineered tracheal transplantation has been hampered by significant morbidity and mortality and a lack of evidence confirming transplant integration and healing. However, the molecular cues responsible for these disappointing outcomes remain unknown. In contrast, we herein provide data that maladaptive TSP1-CD47 is a major impediment to tracheal epithelial and tracheal transplant healing. The findings of this study are novel and include (1) that TSP1 is induced in isolated airway epithelial cells on seeding onto decellularized scaffolds, (2) that hypoxia, as a mimic of the tracheal transplantation injury, is a potent stimulator of TSP1 expression in human airway epithelial cells; (3) that in cell culture systems TSP1 can impede tracheal epithelial cell proliferation and this can be reversed by interference with TSP1-CD47 interaction; (4) that genetic absence of TSP1-CD47 signaling  is associated with an enhanced restorative profile in isolated airway epithelial cells, increased angiogenic sprouting of airways in response to hypoxia and (5) increased tracheal/proximal airway healing after chemical ablation and resurfacing of decellularized tracheal transplants. The translational significance of these findings is emphasized by the fact that humanized CD47 antibodies have been generated [227] and recently entered clinical trials [228].

Regeneration is a function of cell reprograming from differentiated to de-differentiated followed by migration, proliferation and finally differentiation. TSP1 has been previously shown to inhibit the migration of endothelial cells [148] while promoting migration of certain other cell populations [229]. In our study, the presence of TSP1 in media did not alter the rate at which human airway epithelial cells resurfaced a wound. In contrast, the CD47 blocking antibody

B6H12 promoted wound closure in both the presence and absence of TSP1. At the same time TSP1 limited tracheal epithelial cell proliferation via CD47. Together, these data suggest that *in vitro* TSP1 preferentially targets the epithelial cell cycle and thus proliferation rather than migration. Whole tissue data supports this as the lack of TSP1-CD47 signaling in tracheas from null mice was associated with increased expression of the essential proliferation gene Ki67. We recently reported that hypoxia via HIF-2α induced upregulation of TSP1 in pulmonary arterial endothelial cells [159]. We now find that hypoxia also potently induces TSP1 in pulmonary epithelial cells. However, in hypoxic pulmonary endothelial cells TSP1 promoted increased migration [159]. It is possible that under hypoxic conditions TSP1 would alter tracheal epithelial cells migration to enhance in vitro wound closure but this was not tested.

Regardless, these new and published studies suggest that under the ischemic and hypoxic stress of bioengineered tracheal transplantation induction of TSP1 would target multiple cells types including endothelial and epithelial cells to limit cellular reprogramming, restoration and healing. The finding of increased expression of the reprograming/self-renewal cassette OSKM in CD47 null tracheal epithelial cells indicates that the TSP1-CD47 axis is a constitutive and proximate inhibitor of this process in the airway. CD47 null mice enjoyed healing advantages after airway chemical ablation as well as after orthotopic decellularized tracheal transplantation. These new findings are consistent with previous reports indicated improved tissue healing in the absence of CD47 [106, 107]. In some of these situations more rapid healing was associated with increased tissue blood flow in the CD47 null animals. While a tissue perfusion advantage may have promoted enhanced healing in CD47 null mice after naphthalene compared to wild type, this was less likely to have been a factor in the orthotopic decellularized tracheal transplant

model. Thus, in the proximal airway TSP1-CD47 signaling appears to limit healing in both blood flow-dependent and -independent mechanisms.

Limitations of this work are several. First, the murine model of orthotopic transplantation, while providing confirmation of the role of TSP-1CD47 signaling plays in limiting the healing of decellularized tracheal transplants, does not fully recapitulate the complex environment of human tracheal transplantation. Especially obvious is the ability of decellularized transplants to survive in mice in the absence of soft tissue flaps as a source of angiogenesis and immune cells. Although angiogenic activity was greater in CD47 null tracheal explants compared to wild type, the implications of this were not assessed in our analysis of decellularized tracheal transplants. Another limitation is that it is not clear what role, if any, the TSP1-CD47 axis plays in regulating chondrocyte restoration. TSP1 is expressed in mature chondrocytes [230, 231] whereas CD47 is induced during chondrocyte differentiation [232]. Conversely, chondrocyte dedifferentiation is maintained by Klf4 [233], and as we have reported TSP1-CD47 signaling represses Klf4 [187]. Together these results suggest that hypothesis that TSP1-CD47 signaling also targets chondrocytes to limit cartilage restoration. It remains to be seen if chondrocyte repopulation of decellularized tracheal matrix is regulated by TSP1-CD47. Finally, the ability of a CD47 blocking antibody to improve the healing of decellularized tracheal transplant in wild type animals requires testing.

## 6.4    CONCLUSIONS

We hypothesized that TSP1-CD47 signaling is induced in airway epithelial and endothelial cells to limit restoration of decellularized tracheal transplants. The experiments described herein

demonstrate that TSP1-CD47 signaling is upregulated in hypoxic tracheal epithelial cells, in chemically injured airways, in epithelial cells seeded on decellularized grafts, and in engineered tracheal transplants. CD47 null mice have higher tracheal levels of self-renewal factors at baseline and after injury. In keeping with this observation, they show more rapid resurfacing after chemical injury and orthotopic decellularized tracheal transplantation. These findings suggest that modulation of the TSP1-CD47 signaling pathway could be beneficial in bioengineered transplants. Future experiments will examine the role of TSP1 and CD47 signaling in synthetic tracheal grafts, and will explore the use of CD47 blocking antibodies as a therapeutic agent to promote cell survival within tissue engineered grafts.

# APPENDIX A

## CYTOANALYSIS: A PROGRAM TO ANALYZE CYTOSPIN SLIDES

This script was developed in order to perform automated image analysis on cytospin slides, and sort cells into ("high") and ("low") expression categories along one or two axes (in a manner similar to flow sorting.) The program was written by the author. Usage is as follows.

```
runcytoanalysis(folder, filters, markers, universalmarker, minsharedpixelfraction, intensitythreshold,
minArea, maxArea, outputfile)
```

**folder** = the folder containing all the images to be analyzed; **filters** and **markers** = arrays of (1) file type filters and the markers they correspond to. For instance, the first row in each of those arrays might be "*dapi*.tif" and "DAPI"; the program would associate any file matching the filter given with the DAPI marker. **universalmarker** is the index of the marker which should stain all cells (e.g., DAPI). **Intesnitythreshold** is the pixel value threshold corresponding to the boundary between "High" and "Low" expression of a

given marker. **minsharedpixelfraction** tells how much two objects must overlap with the universal marker before they are considered

to be the same object – e.g., if **minsharedpixelfraction** = 0.6, then an object in the red channel must share (60%) of its pixels with an

object in the universal channel in order to associate them in program memory. **minArea** and **maxArea** allow the user to filter out

objects which are too small or two large. **outputfile** is a data file which receives the summary data.

## A.1 RUNCYTOANALYSIS

```
function [allvalues] = runcytoanalysis(folder, filters, markers, universalmarker, minsharedpixelfraction,
intensitythreshold, minArea, maxArea, outputfile)

% minsharedpixelfraction is the fraction of pixels an object must share with a
% cell stained with the universal marker in order to be considered the same
% cell.  The minimum area for this is a fraction of the smaller object'
% area.

xlswrite(outputfile, {' ', 'Mean (I)' , 'Stdev (I)', 'n (I)', 'Intensity Threshold', 'Mean (area)', 'Stdev
(area)'}, 'Summary', 'A1');
summaryrow = 2;

% Build file list for the universal marker, and generate a list of pixels
% for each cell stained by the universal marker.
if ~strcmp(universalmarker, '')
    m = find(ismember(markers, {universalmarker}));
    [status, text] = system(char(strcat('dir "',folder, filters(m),'" /b')));
    umfilelist = strsplit(text, char(10));
    for f = 1:length(umfilelist) - 1
        gray = imread(char(fullfile(folder,umfilelist(f))));
```

```matlab
        mask = im2bw(gray, graythresh(gray));

        % Build pixel lists which can be accessed with
        %        umimstats{[file number]}([cell number]).PxlIdxList
        umimstats{f} = regionprops(mask, gray, {'Area', 'MeanIntensity', 'PixelIdxList'});
        [umimstats{f}(:).IValues] = deal(zeros(length(markers), 1));

        % Remove objects which are too small to be cells
        j = 1;
        while j < length(umimstats{f})
            if (umimstats{f}(j).Area < minArea(m)) || (umimstats{f}(j).Area > maxArea(m))
                umimstats{f}(j) = [];
            else
                umimstats{f}(j).IValues(m) = umimstats{f}(j).MeanIntensity;
                j = j + 1;
            end
        end
        % pp = umimstats{f}(1).PixelIdxList

    end
end

for m = 1:length(markers)
    [status, text] = system(char(strcat('dir "',folder, filters(m),'" /b')));
    filelist = strsplit(text, char(10));

    area = [];
    centroid = [];
    centroidx = [];
    centroidy = [];
    meanI = [];
    minI = [];
    maxI = [];
    threshold = [];



    for i = 1:length(filelist) - 1

        gray = imread(char(fullfile(folder,filelist(i))));
        mask = im2bw(gray, graythresh(gray));
```

126

```matlab
        % Keep in mind that the output of imstats will not necessarily be in the order given below.
        imstats = regionprops(mask, gray, {'Area', 'Centroid', 'PixelIdxList', 'MeanIntensity',
'MinIntensity', 'MaxIntensity'});
        % umimstats{f}(1).area
        j = 1;

        while j < (length(imstats))
            if (imstats(j).Area < minArea(m)) || (imstats(j).Area > maxArea(m))
                imstats(j) = [];
            else
                % See how many of my pixels correspond to a given item in the unversal marker list
                if ~strcmp(universalmarker, '') && ~strcmp(universalmarker, markers(m))
                    for k = 1:length(umimstats{i})
                        overlap = length(intersect(imstats(j).PixelIdxList, umimstats{i}(k).PixelIdxList));
                        if overlap > 0

                            if imstats(j).Area < umimstats{i}(k).Area
                                smallerarea = length(imstats(j).PixelIdxList);
                            else
                                smallerarea = length(umimstats{i}(k).PixelIdxList);
                            end
                            overlapratio = overlap/smallerarea;
                            if minsharedpixelfraction <= overlapratio
                                umimstats{i}(k).IValues(m) = imstats(j).MeanIntensity;

                            end
                            break;  % Leave the loop, since we've found your match
                        end
                    end
                end
            end

            j = j + 1;

        end
    end

    imstatsarray = struct2cell(imstats);
    area = [area cell2mat(imstatsarray(1, :, :))];
    centroid = cell2mat(imstatsarray(2, :, :));
```

127

```matlab
        for c = 1:length(centroid)/2
            centroidx = [centroidx centroid(c*2-1)] ;
            centroidy = [centroidy centroid(c*2)] ;
        end

        meanI = [meanI cell2mat(imstatsarray(4, :, :))];
        minI = [minI cell2mat(imstatsarray(5, :, :))];
        maxI = [maxI cell2mat(imstatsarray(6, :, :))];

    end




    % Determine whether each cell's intensity value exceeded the threshold
    threshold = (meanI >= intensitythreshold(m));

    % Sort intensities and areas depending on whether or not cells
    % exceeded the threshold.
    posI = [];
    posA = [];
    negI = [];
    negA = [];

    for j = 1:length(threshold)
        if threshold(j) == 1
            posI = [posI meanI(j)];
            posA = [posA area(j)];
        else
            negI = [negI meanI(j)];
            negA = [negA area(j)];
        end
    end


    % Write all my data to the sheet in the output file
    header = {'Area', 'CentroidX', 'CentroidY', 'MeanI', 'MinI', ' MaxI', 'Exceeds Threshold'};
    xlsarray = transpose([area; centroidx; centroidy; meanI; double(minI); double(maxI);
double(threshold)]);
    xlswrite(outputfile, header, char(markers(m)));
    xlswrite(outputfile, xlsarray, char(markers(m)), 'A2');
```

128

```matlab
    % Write to summary data to summary sheet in output file
    xlswrite(outputfile, [markers(m), mean(meanI), std(meanI), length(meanI), intensitythreshold(m),
mean(area), std(area)], 'Summary', ['A' int2str(summaryrow)]);
    xlswrite(outputfile, [strcat(markers(m),', I>threshold'), mean(posI), std(posI), length(posI), ' ',
mean(posA), std(posA)], 'Summary', ['A' int2str(summaryrow+1)]);
    xlswrite(outputfile, [strcat(markers(m),', I<threshold'), mean(negI), std(negI), length(negI), ' ',
mean(negA), std(negA)], 'Summary', ['A' int2str(summaryrow+2)]);
    summaryrow = summaryrow + 3;

end
allvalues = [];
for i = 1:(length(filelist) - 1)
    for k = 1:(length(umimstats{i}))
        allvalues = [allvalues ; transpose(umimstats{i}(k).IValues)];
    end
end

xlswrite(outputfile, markers, 'All Cells', 'A1');
xlswrite(outputfile, allvalues, 'All Cells', 'A2');

%
return
```

**EXPLANTDATA: A SCRIPT TO QUANTIFY EXPLANT ASSAYS**

This script was written by me, with the exception of the function `p_poly_dist` which calculates the distance between a point and a polygon. Usage is as follows:

```
explantdata(path, ext, fileOut1, pixelspermicron, maxN)
```

**path** = the folder containing all '.dat' files (without a backslash at the end) ; **ext** = the file extension ('*.dat'); **fileOut** = the output spreadsheet; **pixelspermicron** = a conversion factor which depends on the magnification; and **maxN** = the maximum number of cells to use when calculating distances. The program will calculate the mean distance traveled by the furthest **maxN** cells in the image.

*Example:*

```
explantdata('K:\Data\20130811', '*.dat', '20130811.xls', 1.0, 20)
```

## B.1    FILE: EXPLANTDATA.M

```matlab
function explantdata(path, ext, fileOut1, pixelspermicron, maxN)

files = dir ([path '\*' ext]);
s = size(files);
A = [];
cells = [];
polygon = [];
mymed = 0;
mymean = 0;
mystdev = 0;
myN = 0;
myArea = 0;
myName = '';
fileOut = [path '\' fileOut1];
xlswrite(fileOut, [cellstr('File') cellstr('Mean dist') cellstr('StDev') cellstr('N') cellstr('Median
dist') cellstr('PolyArea')], 'Summary', 'A1:F1');
for f = [1:s(1)]
    A = [];
    cells = [];
    polygon = [];
    mymed = 0;
    mymean = 0;
    mystdev = 0;
    myN = 0;
    myArea = 0;
    myName = files(f).name;
```

```matlab
    xlswrite(fileOut, [cellstr('x') cellstr('y') cellstr('dist')], myName, 'A1:C1');
    xlswrite(fileOut, [cellstr('Mean dist'); cellstr('StDev'); cellstr('N'); cellstr('Median dist');
cellstr('PolyArea')], myName, 'E1:E5');
    xlswrite(fileOut, [cellstr('poly x') cellstr('poly y')], myName, 'H1:I1');

    A = importdata([path '\' myName]);
    disp (['Analyzing ' myName '...']);

    [cells, polygon] = analyzeexplantdata(A.data, 1, 2, pixelspermicron);

    cells = sortrows(cells, 3);

    if length(polygon(:, 1)) < 3
        disp(['Warning: ' files(f).name ' has insufficient polygon points defined.'])

    else
        myArea = polyarea(polygon(:, 1), polygon(:, 2));
        xlswrite(fileOut, myArea, myName, 'F5');
        xlswrite(fileOut, [polygon], myName, ['H2:I' num2str(length(polygon(:, 1))+1)]);
    end

    if size(cells) == [0, 0]
        disp(['Warning: ' files(f).name ' has insufficient cells defined.'])
    else

        myN = length(cells(:, 3));

        if maxN ~= -1
            if myN > maxN
                cells = cells(myN-maxN + 1:myN, :);
                myN = length(cells(:, 3));
            end
        end

        mymed = median(cells(:, 3));
        mymean = mean(cells(:, 3));
        mystdev = std(cells(:, 3));
```

```matlab
        xlswrite(fileOut, [cells], myName, ['A2:C' num2str(myN+1)]);
        xlswrite(fileOut, [mymean; mystdev; myN; mymed], myName, 'F1:F4');

    end
    xlswrite(fileOut, [cellstr(myName) num2str(mymean) num2str(mystdev) num2str(myN) num2str(mymed)
num2str(myArea)], 'Summary', ['A' num2str(f+1) ':F' num2str(f+1)]);


end


disp('Done.');


end


function [cells, polygon] = analyzeexplantdata(datamatrixfromfile, celltypeID, polygontypeID,
pixelspermicron)
s = size(datamatrixfromfile);
polygon = [];
cells = [];
for r = [1:s(1)]
    if datamatrixfromfile(r, 1) == polygontypeID
        newrow = [datamatrixfromfile(r, 3) datamatrixfromfile(r, 4)];
        polygon = [polygon; newrow];
    elseif datamatrixfromfile(r, 1) == celltypeID
        newrow = [datamatrixfromfile(r, 3) datamatrixfromfile(r, 4) -1];
        cells = [cells; newrow];
    end
end


s = size(cells);
for r = [1:s(1)]
    cells(r, 3) = p_poly_dist(cells(r, 1), cells(r, 2), polygon(:, 1), polygon(:, 2));
end
cells = cells / pixelspermicron;
polygon = polygon / pixelspermicron;


end
```

133

```
%*****************************************************************************
% function: p_poly_dist
% Description:  distance from point to polygon whose vertices are specified by the
%               vectors xv and yv
% Input:
%    x - point's x coordinate
%    y - point's y coordinate
%    xv - vector of polygon vertices x coordinates
%    yv - vector of polygon vertices x coordinates
% Output:
%    d - distance from point to polygon (defined as a minimal distance from
%        point to any of polygon's ribs, positive if the point is outside the
%        polygon and negative otherwise)
%    x_poly: x coordinate of the point in the polygon closest to x,y
%    y_poly: y coordinate of the point in the polygon closest to x,y
%
% Routines: p_poly_dist.m
% Revision history:
%    03/31/2008 - return the point of the polygon closest to x,y
%               - added the test for the case where a polygon rib is
%                   either horizontal or vertical. From Eric Schmitz.
%               - Changes by Alejandro Weinstein
%    7/9/2006  - case when all projections are outside of polygon ribs
%    23/5/2004 - created by Michael Yoshpe
% Remarks:
%*****************************************************************************
function [d,x_poly,y_poly] = p_poly_dist(x, y, xv, yv)


% If (xv,yv) is not closed, close it.
xv = xv(:);
yv = yv(:);
Nv = length(xv);
if ((xv(1) ~= xv(Nv)) || (yv(1) ~= yv(Nv)))
    xv = [xv ; xv(1)];
    yv = [yv ; yv(1)];
%     Nv = Nv + 1;
end


% linear parameters of segments that connect the vertices
% Ax + By + C = 0
```

```matlab
A = -diff(yv);
B =  diff(xv);
C = yv(2:end).*xv(1:end-1) - xv(2:end).*yv(1:end-1);

% find the projection of point (x,y) on each rib
AB = 1./(A.^2 + B.^2);
vv = (A*x+B*y+C);
xp = x - (A.*AB).*vv;
yp = y - (B.*AB).*vv;

% Test for the case where a polygon rib is
% either horizontal or vertical. From Eric Schmitz
id = find(diff(xv)==0);
xp(id)=xv(id);
clear id
id = find(diff(yv)==0);
yp(id)=yv(id);

% find all cases where projected point is inside the segment
idx_x = (((xp>=xv(1:end-1)) & (xp<=xv(2:end))) | ((xp>=xv(2:end)) & (xp<=xv(1:end-1))));
idx_y = (((yp>=yv(1:end-1)) & (yp<=yv(2:end))) | ((yp>=yv(2:end)) & (yp<=yv(1:end-1))));
idx = idx_x & idx_y;

% distance from point (x,y) to the vertices
dv = sqrt((xv(1:end-1)-x).^2 + (yv(1:end-1)-y).^2);

if(~any(idx)) % all projections are outside of polygon ribs
    [d,I] = min(dv);
    x_poly = xv(I);
    y_poly = yv(I);
else
    % distance from point (x,y) to the projection on ribs
    dp = sqrt((xp(idx)-x).^2 + (yp(idx)-y).^2);
    [min_dv,I1] = min(dv);
    [min_dp,I2] = min(dp);
    [d,I] = min([min_dv min_dp]);
    if I==1, %the closest point is one of the vertices
        x_poly = xv(I1);
        y_poly = yv(I1);
    elseif I==2, %the closest point is one of the projections
```

```matlab
            idxs = find(idx);
            x_poly = xp(idxs(I2));
            y_poly = yp(idxs(I2));
        end
    end


    if(inpolygon(x, y, xv, yv))
        d = -d;
    end


end
```

# BIBLIOGRAPHY

[1.]     Kutten, J.C., et al., *Decellularized tracheal extracellular matrix supports epithelial migration, differentiation, and function.* Tissue Eng Part A, 2015. **21**(1-2): p. 75-84.

[2.]     Treuting, P.M., et al., *Comparative anatomy and histology : a mouse and human atlas.* 1st ed. 2012, Amsterdam ; Boston: Elsevier/Academic Press. xii, 461 p.

[3.]     Sasson, J.P., et al., *Anatomy, imaging, and pathology of the trachea*, in *Head and Neck Imaging*, P.M. Som and H.D. Curtin, Editors. 2011, Mosby, Inc.: St. Louis, MO. p. 2041-2084.

[4.]     Minnich, D.J. and D.J. Mathisen, *Anatomy of the trachea, carina, and bronchi.* Thorac Surg Clin, 2007. **17**(4): p. 571-85.

[5.]     Ni, A., et al., *Rapid remodeling of airway vascular architecture at birth.* Dev Dyn, 2010. **239**(9): p. 2354-66.

[6.]     McDonald, D.M., L.C. Yao, and P. Baluk, *Dynamics of airway blood vessels and lymphatics: lessons from development and inflammation.* Proc Am Thorac Soc, 2011. **8**(6): p. 504-7.

[7.]     Brand-Saberi, B.E. and T. Schafer, *Trachea: anatomy and physiology.* Thorac Surg Clin, 2014. **24**(1): p. 1-5.

[8.]     Cardoso, W.V. and J. Lu, *Regulation of early lung morphogenesis: questions, facts and controversies.* Development, 2006. **133**(9): p. 1611-24.

[9.]     Domyan, E.T., et al., *Signaling through BMP receptors promotes respiratory identity in the foregut via repression of Sox2.* Development, 2011. **138**(5): p. 971-81.

[10.]    Que, J., et al., *Multiple dose-dependent roles for Sox2 in the patterning and differentiation of anterior foregut endoderm.* Development, 2007. **134**(13): p. 2521-31.

[11.]    Morrisey, E.E. and B.L. Hogan, *Preparing for the first breath: genetic and cellular mechanisms in lung development.* Dev Cell, 2010. **18**(1): p. 8-23.

[12.] Hashimoto, S., et al., *beta-Catenin-SOX2 signaling regulates the fate of developing airway epithelium.* J Cell Sci, 2012. **125**(Pt 4): p. 932-42.

[13.] Tompkins, D.H., et al., *Sox2 activates cell proliferation and differentiation in the respiratory epithelium.* Am J Respir Cell Mol Biol, 2011. **45**(1): p. 101-10.

[14.] Tompkins, D.H., et al., *Sox2 is required for maintenance and differentiation of bronchiolar Clara, ciliated, and goblet cells.* PLoS One, 2009. **4**(12): p. e8248.

[15.] Que, J., et al., *Multiple roles for Sox2 in the developing and adult mouse trachea.* Development, 2009. **136**(11): p. 1899-907.

[16.] Arora, R., R.J. Metzger, and V.E. Papaioannou, *Multiple roles and interactions of Tbx4 and Tbx5 in development of the respiratory system.* PLoS Genet, 2012. **8**(8): p. e1002866.

[17.] Turcatel, G., et al., *Lung mesenchymal expression of Sox9 plays a critical role in tracheal development.* BMC Biol, 2013. **11**: p. 117.

[18.] Grillo, H.C., *Tracheal replacement: a critical review.* Ann Thorac Surg, 2002. **73**(6): p. 1995-2004.

[19.] Delaere, P.R. and D. Van Raemdonck, *The trachea: the first tissue-engineered organ?* J Thorac Cardiovasc Surg, 2014. **147**(4): p. 1128-32.

[20.] Okumura, N., et al., *Experimental study on a new tracheal prosthesis made from collagen-conjugated mesh.* J Thorac Cardiovasc Surg, 1994. **108**(2): p. 337-45.

[21.] Hackett, N.R., et al., *The human airway epithelial basal cell transcriptome.* PLoS One, 2011. **6**(5): p. e18378.

[22.] Hong, K.U., et al., *Basal cells are a multipotent progenitor capable of renewing the bronchial epithelium.* Am J Pathol, 2004. **164**(2): p. 577-88.

[23.] Hong, K.U., et al., *In vivo differentiation potential of tracheal basal cells: evidence for multipotent and unipotent subpopulations.* Am J Physiol Lung Cell Mol Physiol, 2004. **286**(4): p. L643-9.

[24.] Rock, J.R., et al., *Basal cells as stem cells of the mouse trachea and human airway epithelium.* Proc Natl Acad Sci U S A, 2009. **106**(31): p. 12771-5.

[25.] Rock, J.R., S.H. Randell, and B.L. Hogan, *Airway basal stem cells: a perspective on their roles in epithelial homeostasis and remodeling.* Dis Model Mech, 2010. **3**(9-10): p. 545-56.

[26.] Sonar, S.S. and J.C. Dudda, *Clara epithelial cell depletion in the lung.* Methods Mol Biol, 2013. **1032**: p. 229-34.

[27.] Liu, X., R.R. Driskell, and J.F. Engelhardt, *Stem cells in the lung.* Methods Enzymol, 2006. **419**: p. 285-321.

[28.] Liu, X., et al., *Characterization of Lef-1 promoter segments that facilitate inductive developmental expression in skin.* J Invest Dermatol, 2004. **123**(2): p. 264-74.

[29.] Rock, J.R., et al., *Notch-dependent differentiation of adult airway basal stem cells.* Cell Stem Cell, 2011. **8**(6): p. 639-48.

[30.] Musah, S., J. Chen, and G.W. Hoyle, *Repair of tracheal epithelium by basal cells after chlorine-induced injury.* Respir Res, 2012. **13**: p. 107.

[31.] Reynolds, S.D. and A.M. Malkinson, *Clara cell: progenitor for the bronchiolar epithelium.* Int J Biochem Cell Biol, 2010. **42**(1): p. 1-4.

[32.] Smith, P., D. Heath, and H. Moosavi, *The Clara cell.* Thorax, 1974. **29**(2): p. 147-63.

[33.] Roomans, G.M., *Tissue engineering and the use of stem/progenitor cells for airway epithelium repair.* Eur Cell Mater, 2010. **19**: p. 284-99.

[34.] Luo, X., et al., *Long-term functional reconstruction of segmental tracheal defect by pedicled tissue-engineered trachea in rabbits.* Biomaterials, 2013. **34**(13): p. 3336-44.

[35.] Stoelben, E., et al., *Benign stenosis of the trachea.* Thorac Surg Clin, 2014. **24**(1): p. 59-65.

[36.] Kugler, C. and F. Stanzel, *Tracheomalacia.* Thorac Surg Clin, 2014. **24**(1): p. 51-8.

[37.] Rutter, M.J., et al., *Slide tracheoplasty for the management of complete tracheal rings.* J Pediatr Surg, 2003. **38**(6): p. 928-34.

[38.] Kim, H.K., et al., *Management of congenital tracheal stenosis.* Eur J Cardiothorac Surg, 2004. **25**(6): p. 1065-71.

[39.] Grillo, H.C., et al., *Management of congenital tracheal stenosis by means of slide tracheoplasty or resection and reconstruction, with long-term follow-up of growth after slide tracheoplasty.* J Thorac Cardiovasc Surg, 2002. **123**(1): p. 145-52.

[40.] ten Hallers, E.J., et al., *Animal models for tracheal research.* Biomaterials, 2004. **25**(9): p. 1533-43.

[41.] Tsang, V., et al., *Slide tracheoplasty for congenital funnel-shaped tracheal stenosis.* Ann Thorac Surg, 1989. **48**(5): p. 632-5.

[42.] Ergun, S., T. Tewfik, and S. Daniel, *Tracheal agenesis: A rare but fatal congenital anomaly.* Mcgill J Med, 2011. **13**(1): p. 10.

[43.] de Groot-van der Mooren, M.D., et al., *Tracheal agenesis: approach towards this severe diagnosis. Case report and review of the literature.* Eur J Pediatr, 2012. **171**(3): p. 425-31.

[44.] Junker, K., *Pathology of tracheal tumors.* Thorac Surg Clin, 2014. **24**(1): p. 7-11.

[45.] Behringer, D., S. Konemann, and E. Hecker, *Treatment approaches to primary tracheal cancer.* Thorac Surg Clin, 2014. **24**(1): p. 73-6.

[46.] Lancet, E., *Expression of concern--Tracheobronchial transplantation with a stem-cell-seeded bioartificial nanocomposite: a proof-of-concept study.* Lancet, 2016. **387**(10026): p. 1359.

[47.] Haykal, S., et al., *Advances in tracheal reconstruction.* Plast Reconstr Surg Glob Open, 2014. **2**(7): p. e178.

[48.] Tan, Q., et al., *Tissue-engineered trachea: History, problems and the future.* Eur J Cardiothorac Surg, 2006. **30**(5): p. 782-6.

[49.] Gilbert, T.W., *Strategies for tissue and organ decellularization.* J Cell Biochem, 2012. **113**(7): p. 2217-22.

[50.] Gilbert, T.W., T.L. Sellaro, and S.F. Badylak, *Decellularization of tissues and organs.* Biomaterials, 2006. **27**(19): p. 3675-83.

[51.] Chiang, T., et al., *Clinical Translation of Tissue Engineered Trachea Grafts.* Ann Otol Rhinol Laryngol, 2016.

[52.] Hamilton, N., et al., *Tissue engineering airway mucosa: a systematic review.* Laryngoscope, 2014. **124**(4): p. 961-8.

[53.] Bogan, S.L., G.Z. Teoh, and M.A. Birchall, *Tissue Engineered Airways: A Prospects Article.* J Cell Biochem, 2016. **117**(7): p. 1497-505.

[54.] Lange, P., et al., *Pilot study of a novel vacuum-assisted method for decellularization of tracheae for clinical tissue engineering applications.* J Tissue Eng Regen Med, 2015.

[55.] Viera, M., *A Leap of Faith*, in *Dateline NBC*. 2014, NBC News: New York. p. 82 minutes.

[56.] Jungebluth, P. and P. Macchiarini, *Airway transplantation.* Thorac Surg Clin, 2014. **24**(1): p. 97-106.

[57.]    Vogel, G., *Trachea transplants test the limits.* Science, 2013. **340**(6130): p. 266-8.

[58.]    Brånstad, J., *Experimenten.* 2016, SVT. p. 3 hours.

[59.]    Vogel, G., *Regenerative medicine. Report finds misconduct by surgeon.* Science, 2015. **348**(6238): p. 954-5.

[60.]    Vogel, G., *SCIENTIFIC MISCONDUCT. Karolinska to reopen inquiry into surgeon's work.* Science, 2016. **351**(6273): p. 546.

[61.]    Polyakov, I., et al. *Artificialtracheo-Laryngeal Complex Transplantation In Patients With Tracheal Diseases. Early Results (A 6-Month Follow-Up Period). Krasnodar (Russian Federation) Experience*. in *21st European Conference onGeneral Thoracic Surgery* 2013. Birmingham, UK: InteractiveCardioVascularand Thoracic Surgery.

[62.]    Corbascio, M., et al., *Analysis of Clinical Outcome of Synthetic Tracheal Transplantation Compared to Results Published in 6 Articles by Macchiarini et al.* 2014, Karolinska University Hospital, Stockholm, Sweden: RetractionWatch.com. p. 40.

[63.]    Ferguson, C., *Revealed: Complaint lodged against Macchiarini, "super-surgeon" under investigation*, in *Retraction Watch*, A. McCook, Editor. 2014.

[64.]    Macchiarini, P., et al., *Clinical transplantation of a tissue-engineered airway.* Lancet, 2008. **372**(9655): p. 2023-30.

[65.]    Curcio, E., P. Macchiarini, and L. De Bartolo, *Oxygen mass transfer in a human tissue-engineered trachea.* Biomaterials, 2010. **31**(19): p. 5131-6.

[66.]    Gonfiotti, A., et al., *The first tissue-engineered airway transplantation: 5-year follow-up results.* Lancet, 2014. **383**(9913): p. 238-44.

[67.]    Elliott, M.J., et al., *Stem-cell-based, tissue engineered tracheal replacement in a child: a 2-year follow-up study.* Lancet, 2012. **380**(9846): p. 994-1000.

[68.]    Hamilton, N.J., et al., *Tissue-Engineered Tracheal Replacement in a Child: A 4-Year Follow-Up Study.* Am J Transplant, 2015. **15**(10): p. 2750-7.

[69.]    Jungebluth, P., et al., *Tracheobronchial transplantation with a stem-cell-seeded bioartificial nanocomposite: a proof-of-concept study.* Lancet, 2011. **378**(9808): p. 1997-2004.

[70.]    Schneider, L., *Macchiarni's patients, the real situation*, in *For Better Science*. 2016.

[71.]    Ajalloueian, F., et al., *Biomechanical and biocompatibility characteristics of electrospun polymeric tracheal scaffolds.* Biomaterials, 2014. **35**(20): p. 5307-15.

[72.] Badylak, S.F., et al., *Engineered whole organs and complex tissues.* Lancet, 2012. **379**(9819): p. 943-52.

[73.] Fountain, H., *A First: Organs Tailor-Made with Body's Own Cells*, in *New York Times*. 2012, The New York Times Company: New York, NY.

[74.] Claesson-Welsh, L., G.K. Hansson, and S. Royal Swedish Academy of, *Tracheobronchial transplantation: The Royal Swedish Academy of Sciences' concerns.* Lancet, 2016. **387**(10022): p. 942.

[75.] Del Gaudio, C., et al., *Are synthetic scaffolds suitable for the development of clinical tissue-engineered tubular organs?* J Biomed Mater Res A, 2014. **102**(7): p. 2427-47.

[76.] Cyranoski, D., *Artificial-windpipe pioneer under scrutiny again.* Nature, 2016.

[77.] Cyranoski, D., *Investigations launched into artificial tracheas.* Nature, 2014. **516**(7529): p. 16-7.

[78.] Cyranoski, D., *Surgeon commits misconduct.* Nature, 2015. **521**(7553): p. 406-7.

[79.] *The patients were dischargedd after the first bioartificial stem-cell based laryngo-tracheal transplantation*. [Text] 2012  [cited 2016 July 13, 2016]; The official website of the project "Investigating the molecular mechanisms and underlying pathways of regenerative medicine approaches the tissue-engineering and cell therapy of airways and lungs," grant agreement No. 11.G34.31.0065 dated October 19, 2011]. Available from: http://regmedgrant.ksma.ru/index.php?id=6&news=18&lang=eng.

[80.] Åstrand, Y. and C. Attalah. *In english: Still in hospital three years after surgery nightmare*. 2015 May 27, 2015 [cited 2016 July 11, 2016]; Available from: http://www.svt.se/ug/yesim-stuck-in-intensive-care-for-three-years-after-surgery-nightmare.

[81.] Jungebluth, P., et al., *Verification of cell viability in bioengineered tissues and organs before clinical transplantation.* Biomaterials, 2013. **34**(16): p. 4057-67.

[82.] Fountain, H., *Groundbreaking surgery for girl born without windpipe*, in *New York Times*. 2013: New York.

[83.] *A foreign patient underwent trachea transplantation in Krasnodar*. [Text] 2012 2012 [cited 2016 July, 13, 2016 ]; The official website of the project "Investigating the molecular mechanisms and underlying pathways of regenerative medicine approaches the tissue-engineering and cell therapy of airways and lungs"]. Available from: http://regmedgrant.ksma.ru/index.php?id=6&news=25&lang=eng.

[84.] Gonfiotti, A., et al., *The first tissue-engineered airway transplantation: 5-year follow-up results.* Lancet, 2013.

[85.] *Trachea recipient graduates from the University of Iceland.* [Text] 2014 May 27. 2014 [cited 2016 July 15]; Available from: http://english.hi.is/frettir/trachea_recipient_graduates_university_iceland.

[86.] Macchiarini, P., *Primary tracheal tumours.* Lancet Oncol, 2006. **7**(1): p. 83-91.

[87.] *Surgery of the Trachea and the Bronchi.* BC Decker.

[88.] *The Macchiarini case: The story so far.* 2016 April 5, 2016 [cited 2016 July 17]; Available from: http://ki.se/en/news/the-macchiarini-case-the-story-so-far.

[89.] Ciralsky, A., *The Celebrity Surgeon Who Used Love, Money, and the Pope to Scam an NBC News Producer*, in *Vanity Fair*. 2016, Conde Nast.

[90.] Hamsten, A. and L. Samuelsson, *Suspected scientific misconduct in the case of Professor Paolo Macchiarini*. 2014, Karolinska Institutet. p. 16.

[91.] *Paolo Macchiarini is not guilty of scientific misconduct.* Lancet, 2015. **386**(9997): p. 932.

[92.] *Department of Error.* Lancet, 2016. **387**(10025): p. 1276.

[93.] *Department of Error.* Lancet, 2016. **387**(10026): p. 1376.

[94.] Press, A., *Stem cell doc faces manslaughter charge over transplants*. 2016.

[95.] Projects, H. *Funds for replacement trachea trial.* [Text] 2015 Dec 11 [cited 2016 July 21]; Available from: http://horizon2020projects.com/sc-health/replacement-trachea-trial-wins-h2020-funding/.

[96.] Sibbald, B., *Death but one unintended consequence of gene-therapy trial.* CMAJ, 2001. **164**(11): p. 1612.

[97.] De Los Angeles, A., et al., *Corrigendum: Failure to replicate the STAP cell phenomenon.* Nature, 2016. **531**(7594): p. 400.

[98.] Delaere, P. and D. Van Raemdonck, *Tracheal replacement.* J Thorac Dis, 2016. **8**(Suppl 2): p. S186-96.

[99.] Isenberg, J.S., et al., *Treatment of liver ischemia-reperfusion injury by limiting thrombospondin-1/CD47 signaling.* Surgery, 2008. **144**(5): p. 752-61.

[100.] Rogers, N.M., A.W. Thomson, and J.S. Isenberg, *Activation of parenchymal CD47 promotes renal ischemia-reperfusion injury.* J Am Soc Nephrol, 2012. **23**(9): p. 1538-50.

[101.] Jin, G., et al., *CD47 gene knockout protects against transient focal cerebral ischemia in mice.* Exp Neurol, 2009. **217**(1): p. 165-70.

[102.] Xing, C., et al., *Neurovascular effects of CD47 signaling: promotion of cell death, inflammation, and suppression of angiogenesis in brain endothelial cells in vitro.* J Neurosci Res, 2009. **87**(11): p. 2571-7.

[103.] Rogers, N.M., et al., *CD47 regulates renal tubular epithelial cell self-renewal and proliferation following renal ischemia reperfusion.* Kidney Int, 2016.

[104.] Xiao, Z., et al., *Attenuation of Ischemia-Reperfusion Injury and Improvement of Survival in Recipients of Steatotic Rat Livers Using CD47 Monoclonal Antibody.* Transplantation, 2016. **100**(7): p. 1480-9.

[105.] Lin, Y., et al., *CD47 blockade reduces ischemia-reperfusion injury and improves outcomes in a rat kidney transplant model.* Transplantation, 2014. **98**(4): p. 394-401.

[106.] Isenberg, J.S., et al., *Gene silencing of CD47 and antibody ligation of thrombospondin-1 enhance ischemic tissue survival in a porcine model: implications for human disease.* Ann Surg, 2008. **247**(5): p. 860-8.

[107.] Isenberg, J.S., et al., *Blockade of thrombospondin-1-CD47 interactions prevents necrosis of full thickness skin grafts.* Ann Surg, 2008. **247**(1): p. 180-90.

[108.] Isenberg, J.S., et al., *Thrombospondin-1 and CD47 limit cell and tissue survival of radiation injury.* Am J Pathol, 2008. **173**(4): p. 1100-12.

[109.] Maxhimer, J.B., et al., *Radioprotection in normal tissue and delayed tumor growth by blockade of CD47 signaling.* Sci Transl Med, 2009. **1**(3): p. 3ra7.

[110.] Soto-Pantoja, D.R., J.S. Isenberg, and D.D. Roberts, *Therapeutic Targeting of CD47 to Modulate Tissue Responses to Ischemia and Radiation.* J Genet Syndr Gene Ther, 2011. **2**(2).

[111.] Soto-Pantoja, D.R., S. Kaur, and D.D. Roberts, *CD47 signaling pathways controlling cellular differentiation and responses to stress.* Crit Rev Biochem Mol Biol, 2015. **50**(3): p. 212-30.

[112.] Rogers, N.M., et al., *Thrombospondin-1 and CD47 regulation of cardiac, pulmonary and vascular responses in health and disease.* Matrix Biol, 2014.

[113.] *Treatment of childhood tuberculosis: Consensus Statement of IAP Working Group. Indian Academy of Pediatrics.* Indian Pediatr, 1997. **34**(12): p. 1093-6.

[114.] Kocyildirim, E., et al., *Long-segment tracheal stenosis: slide tracheoplasty and a multidisciplinary approach improve outcomes and reduce costs.* J Thorac Cardiovasc Surg, 2004. **128**(6): p. 876-82.

[115.] Wurtz, A. and E. Kipnis, *Tissue-engineered airway in the clinical setting: a call for information disclosure.* Clin Pharmacol Ther, 2012. **91**(6): p. 973; author reply 974.

[116.] Birchall, M. and P. Macchiarini, *Airway transplantation: a debate worth having?* Transplantation, 2008. **85**(8): p. 1075-80.

[117.] Teramachi, M., et al., *Intrathoracic tracheal reconstruction with a collagen-conjugated prosthesis: evaluation of the efficacy of omental wrapping.* J Thorac Cardiovasc Surg, 1997. **113**(4): p. 701-11.

[118.] Berg, M., et al., *Replacement of a tracheal stenosis with a tissue-engineered human trachea using autologous stem cells: a case report.* Tissue Eng Part A, 2014. **20**(1-2): p. 389-97.

[119.] Omori, K., et al., *Regenerative medicine of the trachea: the first human case.* Ann Otol Rhinol Laryngol, 2005. **114**(6): p. 429-33.

[120.] Azorin, J.F., et al., *Tracheal replacement with an aortic autograft.* Eur J Cardiothorac Surg, 2006. **29**(2): p. 261-3.

[121.] Baiguera, S., et al., *Long-term changes to in vitro preserved bioengineered human trachea and their implications for decellularized tissues.* Biomaterials, 2012. **33**(14): p. 3662-72.

[122.] Baiguera, S., et al., *Tissue engineered human tracheas for in vivo implantation.* Biomaterials, 2010. **31**(34): p. 8931-8.

[123.] Macchiarini, P., *[First successful trachea transplantation. New trachea from the bioreactor (interview by Dr. Judith Neumaier)].* MMW Fortschr Med, 2009. **151**(8): p. 6.

[124.] Macchiarini, P., et al., *First human transplantation of a bioengineered airway tissue.* J Thorac Cardiovasc Surg, 2004. **128**(4): p. 638-41.

[125.] Mertsching, H., T. Walles, and P. Macchiarini, *Replacement of the trachea with an autologous aortic graft.* Ann Thorac Surg, 2004. **78**(3): p. 1132-3; author reply 1133.

[126.] National Research Council (U.S.). Committee for the Update of the Guide for the Care and Use of Laboratory Animals., Institute for Laboratory Animal Research (U.S.), and National Academies Press (U.S.), *Guide for the care and use of laboratory animals.* 2011, National Academies Press,: Washington, D.C. p. xxv, 220 p.

[127.] Hua, X., et al., *Heterotopic and orthotopic tracheal transplantation in mice used as models to study the development of obliterative airway disease.* J Vis Exp, 2010(35).

[128.] Genden, E.M., et al., *Orthotopic tracheal transplantation in the murine model.* Transplantation, 2002. **73**(9): p. 1420-5.

[129.] Genden, E.M., et al., *The kinetics and pattern of tracheal allograft re-epithelialization.* Am J Respir Cell Mol Biol, 2003. **28**(6): p. 673-81.

[130.] Genden, E.M., et al., *Orthotopic tracheal allografts undergo reepithelialization with recipient-derived epithelium.* Arch Otolaryngol Head Neck Surg, 2003. **129**(1): p. 118-23.

[131.] Crapo, P.M., T.W. Gilbert, and S.F. Badylak, *An overview of tissue and whole organ decellularization processes.* Biomaterials, 2011. **32**(12): p. 3233-43.

[132.] Zang, M., et al., *Decellularized tracheal matrix scaffold for tracheal tissue engineering: in vivo host response.* Plast Reconstr Surg, 2013. **132**(4): p. 549e-559e.

[133.] Remlinger, N.T., et al., *Hydrated xenogeneic decellularized tracheal matrix as a scaffold for tracheal reconstruction.* Biomaterials, 2010. **31**(13): p. 3520-6.

[134.] Gilbert, T.W., et al., *Morphologic assessment of extracellular matrix scaffolds for patch tracheoplasty in a canine model.* Ann Thorac Surg, 2008. **86**(3): p. 967-74; discussion 967-74.

[135.] Jungebluth, P., et al., *Structural and morphologic evaluation of a novel detergent-enzymatic tissue-engineered tracheal tubular matrix.* J Thorac Cardiovasc Surg, 2009. **138**(3): p. 586-93; discussion 592-3.

[136.] Cole, B.B., et al., *Tracheal Basal cells: a facultative progenitor cell pool.* Am J Pathol, 2010. **177**(1): p. 362-76.

[137.] Hajj, R., et al., *Basal cells of the human adult airway surface epithelium retain transit-amplifying cell properties.* Stem Cells, 2007. **25**(1): p. 139-48.

[138.] Isenberg, J.S., et al., *Increasing survival of ischemic tissue by targeting CD47.* Circ Res, 2007. **100**(5): p. 712-20.

[139.] Lee, J.H., et al., *Lung stem cell differentiation in mice directed by endothelial cells via a BMP4-NFATc1-thrombospondin-1 axis.* Cell, 2014. **156**(3): p. 440-55.

[140.] Murphy-Ullrich, J.E. and E.H. Sage, *Revisiting the matricellular concept.* Matrix Biol, 2014. **37**: p. 1-14.

[141.] Bornstein, P., *Thrombospondins: structure and regulation of expression.* FASEB J, 1992. **6**(14): p. 3290-9.

[142.] Wolf, F.W., et al., *Structure and chromosomal localization of the human thrombospondin gene.* Genomics, 1990. **6**(4): p. 685-91.

[143.] Bornstein, P., *Diversity of function is inherent in matricellular proteins: an appraisal of thrombospondin 1.* J Cell Biol, 1995. **130**(3): p. 503-6.

[144.] Resovi, A., et al., *Current understanding of the thrombospondin-1 interactome.* Matrix Biol, 2014. **37**: p. 83-91.

[145.] Sweetwyne, M.T., et al., *The calreticulin-binding sequence of thrombospondin 1 regulates collagen expression and organization during tissue remodeling.* Am J Pathol, 2010. **177**(4): p. 1710-24.

[146.] Lafyatis, R., *Transforming growth factor beta--at the centre of systemic sclerosis.* Nat Rev Rheumatol, 2014. **10**(12): p. 706-19.

[147.] Ahamed, J., et al., *In vitro and in vivo evidence that thrombospondin-1 (TSP-1) contributes to stirring- and shear-dependent activation of platelet-derived TGF-beta1.* PLoS One, 2009. **4**(8): p. e6608.

[148.] Short, S.M., et al., *Inhibition of endothelial cell migration by thrombospondin-1 type-1 repeats is mediated by beta1 integrins.* J Cell Biol, 2005. **168**(4): p. 643-53.

[149.] Lawler, J., et al., *Thrombospondin-1 is required for normal murine pulmonary homeostasis and its absence causes pneumonia.* J Clin Invest, 1998. **101**(5): p. 982-92.

[150.] Iruela-Arispe, M.L., et al., *Differential expression of thrombospondin 1, 2, and 3 during murine development.* Dev Dyn, 1993. **197**(1): p. 40-56.

[151.] Sherbina, N.V. and P. Bornstein, *Modulation of thrombospondin gene expression during osteoblast differentiation in MC3T3-E1 cells.* Bone, 1992. **13**(2): p. 197-201.

[152.] Rice, L.M., et al., *A longitudinal biomarker for the extent of skin disease in patients with diffuse cutaneous systemic sclerosis.* Arthritis Rheumatol, 2015. **67**(11): p. 3004-15.

[153.] Matsuo, Y., et al., *Thrombospondin 1 as a novel biological marker of obesity and metabolic syndrome.* Metabolism, 2015. **64**(11): p. 1490-9.

[154.] von Toerne, C., et al., *MASP1, THBS1, GPLD1 and ApoA-IV are novel biomarkers associated with prediabetes: the KORA F4 study.* Diabetologia, 2016.

[155.] Dong, X.Q., et al., *Changes in plasma thrombospondin-1 concentrations following acute intracerebral hemorrhage.* Clin Chim Acta, 2015. **450**: p. 349-55.

[156.] Gao, J.B., et al., *Predictive value of thrombospondin-1 for outcomes in patients with acute ischemic stroke.* Clin Chim Acta, 2015. **450**: p. 176-80.

[157.] Smadja, D.M., et al., *Thrombospondin-1 is a plasmatic marker of peripheral arterial disease that modulates endothelial progenitor cell angiogenic properties.* Arterioscler Thromb Vasc Biol, 2011. **31**(3): p. 551-9.

[158.] Ochoa, C.D., B.W. Fouty, and C.A. Hales, *Thrombospondin-1, endothelium and systemic vascular tone.* Future Cardiol, 2011. **7**(2): p. 169-72.

[159.] Labrousse-Arias, D., et al., *HIF-2alpha-mediated induction of pulmonary thrombospondin-1 contributes to hypoxia-driven vascular remodelling and vasoconstriction.* Cardiovasc Res, 2016. **109**(1): p. 115-30.

[160.] Yao, M., et al., *Thrombospondin-1 Activation of Signal-Regulatory Protein-alpha Stimulates Reactive Oxygen Species Production and Promotes Renal Ischemia Reperfusion Injury.* J Am Soc Nephrol, 2014. **25**(6): p. 1171-86.

[161.] Zeisberg, M., et al., *Thrombospondin-1 deficiency causes a shift from fibroproliferative to inflammatory kidney disease and delays onset of renal failure.* Am J Pathol, 2014. **184**(10): p. 2687-98.

[162.] Daniel, C., et al., *Thrombospondin-1 is a major activator of TGF-beta in fibrotic renal disease in the rat in vivo.* Kidney Int, 2004. **65**(2): p. 459-68.

[163.] Lindberg, F.P., et al., *Molecular cloning of integrin-associated protein: an immunoglobulin family member with multiple membrane-spanning domains implicated in alpha v beta 3-dependent ligand binding.* J Cell Biol, 1993. **123**(2): p. 485-96.

[164.] Reinhold, M.I., et al., *In vivo expression of alternatively spliced forms of integrin-associated protein (CD47).* J Cell Sci, 1995. **108 ( Pt 11**): p. 3419-25.

[165.] Oldenborg, P.A., et al., *Role of CD47 as a marker of self on red blood cells.* Science, 2000. **288**(5473): p. 2051-4.

[166.] Willingham, S.B., et al., *The CD47-signal regulatory protein alpha (SIRPa) interaction is a therapeutic target for human solid tumors.* Proc Natl Acad Sci U S A, 2012. **109**(17): p. 6662-7.

[167.] Zhang, H., et al., *HIF-1 regulates CD47 expression in breast cancer cells to promote evasion of phagocytosis and maintenance of cancer stem cells.* Proc Natl Acad Sci U S A, 2015. **112**(45): p. E6215-23.

[168.] McCracken, M.N., A.C. Cha, and I.L. Weissman, *Molecular Pathways: Activating T Cells after Cancer Cell Phagocytosis from Blockade of CD47 "Don't Eat Me" Signals.* Clin Cancer Res, 2015. **21**(16): p. 3597-601.

[169.] Kojima, Y., et al., *CD47-blocking antibodies restore phagocytosis and prevent atherosclerosis.* Nature, 2016.

[170.] Tengood, J.E., R.J. Levy, and S.J. Stachelek, *The use of CD47-modified biomaterials to mitigate the immune response.* Exp Biol Med (Maywood), 2016. **241**(10): p. 1033-41.

[171.] Tena, A.A., et al., *Prolonged Survival of Pig Skin on Baboons After Administration of Pig Cells Expressing Human CD47.* Transplantation, 2016.

[172.] Soto-Pantoja, D.R., et al., *Inhibitory signaling through signal regulatory protein-alpha is not sufficient to explain the antitumor activities of CD47 antibodies.* Proc Natl Acad Sci U S A, 2012. **109**(42): p. E2842; author reply E2844-5.

[173.] Zhao, X., et al., *On the mechanism and benefit of siRNA-mediated targeting of CD47 in cancer.* Mol Ther, 2013. **21**(10): p. 1811.

[174.] Rogers, N.M., et al., *Thrombospondin-1 and CD47 regulation of cardiac, pulmonary and vascular responses in health and disease.* Matrix Biol, 2014. **37**: p. 92-101.

[175.] McDonald, J.F., J.M. Dimitry, and W.A. Frazier, *An amyloid-like C-terminal domain of thrombospondin-1 displays CD47 agonist activity requiring both VVM motifs.* Biochemistry, 2003. **42**(33): p. 10001-11.

[176.] Kaur, S., et al., *Heparan sulfate modification of the transmembrane receptor CD47 is necessary for inhibition of T cell receptor signaling by thrombospondin-1.* J Biol Chem, 2011. **286**(17): p. 14991-5002.

[177.] Wu, A.L., et al., *Ubiquitin-related proteins regulate interaction of vimentin intermediate filaments with the plasma membrane.* Mol Cell, 1999. **4**(4): p. 619-25.

[178.] N'Diaye, E.N. and E.J. Brown, *The ubiquitin-related protein PLIC-1 regulates heterotrimeric G protein function through association with Gbetagamma.* J Cell Biol, 2003. **163**(5): p. 1157-65.

[179.] Brown, E.J. and W.A. Frazier, *Integrin-associated protein (CD47) and its ligands.* Trends Cell Biol, 2001. **11**(3): p. 130-5.

[180.] Lindberg, F.P., et al., *Integrin-associated protein immunoglobulin domain is necessary for efficient vitronectin bead binding.* J Cell Biol, 1996. **134**(5): p. 1313-22.

[181.] Kaur, S., et al., *Thrombospondin-1 inhibits VEGF receptor-2 signaling by disrupting its association with CD47.* J Biol Chem, 2010. **285**(50): p. 38923-32.

[182.]  Isenberg, J.S., et al., *Thrombospondin-1 stimulates platelet aggregation by blocking the antithrombotic activity of nitric oxide/cGMP signaling.* Blood, 2008. **111**(2): p. 613-23.

[183.]  Isenberg, J.S., et al., *CD47 is necessary for inhibition of nitric oxide-stimulated vascular cell responses by thrombospondin-1.* J Biol Chem, 2006. **281**(36): p. 26069-80.

[184.]  Isenberg, J.S., et al., *Thrombospondin-1 inhibits endothelial cell responses to nitric oxide in a cGMP-dependent manner.* Proc Natl Acad Sci U S A, 2005. **102**(37): p. 13141-6.

[185.]  Bauer, E.M., et al., *Thrombospondin-1 supports blood pressure by limiting eNOS activation and endothelial-dependent vasorelaxation.* Cardiovasc Res, 2010. **88**(3): p. 471-81.

[186.]  Kaur, S. and D.D. Roberts, *CD47 applies the brakes to angiogenesis via vascular endothelial growth factor receptor-2.* Cell Cycle, 2011. **10**(1): p. 10-2.

[187.]  Kaur, S., et al., *Thrombospondin-1 signaling through CD47 inhibits self-renewal by regulating c-Myc and other stem cell transcription factors.* Sci Rep, 2013. **3**: p. 1673.

[188.]  Jackson Laboratory, T. *Mouse Strain Datasheet - 003173. B6.129S7-Cd47<tm1Fpl>/J* [cited 2016 July 13, 2016]; Product datasheet for Jackson Laboratories Mouse Stock no. 003173, CD47-null.]. Available from: https://www.jax.org/strain/003173.

[189.]  Jackson Laboratory, T. *Mouse Strain Datasheet - 006141. B6.129S2-Thbs1<tm1Hyn>/J.* [Text]  [cited 2016 July 26]; Product information for the TSP1 null mouse.]. Available from: https://www.jax.org/strain/006141.

[190.]  Lindberg, F.P., et al., *Decreased resistance to bacterial infection and granulocyte defects in IAP-deficient mice.* Science, 1996. **274**(5288): p. 795-8.

[191.]  Frazier, E.P., et al., *Age-dependent regulation of skeletal muscle mitochondria by the thrombospondin-1 receptor CD47.* Matrix Biol, 2011. **30**(2): p. 154-61.

[192.]  Isenberg, J.S., et al., *Thrombospondin-1 and CD47 regulate blood pressure and cardiac responses to vasoactive stress.* Matrix Biol, 2009. **28**(2): p. 110-9.

[193.]  Amend, S.R., et al., *Thrombospondin-1 regulates bone homeostasis through effects on bone matrix integrity and nitric oxide signaling in osteoclasts.* J Bone Miner Res, 2015. **30**(1): p. 106-15.

[194.]  Koskinen, C., et al., *Lack of CD47 impairs bone cell differentiation and results in an osteopenic phenotype in vivo due to impaired signal regulatory protein alpha (SIRPalpha) signaling.* J Biol Chem, 2013. **288**(41): p. 29333-44.

[195.] Contreras-Ruiz, L., et al., *Sjogren's syndrome associated dry eye in a mouse model is ameliorated by topical application of integrin alpha4 antagonist GW559090.* Exp Eye Res, 2016. **143**: p. 1-8.

[196.] International Mouse Knockout, C., et al., *A mouse for all reasons.* Cell, 2007. **128**(1): p. 9-13.

[197.] Austin, C.P., et al., *The knockout mouse project.* Nat Genet, 2004. **36**(9): p. 921-4.

[198.] Skarnes, W.C., *Two ways to trap a gene in mice.* Proc Natl Acad Sci U S A, 2005. **102**(37): p. 13001-2.

[199.] Guan, C., et al., *A review of current large-scale mouse knockout efforts.* Genesis, 2010. **48**(2): p. 73-85.

[200.] Accili, D., *A note of caution on the Knockout Mouse Project.* Nat Genet, 2004. **36**(11): p. 1132.

[201.] Skarnes, W.C., et al., *A conditional knockout resource for the genome-wide study of mouse gene function.* Nature, 2011. **474**(7351): p. 337-42.

[202.] Testa, G., et al., *A reliable lacZ expression reporter cassette for multipurpose, knockout-first alleles.* Genesis, 2004. **38**(3): p. 151-8.

[203.] Consortium, I.M.P. *Cd47<tm1a(KOMP)>Mbp* [cited 2016 July 13, 2016]; Allele map for the CD47 tm1a allele.]. Available from: http://www.mousephenotype.org/data/alleles/MGI:96617/tm1a(KOMP)Mbp.

[204.] Dimitry, J., *CD47 flox protocol*, N. Rogers, W. Frazier, and B. Capoccia, personal communication, September 25, 2014.

[205.] Jackson Laboratory, T. *Master Protocol Details*. [Text] 2014 August 4, 2014 [cited 2016 July 20]; Protocol details for genotyping for the flp allele.]. Available from: https://www2.jax.org/protocolsdb/f?p=116:5:0::NO:5:P5_MASTER_PROTOCOL_ID,P5_JRS_CODE:12398,009086.

[206.] Silver, L.M., *Mouse Genetics: Concepts and Applications*. 1995: Oxford University Press.

[207.] Coleman, J.L., et al., *Rapid Knockout and Reporter Mouse Line Generation and Breeding Colony Establishment Using EUCOMM Conditional-Ready Embryonic Stem Cells: A Case Study.* Front Endocrinol (Lausanne), 2015. **6**: p. 105.

[208.] Rogers, N.M., A.W. Thomson, and J.S. Isenberg, *Activation of Parenchymal CD47 Promotes Renal Ischemia-Reperfusion Injury.* J Am Soc Nephrol, 2012.

[209.] Johansson, U., K. Higginbottom, and M. Londei, *CD47 ligation induces a rapid caspase-independent apoptosis-like cell death in human monocytes and dendritic cells.* Scand J Immunol, 2004. **59**(1): p. 40-9.

[210.] Mateo, V., et al., *Mechanisms of CD47-induced caspase-independent cell death in normal and leukemic cells: link between phosphatidylserine exposure and cytoskeleton organization.* Blood, 2002. **100**(8): p. 2882-90.

[211.] Mateo, V., et al., *CD47 ligation induces caspase-independent cell death in chronic lymphocytic leukemia.* Nat Med, 1999. **5**(11): p. 1277-84.

[212.] You, Y. and S.L. Brody, *Culture and differentiation of mouse tracheal epithelial cells.* Methods Mol Biol, 2013. **945**: p. 123-43.

[213.] Maxhimer, J.B., et al., *Thrombospondin-1/CD47 blockade following ischemia-reperfusion injury is tissue protective.* Plast Reconstr Surg, 2009. **124**(6): p. 1880-9.

[214.] Isenberg, J.S., S. Shiva, and M. Gladwin, *Thrombospondin-1-CD47 blockade and exogenous nitrite enhance ischemic tissue survival, blood flow and angiogenesis via coupled NO-cGMP pathway activation.* Nitric Oxide, 2009. **21**(1): p. 52-62.

[215.] Isenberg, J.S., et al., *Blocking thrombospondin-1/CD47 signaling alleviates deleterious effects of aging on tissue responses to ischemia.* Arterioscler Thromb Vasc Biol, 2007. **27**(12): p. 2582-8.

[216.] Johansson, M.W. and D.F. Mosher, *Activation of beta1 integrins on blood eosinophils by P-selectin.* Am J Respir Cell Mol Biol, 2011. **45**(4): p. 889-97.

[217.] Danahay, H., et al., *Notch2 is required for inflammatory cytokine-driven goblet cell metaplasia in the lung.* Cell Rep, 2015. **10**(2): p. 239-52.

[218.] Myerburg, M.M., et al., *Acute regulation of the epithelial sodium channel in airway epithelia by proteases and trafficking.* Am J Respir Cell Mol Biol, 2010. **43**(6): p. 712-9.

[219.] Lee, A.H., et al., *Rho-kinase inhibitor prevents bleomycin-induced injury in neonatal rats independent of effects on lung inflammation.* Am J Respir Cell Mol Biol, 2014. **50**(1): p. 61-73.

[220.] Rogers, N.M., D.D. Roberts, and J.S. Isenberg, *Age-associated induction of cell membrane CD47 limits basal and temperature-induced changes in cutaneous blood flow.* Ann Surg, 2013. **258**(1): p. 184-91.

[221.] Azcutia, V., et al., *CD47 plays a critical role in T-cell recruitment by regulation of LFA-1 and VLA-4 integrin adhesive functions.* Mol Biol Cell, 2013. **24**(21): p. 3358-68.

[222.] Iatropoulos, M.J. and G.M. Williams, *Proliferation markers.* Exp Toxicol Pathol, 1996. **48**(2-3): p. 175-81.

[223.] Takahashi, K., et al., *Induction of pluripotent stem cells from adult human fibroblasts by defined factors.* Cell, 2007. **131**(5): p. 861-72.

[224.] Volckaert, T., A. Campbell, and S. De Langhe, *c-Myc regulates proliferation and Fgf10 expression in airway smooth muscle after airway epithelial injury in mouse.* PLoS One, 2013. **8**(8): p. e71426.

[225.] Warner, S.M., et al., *Transcription factor p63 regulates key genes and wound repair in human airway epithelial basal cells.* Am J Respir Cell Mol Biol, 2013. **49**(6): p. 978-88.

[226.] Arason, A.J., et al., *deltaNp63 has a role in maintaining epithelial integrity in airway epithelium.* PLoS One, 2014. **9**(2): p. e88683.

[227.] Liu, J., et al., *Pre-Clinical Development of a Humanized Anti-CD47 Antibody with Anti-Cancer Therapeutic Potential.* PLoS One, 2015. **10**(9): p. e0137345.

[228.] *Clinical Trials: CD47.* 2016 [cited 2016 Aug 28]; Available from: https://clinicaltrials.gov/ct2/results?term=CD47&Search=Search.

[229.] Firlej, V., et al., *Thrombospondin-1 triggers cell migration and development of advanced prostate tumors.* Cancer Res, 2011. **71**(24): p. 7649-58.

[230.] Pfander, D., et al., *Expression of thrombospondin-1 and its receptor CD36 in human osteoarthritic cartilage.* Ann Rheum Dis, 2000. **59**(6): p. 448-54.

[231.] DiCesare, P.E., et al., *Cartilage oligomeric matrix protein and thrombospondin 1. Purification from articular cartilage, electron microscopic structure, and chondrocyte binding.* Eur J Biochem, 1994. **223**(3): p. 927-37.

[232.] Goessler, U.R., et al., *In vitro analysis of integrin expression during chondrogenic differentiation of mesenchymal stem cells and chondrocytes upon dedifferentiation in cell culture.* Int J Mol Med, 2006. **17**(2): p. 301-7.

[233.] Michikami, I., et al., *Kruppel-like factor 4 regulates membranous and endochondral ossification.* Exp Cell Res, 2012. **318**(4): p. 311-25.